AWARD NUMBER: **W81XWH-15-C-0125**

TITLE: **A Modular Multi-DoF Prosthetic Wrist and Low-Level Autonomous Control for Ease-of-Use**

PRINCIPAL INVESTIGATOR: **Aaron Dollar, PhD**

CONTRACTING ORGANIZATION: **Yale University**

REPORT DATE: October 2019

TYPE OF REPORT: Annual

PREPARED FOR: U.S. Army Medical Research and Materiel Command
Fort Detrick, Maryland 21702-5012

REPORT DOCUMENTATION PAGE

Form Approved
OMB No. 0704-0188

1. REPORT DATE Oct 2019	**2. REPORT TYPE** Annual	**3. DATES COVERED** 09/30/18 - 9/29/19

4. TITLE AND SUBTITLE
A Modular Multi-DOF Prosthetic Wrist and Low-Level Autonomous

5a. CONTRACT NUMBER
W81XWH-15-C-0125

5b. GRANT NUMBER

5c. PROGRAM ELEMENT NUMBER

6. AUTHOR(S)
Aaron Dollar, Neil Bajaj, Linda Resnik, He Huang

5d. PROJECT NUMBER

5e. TASK NUMBER

5f. WORK UNIT NUMBER

7. PERFORMING ORGANIZATION NAME(S) AND ADDRESS(ES)
Yale University, New Haven, CT 06511

8. PERFORMING ORGANIZATION REPORT

9. SPONSORING / MONITORING AGENCY NAME(S) AND ADDRESS(ES)

U.S. Army Medical Research and Materiel Command
Fort Detrick, Maryland 21702-5012

10. SPONSOR/MONITOR'S ACRONYM(S)

11. SPONSOR/MONITOR'S REPORT NUMBER(S)

12. DISTRIBUTION / AVAILABILITY STATEMENT

Approved for Public Release; Distribution Unlimited

13. SUPPLEMENTARY NOTES

14. ABSTRACT

The proposed project centers on developing and evaluating a novel class of spherical prosthetic wrist that provides a range of motion equal to the unaffected human wrist while adding only two inches to the length of the residual limb. This device will be enabled by an intuitive pattern recognition-based surface EMG control scheme to directly control the three degrees of freedom of the wrist and one degree of freedom of the user's terminal device, as well as smart low-level autonomy to enable functions such as ''autolevel'' to reduce cognitive loads for tasks such as keeping a soup spoon level during eating. These concepts will be tested through both a participatory research plan involving amputee end-users from conception, refinement to preliminary testing, as well as a six-subject amputee pilot study in the final year, conducted at the VA New York Harbor Health Care System (Manhattan)

15. SUBJECT TERMS
Upper Limb Prosthetics, Amputee, Assistive Technology, Motion Capture

16. SECURITY CLASSIFICATION OF:			**17. LIMITATION OF ABSTRACT**	**18. NUMBER OF PAGES**	**19a. NAME OF RESPONSIBLE PERSON** USAMRMC
a. REPORT	**b. ABSTRACT**	**c. THIS PAGE**			**19b. TELEPHONE NUMBER** *(include area code)*
U	U	U	UU	51	

Standard Form 298 (Rev. 8-98)
Prescribed by ANSI Std. Z39.18

Table of Contents

Page

1. INTRODUCTION

The proposed project centers on developing and evaluating a novel class of spherical prosthetic wrist that provides a range of motion equal to the unaffected human wrist while adding only two inches to the length of the residual limb. This device will be enabled by an intuitive pattern recognition-based surface EMG control scheme to directly control the three degrees of freedom of the wrist and one degree of freedom of the user's terminal device, as well as smart low-level autonomy to enable functions such as "autolevel" to reduce cognitive loads for tasks such as keeping a soup spoon level during eating. These concepts will be tested through both a participatory research plan involving amputee end-users from conception, refinement to preliminary testing, as well as a six-subject amputee pilot study in the final year.

2. KEYWORDS

Upper Limb Prosthetics, Amputee, Assistive Technology, Motion Capture

3. ACCOMPLISHMENTS

This reporting period covers the third year of the project. This portion of the project has been largely dedicated to the development of novel hardware and control software integration. The group at Yale developed a 3-DOF robotic wrist suitable for subject testing and optimized the 1 DOF Yale MultiGrasp hand, while the group at NC State created an EMG-driven musculoskeletal model-based real-time control of a 3-DOF combined system simulating a 2-DOF wrist and 1-DOF hand.

What were the major goals of the project?

The major goals of this project are to develop a novel 3DOF prosthetic wrist and associated pattern recognition based myoelectric (surface EMG) control scheme. This scheme will simplify the challenges associated with controlling multiple DOF simultaneously, from limited control sites on the residual limb. The scheme will also grant the user access to semi-autonomous 'smart control modes'. These modes involve such functions as keeping the spoon level while eating or taking care of some of the wrist motion that exists when bringing a cup to one's mouth for drinking.

The technical components and smart control concepts are to be tested and iteratively developed via able-bodied participants via a number of sub-studies to be carried out at both Yale and NC STATE. A final study involving amputees will be conducted as well at Yale.

What was accomplished under these goals?

The group at Yale carried out design and fabrication work for the prosthetic wrist device and explored ways to optimize the single DOF prosthetic hand. In particular, the following achievements have been made:

1. A 3DOF prototype that is wearable on either a bypass socket or prosthetic socket was designed and manufactured. Many of these components were designed to reduce to overall weight and size of the device while maintaining an acceptable degree of usability of the wrist device in terms of torque and speed requirements. This included motor selection and integration of drive-train and power transmission components into custom made structural elements.

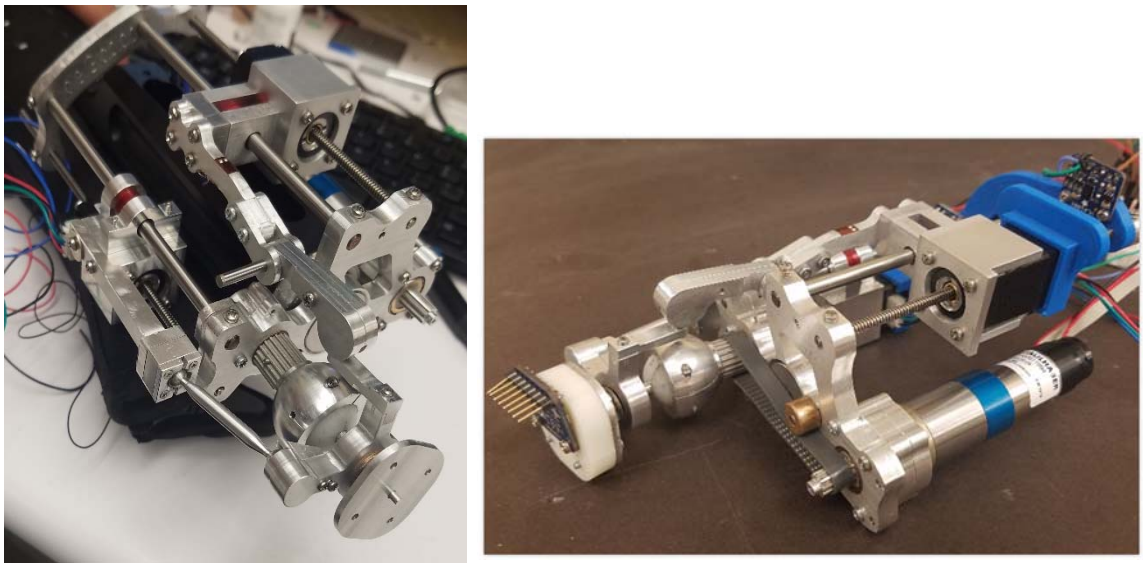

Fig. 1. The new 3 DOF wrist prototype.

2. Multiple methods for providing feedback to the wrist device were explored. The feedback methods include indirect methods by measuring the motor positions and then solving the forward kinematics to determine the orientation of the wrist, and direct methods. The indirect methods implemented used magnetic contactless potentiometers to measure linear motor position with a low noise margin but significant additional hardware, and laser based solutions, which required little hardware but had significantly more noise. The direct method was implemented through use of state of the art inertial measurement units (IMUs), which capture the orientation of both the base of the wrist and the distal terminal device, and can determine the wrist posture by calculating the relative orientation between the two.

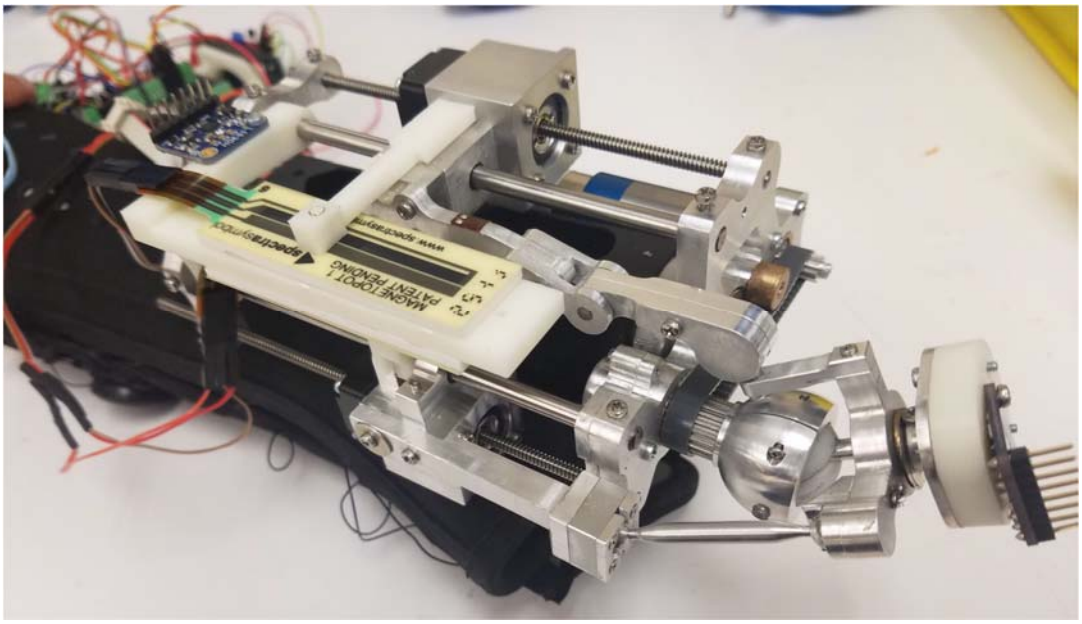

Fig. 1. The new 3 DOF wrist prototype with the magnetic potentiometers and IMUs mounted on board.

3. Low-level control circuit boards were designed, manufactured, and developed to control the wrist. These boards handle the motor control and processing for the sensing elements. Two version of these control boards were made. The first handled very basic motor control and required fast processing to control the wrist with high fidelity, and required multiple power supplies, thus many power cables and communication wires needed to go between the master device, controller boards, and the wrist. The second version handled power management, sensor conditioning, pulse generation for the stepper motors, and over current protection fully onboard, reducing the amount of processing required for the master device. This increases speed and simplifies the control code.

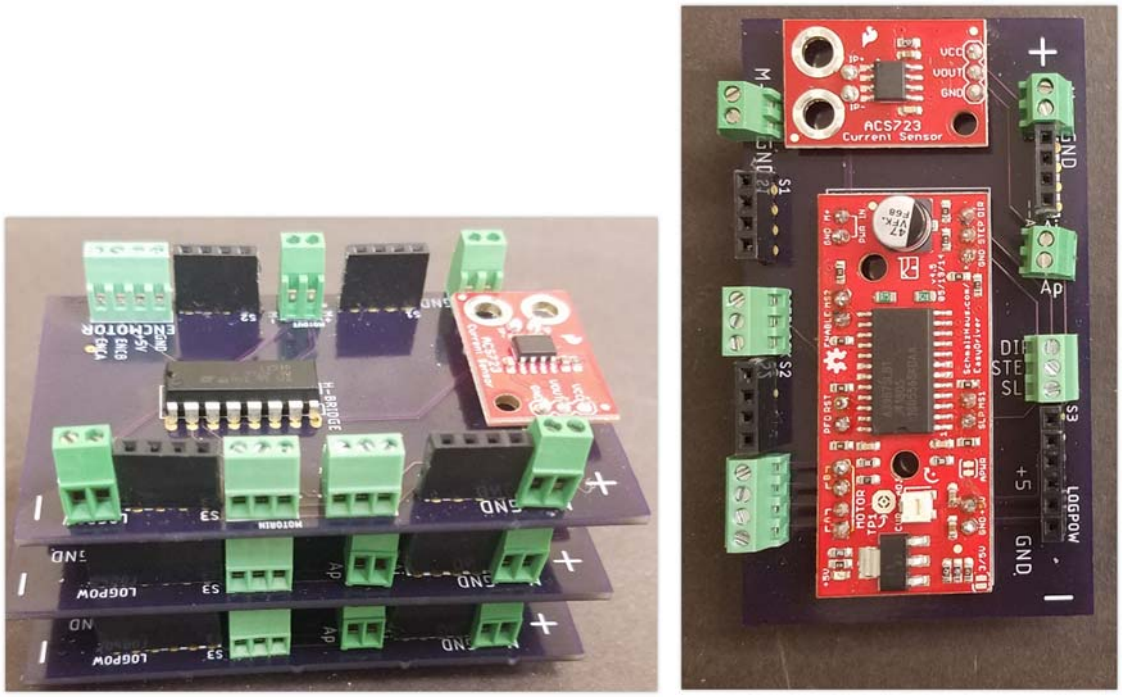

Fig. 3. Version 1 of the wrist control boards. Stacked configuration on the left, exemplar individual board on the right.

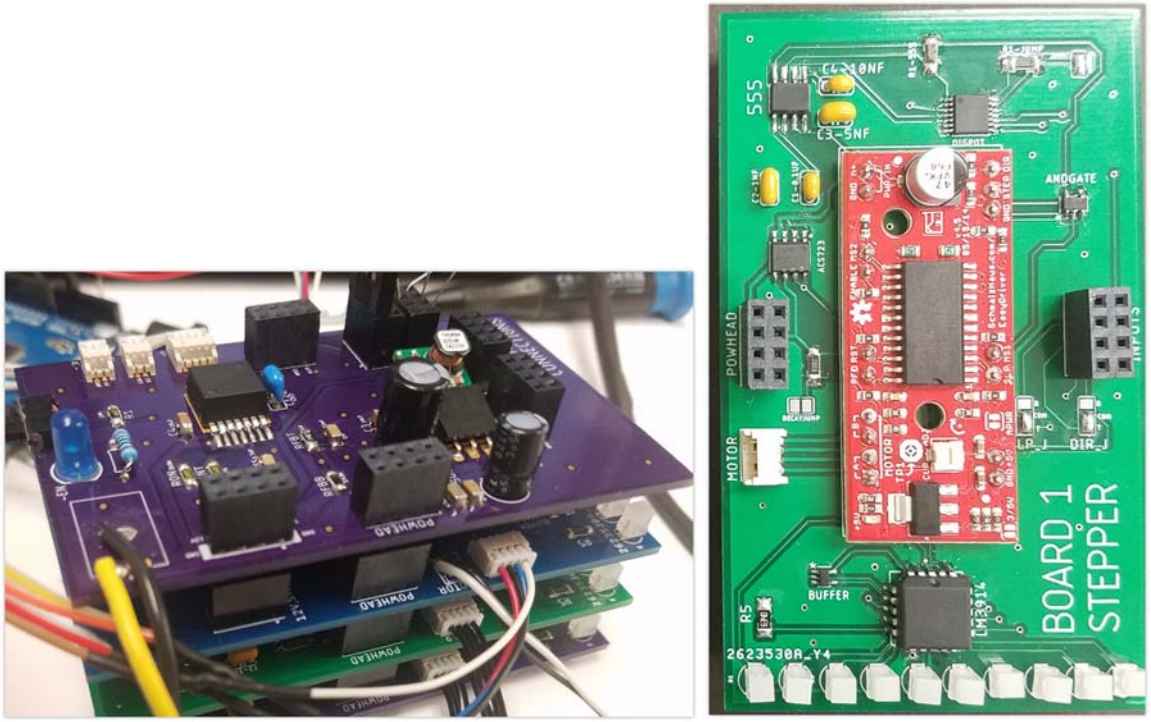

Fig. 4. Version 2 of the wrist control boards. Stacked configuration on the left, exemplar individual board on the right. The boards are designed to stack to minimize horizontal footprint.

4. The finger parameters and gripping surfaces of a single actuator anthropomorphic prosthetic hand were optimized to be used in conjunction with the multiple degree of freedom wrist.

    a. A parameter search was completed to find optimal finger configurations for precision grasping from a single actuator. An optimization framework was created to evaluate the stability of the gripper for a variety of object sizes including heuristics on minimizing post contact work and maximizing the resistance to external disturbances while grasping. (Figure X).

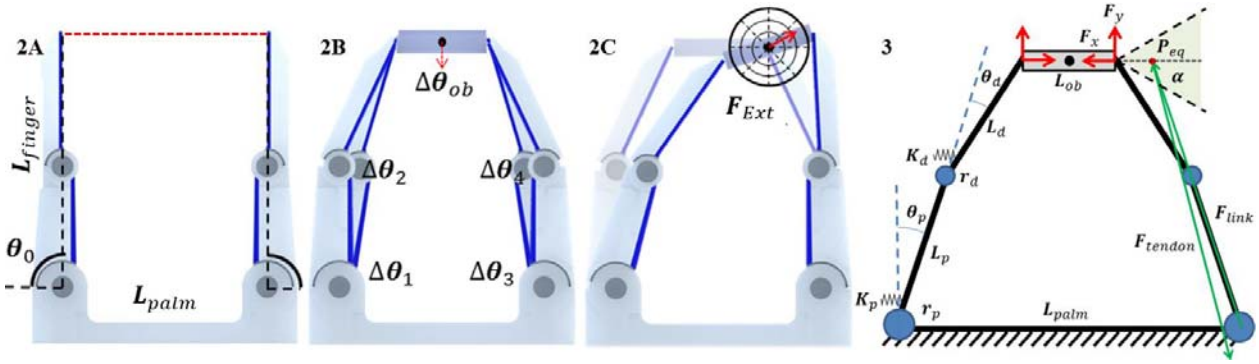

Figure 5. [2A-2C] The process for evaluating stability for two-fingered precision grasping including (a) the starting position of the hand and (b) a constrained optimization of the six bar mechanism to determine reconfiguration and (c) evaluating the stability of configurations to external wrenches. [3] A kinematic model of the two fingered system describing the starting positions, design parameters, kinematics and contact model.

    b. The design of effective robotic finger pads was investigated for precision grippers or multi-fingered hands. The advantages and disadvantages of primitive geometries were compared to the performance of the human hand using a custom testing apparatus for rubber based gripping surfaces. (Figure X).

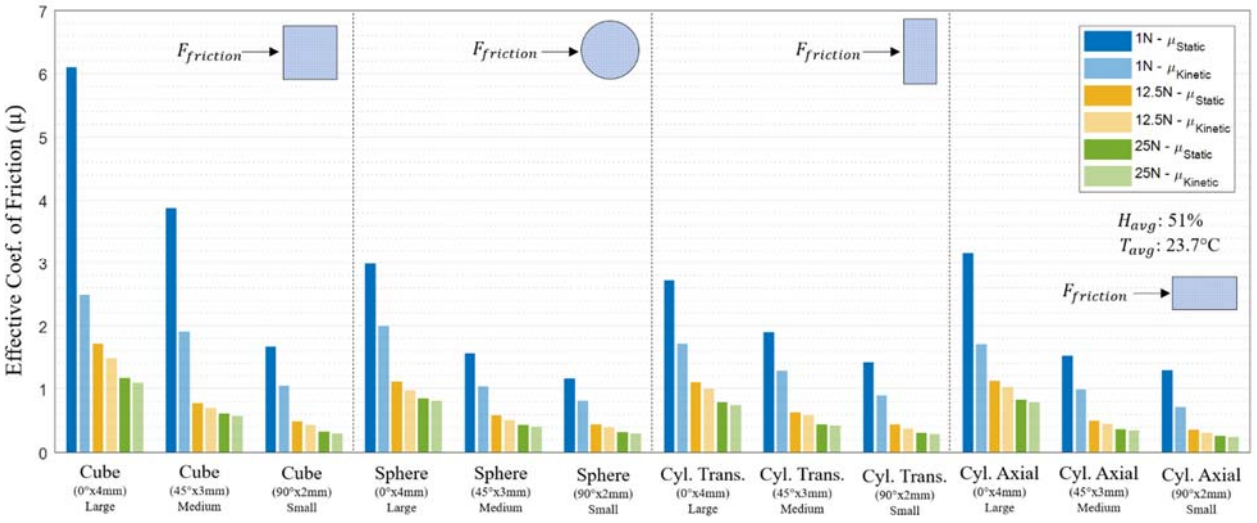

Figure 6. Evaluation of the variation in the effective static and kinetic coefficients of friction relative to a low (1N), medium (12.5N) and high (25N) normal loading force for the fabricated finger pad primitives. The three primitive geometries grip pads are listed in descending order from the pad of that geometry with the largest contact area and

displacement to the smallest contact area and displacement. The cylinder is evaluated in two sliding modes, one sliding across the cylinder round or transverse direction and one sliding across the cylinder length or axial direction.

The group at NC STATE focused on myoelectric control and established the EMG-driven musculoskeletal model-based prosthesis control in real-time. Particularly, the following achievements have been done:

1. We added joint position sensors to the 3 degrees of freedom (wrist pronation/supination, wrist flexion/extension, and hand open/close) and setup the data acquisition of these sensors to stream data to MATLAB. Two angular magnetic encoders were attached to measure hand open/close and wrist flexion extension. An off-axis rotary absolute encoder was attached measure wrist pronation/supination. The setup is shown in Figure 7.
2. We developed a PID controller, allowing for low-level, closed-loop position control of the 3 degrees of freedom (DoFs) of the RIC hand. The controller was implemented using the aforementioned sensors and data streaming in MATLAB.
3. We proposed and developed a reinforcement learning method capable of performing inverse dynamics analysis and predict the torques of the hand joints (Figure 8). This method uses surface EMG and kinematic measurements to predict the torques without external force measurements. The predicted joint moments were used to perform forward dynamics calculations to generate kinematic profiles closely matching the cross-validation datasets, as shown in Figure 9.
4. The previously mentioned reinforcement learning method was further evaluated, demonstrating fast training and the ability to generate subject-specific joint torque profiles, which is helpful in generating subject-specific musculoskeletal models. An example profile is shown in Figure 10.
5. We contacted physicians at OrthoCarolina (located in Charlotte, NC) regarding subject recruitment assistance. Following this effort, two transradial amputees have been brought in for evaluation for participation in pilot testing.

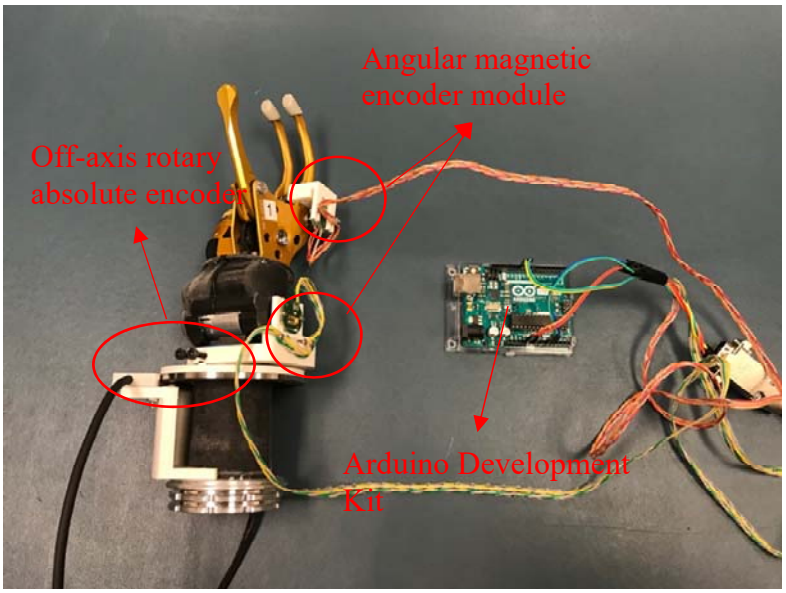

Figure 7. Three position sensors are attached to the three degrees of freedom of the RIC hand. These sensors output data to MATLAB through the Arduino Development Kit. These sensors are used in the developed PID position controller.

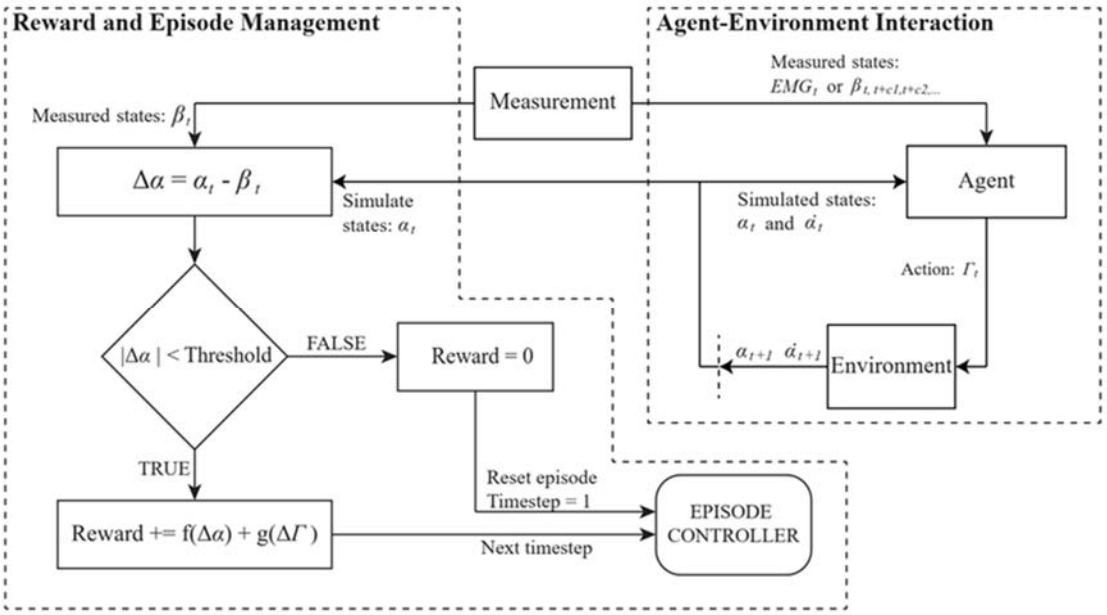

Figure 8. Block diagram outlining the reinforcement learning method for performing inverse dynamics using kinematic and surface EMG data.

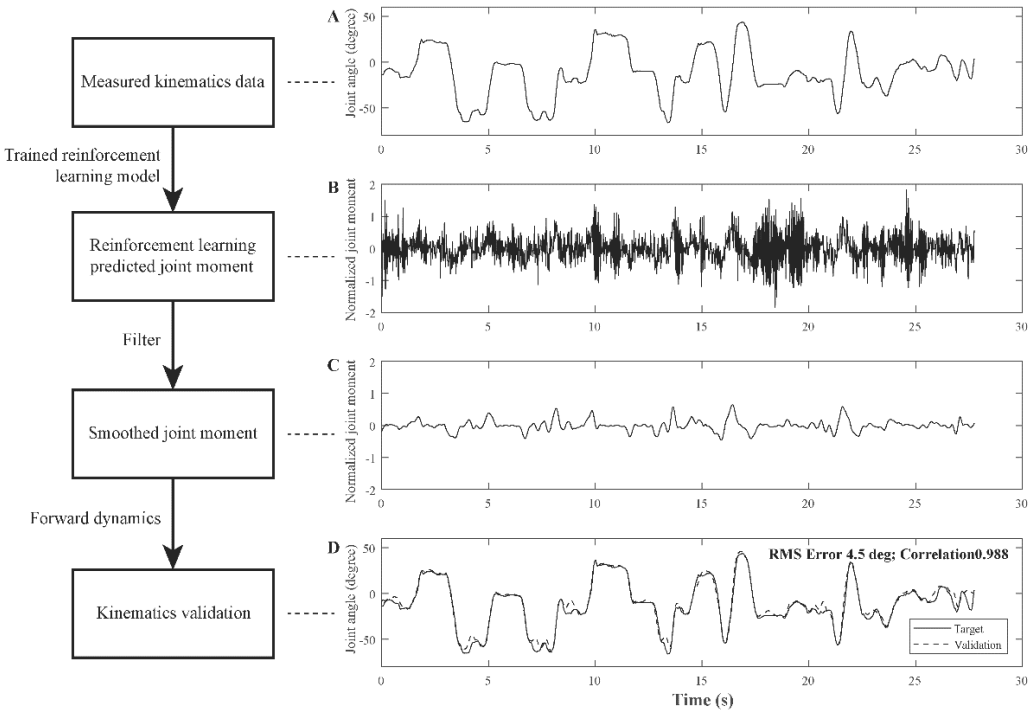

Figure 9. A diagram and example dataset of the reinforcement learning method. Kinematic data (A) are input to the trained reinforcement learning model to output joint moments (B), which are then smoothed (C) using a local regression filter. The joint moments from (C) are then used to calculate forward dynamics for validation.

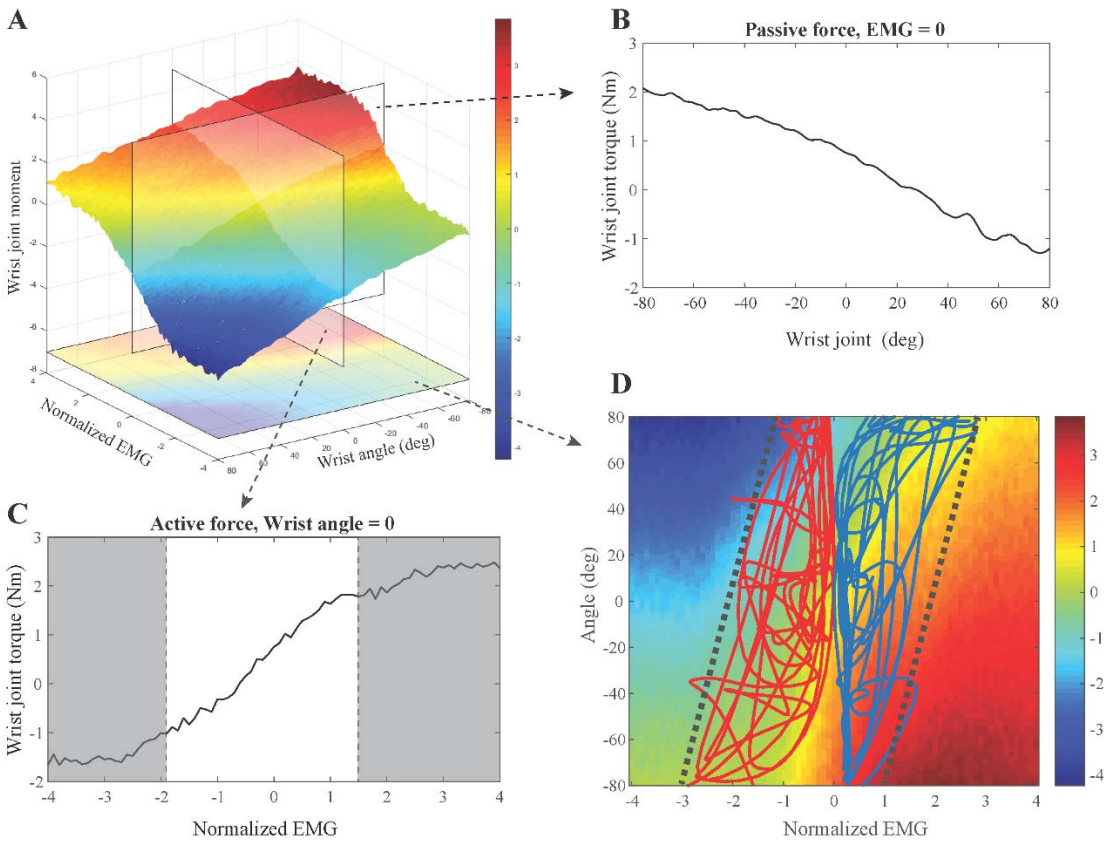

Figure 10. An example of the moment generating profile of the wrist joint for a subject as determined by the reinforcement learning method. The model determines joint moment features based on normalized EMG and joint angle (A). In (B), the joint moment as a function of joint angle, while all EMG is 0 demonstrates the passive force/moment profile. In (C), the active force/moment of the joint is shown by keeping the joint angle constant while changing muscle activity. (D) shows the dataset used to train the reinforcement learning model, with the blue curve representing the flexor EMG-wrist angle relationship and the red curve representing the extensor EMG-wrist angle relationship.

What opportunities for training and professional development has the project provided?

For the team at Yale – the project provided opportunities to connect and learn from researchers in the field of robotics at ICRA 2019. And ASME IDETC 2019. The project also provided opportunities to iterate and address common issues in the field of robotics and hardware design.

For the team at NC STATE - the project provided opportunities to understand the state-of-the-art of myoelectric control for 3-DOF wrist more clearly and deeply.

How were the results disseminated to communities of interest?

At Yale, the related publications are as follows:

M. Leddy and A. Dollar. “Stability Optimization of Two-Fingered Anthropomorphic Hands for Precision Grasping with a Single Actuator”. The IEEE International Conference on Robotics and Automation (ICRA), Montreal, Canada, 2019.

NM Bajaj, AJ Spiers, AM Dollar “State of the Art in Artificial Wrists: A Review of Prosthetic and Robotic Wrist Design.” - IEEE Transactions on Robotics, 2019

NM Bajaj, AM Dollar, “KINEMATIC OPTIMIZATION OF A 2-DOF U, 2PSS PARALLEL WRIST DEVICE” ASME IDETC, 2019.

What do you plan to do during the next reporting period to accomplish the goals?

The team at Yale will conduct an evaluation of both the 3 DOF wrist and 1 DOF multigrasp hand on healthy subjects (using a prosthetic socket simulator) and amputees. This testing will be comprehensive enough to determine points of improvement for both devices and control systems of said devices as well as their general success in accomplishing activities of daily living.

The team at NC State plans to implement low-level, PID position controller of the RIC hand in an embedded system. We will also use the musculoskeletal and reinforcement learning-based models to control the RIC robotic hand. We will then use the hand in pilot testing with amputee and able-bodied subjects.

4. IMPACT

What was the impact on the development of the principal discipline(s) of the project?

This project will serve to introduce new design ideas into the underdeveloped field of parallel mechanism wrist prostheses. Subsequent publications will inform prosthesis designers of the advantages and disadvantages of parallel mechanisms versus their counterparts: serial mechanisms.

More generally, this project has identified areas in which prosthetic design may improve from non-traditional mechanism design, which is commonly not seen in currently available prosthetics on the market.

What was the impact on other disciplines?

The wrist design has a number of aspects of it that make it attractive in other fields, such as robotics and medical devices.

What was the impact on technology transfer?

Nothing to report

What was the impact on society beyond science and technology?

Nothing to report

5. CHANGES/PROBLEMS:

Changes in approach and reasons for change

Nothing to report

Actual or anticipated problems or delays and actions or plans to resolve them

We have received a no-cost extension for a fifth year for the project due to typical delays, mostly form prior years. We should be all set completing the work within this year, or perhaps a few additional months afterwards.

6. PRODUCTS:

Publications, conference papers, and presentations

M. Leddy and A. Dollar. “Stability Optimization of Two-Fingered Anthropomorphic Hands for Precision Grasping with a Single Actuator”. The IEEE International Conference on Robotics and Automation (ICRA), Montreal, Canada, 2019.

NM Bajaj, AJ Spiers, AM Dollar “State of the Art in Artificial Wrists: A Review of Prosthetic and Robotic Wrist Design.” - IEEE Transactions on Robotics, 2019

NM Bajaj, AM Dollar, “KINEMATIC OPTIMIZATION OF A 2-DOF U, 2PSS PARALLEL WRIST DEVICE” ASME IDETC, 2019.

Website(s) or other Internet site(s)

Nothing to report

Technologies or techniques

Nothing to report

Inventions, patent applications, and/or licenses

Nothing to report

Other Products

Nothing to report

7. PARTICIPANTS & OTHER COLLABORATING ORGANIZATIONS

What individuals have worked on the project?

Name:	Aaron Dollar
Project Role:	PI
Researcher Identifier (e.g. ORCID ID):	Aaron.dollar@yale.edu
Nearest person month worked:	1.5
Contribution to Project:	**An expert on human hand functional use and robot / prosthetic hand development. Contributed to protocol development, measurement equipment selection, and setup.**
Funding Support:	This award.

Name:	Linda Resnik
Project Role:	Co-PI
Researcher Identifier (e.g. ORCID ID):	linda_resnik@brown.edu
Nearest person month worked:	1
Contribution to Project:	**An expert on upper limb prosthetics and measures of upper limb functionality and rehabilitation outcomes. Contributed to protocol development.**
Funding Support:	This award

Name:	Helen Huang
Project Role:	Co-PI
Researcher Identifier (e.g. ORCID ID):	hhuang11@NC State.edu
Nearest person month worked:	1
Contribution to Project:	**An expert on myoelectric control. Contributed to protocol development.**
Funding Support:	This award

Name:	Neil Bajaj
Project Role:	Graduate Student
Researcher Identifier (e.g. ORCID ID):	neil.bajaj@yale.edu

Nearest person month worked:	12
Contribution to Project:	**Wrist technology review and publication. Wrist hardware prototype development.**
Funding Support:	This award.

Name:	Michael Leddy
Project Role:	Graduate Student
Researcher Identifier (e.g. ORCID ID):	michael.leddy@yale.edu
Nearest person month worked:	12
Contribution to Project:	**Terminal Device research, design, and evaluation**
Funding Support:	This award.

Name:	Marguerite Bowker
Project Role:	Administrative Lead
Researcher Identifier (e.g. ORCID ID):	Marguerite.Bowker@va.gov
Nearest person month worked:	0.5
Contribution to Project:	**Protocol development. IRB submissions (all institutions and DOD). Project administration.**
Funding Support:	This award

Name:	Ting Zhang
Project Role:	Postdoctoral Associate
Researcher Identifier (e.g. ORCID ID):	tzhang13@NC State.edu
Nearest person month worked:	1
Contribution to Project:	**Protocol development, IRB preparation, and submission,**
Funding Support:	This award

Name:	Lizhi Pan
Project Role:	Postdoctoral Associate
Researcher Identifier (e.g. ORCID ID):	lpan3@NC State.edu

Nearest person month worked:	1
Contribution to Project:	**Algorithm development for myoelectric control**
Funding Support:	This award

Name:	Wen Wu
Project Role:	Postdoctoral Associate
Researcher Identifier (e.g. ORCID ID):	wwu22@ncsu.edu
Nearest person month worked:	1
Contribution to Project:	**Protocol development, hardware programming, efforts related to reinforcement learning.**
Funding Support:	This award

Name:	Boxuan Zhong
Project Role:	Graduate student
Researcher Identifier (e.g. ORCID ID):	bzhong2@ncsu.edu
Nearest person month worked:	2
Contribution to Project:	**Protocol development and human subject testing**
Funding Support:	This award

Has there been a change in the active other support of the PD/PI(s) or senior/key personnel since the last reporting period?

The PI has received additional funding from the National Science Foundation to support his robotics research, but nothing new related to rehabilitation.

What other organizations were involved as partners?

Nothing to report

8. SPECIAL REPORTING REQUIREMENTS

A Quad Chart accompanies this report

9. APPENDICIES

M. Leddy and A. Dollar. “Stability Optimization of Two-Fingered Anthropomorphic Hands for Precision Grasping with a Single Actuator”. The IEEE International Conference on Robotics and Automation (ICRA), Montreal, Canada, 2019.

NM Bajaj, AJ Spiers, AM Dollar “State of the Art in Artificial Wrists: A Review of Prosthetic and Robotic Wrist Design.” - IEEE Transactions on Robotics, 2019

NM Bajaj, AM Dollar, “KINEMATIC OPTIMIZATION OF A 2-DOF U, 2PSS PARALLEL WRIST DEVICE” ASME IDETC, 2019.

2019 International Conference on Robotics and Automation (ICRA)
Palais des congres de Montreal, Montreal, Canada, May 20-24, 2019

Stability Optimization of Two-Fingered Anthropomorphic Hands for Precision Grasping with a Single Actuator

Michael T. Leddy, *Student Member, IEEE* and Aaron M. Dollar, *Senior Member, IEEE*

***Abstract*— In this paper, we present a constrained optimization framework for evaluating the post-contact stability of underactuated precision grasping configurations with a single degree of actuation. Relationships between key anthropomorphic design parameters including link length ratios, transmission ratios, joint stiffness ratios and palm width are developed with applications in upper limb prosthetic design. In addition to grasp stability, we examine post-contact system work, to reduce reconfiguration, and consider the range of objects that can be stably grasped. External wrenches were simulated on a subset of the heuristically evaluated optimal solutions and an optimal configuration was experimentally tested to determine favorable wrench resistible gripper orientations for grasp planning applications.**

I. Introduction

Underactuated mechanical systems with significantly more degrees of freedom than actuators have been utilized in the field of robotic grasping to provide a grasp that is adaptive and robust without the need for complex control. This approach is extensively applied in the field of upper limb prosthetics [1-4] in which nominally ten to fifteen degrees of freedom are controlled by only a few actuators using coupling mechanisms in the palm and fingers. The compliance in these mechanisms facilitate multiple points of contact during enveloping grasps that can accommodate the arbitrary object positioning, orientation and size seen in unstructured environments [5][6]. However, in a two-fingered precision grasp, which is generally necessary to grasp small objects, unconstrained degrees of freedom and decreased force production from passive elastic elements provide potential reconfiguration and instability. An ideal underactuated hand should combine both wrap grasp performance with precision grasps stability to be effective for a variety of objects.

To ensure that the precision grasp of an object remains stable, the hand-object system must remain stable at contact and as it reconfigures. To determine stability, concepts such as force closure and the equilibrium point may be examined. Finger stability occurs in underactuated two link fingers when the equilibrium point, the location in which the contact, actuation and interlink force lines of action intersect, is within the friction cone [7]. An object is considered to be stable in precision grasp when it satisfies force closure, indicating the forces applied between antipodal contact points on an object are positive or zero, the contact line lies within each friction cone and net wrench on the object is zero [8].

This work was supported by the US Army Medical Research and Material Command, under contract W81XWH-15-C-0125. Authors are with the Department of Mechanical Engineering and Materials Science, Yale University, New Haven CT, 06511, USA, michael.leddy@yale.edu and aaron.dollar@yale.edu.

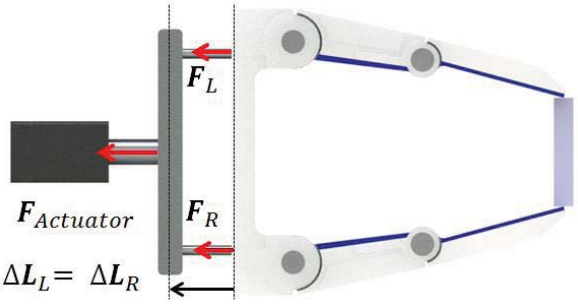

Figure 1. A two-fingered underactuated tendon driven hand model precision grasping an object with a single actuator in force control.

Recent research has taken many different approaches to address the stability issue seen in underactuated precision grasping. In [9], the equilibrium point was investigated to develop mechanical joint limits and determine optimal contact locations for a single actuator grasper with a force differential. On-contact stability was further investigated in a finger that could manipulate its static equilibrium point by mechanically changing its transmission ratio [10]. A constrained optimization was implemented to determine finger parameters for successful form closure of a single actuator multi-link robotic gripper [11] and to determine the passive wrench resistibility of a two-fingered hand fixed in force control [12]. Stable reconfiguration has been investigated for controlled manipulation of two separately actuated, underactuated fingers [13] and for the motion compensation of a similar underactuated gripper [14]. Although stability has been investigated in two finger precision grasping, minimal research addresses the optimality of these configurations for grasping where sophisticated control of the end effector is not possible due to limited number of actuators nominally controlled open loop.

In this paper, we present a multi-step constrained optimization framework for evaluating grasp stability including the post contact reconfiguration and the wrench resistibility of two-fingered precision grasping configurations in which parameters are sampled in anthropomorphic configurations. The optimization platform is modeled off of the kinematics of tendon-driven underactuated hands that are driven from a single actuator. To determine optimal solutions, additional criteria were evaluated including a minimization of post-contact work, to reduce reconfiguration, and maximize the stable object size (Fig. 2A,2B). Maximally performing configurations were simulated and one configuration was experimentally tested to determine favorable wrench resistible gripper orientations for grasp planning applications (Fig. 2C). Relationships between key anthropomorphic design parameters were developed and

978-1-5386-6027-0/19/$31.00 ©2019 IEEE

interpreted for implications in robotic end effectors and upper limb prosthetic design.

II. Methods

A. Stability and Contact Model

When defining stability of the hand-object system in precision grasp, we determined that both the finger and object should be in quasistatic equilibrium at contact and while reconfiguring. The underactuated hand was modeled as two symmetric two-link fingers grasping orthogonal rectangular objects in point contact with coulomb friction (Fig 3.), where contact force ($\boldsymbol{F}_c$)can be applied at any direction with the friction cone angle $\alpha = arctan(\mu)$. Force closure determined object stability in this model, requiring the forces applied between antipodal contact points on an object to be positive or zero, the contact line to lie within each friction cone and the net wrench on the object is zero. However, the antipodal grasp theorem tells us that the object will remain stable with our contact model. As an additional heuristic, the equilibrium point (P_{EQ}) location relative to the friction cone, was introduced to evaluate the quality of grasp stability for a given grasp. When the equilibrium point is within the friction cone there exists a wrench that the finger can exert without slipping or reconfiguring to stabilize the object [7]. We described this equilibrium point configuration as a reliable precision grasp and implemented grasp reliability as an additional criteria for evaluating finger stability under arbitrary external disturbances.

Failure to stabilize the object was determined when force closure of the object was broken or finger equilibrium was not ensured with the grasp reliability heuristic. This was simplified into four main stability criteria for each finger. First, the tendon force magnitude (F_T) being positive or zero, the contact force magnitude $\|F_c\|$ being positive or zero, the contact force vector ($\vec{F_c}$) between antipodal points is located in the friction cone manifold given object tilt (θ_{ob}) and the finger contact force vector and contact moment arm ($\boldsymbol{F}_c, \boldsymbol{R}_c$), interlink force vector and moment arm ($\boldsymbol{F}_l, \boldsymbol{R}_l$), and tendon force vector and moment ($\boldsymbol{F}_T$,$\boldsymbol{R}_T$) are in force and torque equilibrium. It is noted that under external wrenches the contact force vector and antipodal line are not collinear, when the contact force vector points outside of the friction cones the object experiences slip. When these criteria, listed below, are satisfied the hand-object system reconfigures like a constrained six bar mechanism.

$$F_{TL} \geq 0 \quad , \quad \|F_C\| \geq 0 \tag{1}$$

$$\mu - \tan(\theta_{obj}) \leq \frac{|F_{cy}|}{|F_{cx}|} \leq \mu + \tan(\theta_{obj}) \tag{2}$$

$$\sum \vec{r}_i x \, \vec{F}_i = 0 \tag{3}$$

B. Parameter Reduction and Constraints

Constraints were placed on feasible parameters to reduce the sample space of the optimization. Configurations were normalized and sampling ranges were limited to reflect that of anthropomorphic configurations that were kinematically feasible. Anthropomorphism was preferred for the underactuated hand parameters because these configurations nominally produce favorable wrap grasp performance [7] and we aimed to retain these benefits as we further optimized the precision grasping performance. The initial sampled parameters were simplified to three normalized independent variables, the distal radius (r_d), the distal link length (L_d), and the palm width L_{palm}. The proximal finger length (L_p) was determined by keeping the total finger length constant such that $L_p = 1 - L_d$. The value for the proximal radius r_p was kept consistent to determine the transmission ratio and the proximal joint stiffness (K_p)was kept consistent to determine the distal stiffness (K_d) given a predetermined anthropomorphic free swing trajectory constant ($\boldsymbol{c}_{fs}$) that maps the relative movement of the finger proximal joint (θ_p) and distal joint (θ_d) in free swing.

$$c_{fs} = \frac{r_d}{r_p}\frac{K_p}{K_d} \tag{4}$$

The post-contact reconfiguration of the system from increased actuator force or external disturbances was modeled as a constrained six bar mechanism. The system kinematics were evenly constrained to regularize the optimization. This produced a unique solution for each of the eleven variables that kinematically determined our model. Variables included are the proximal and distal joint angle for the left and right fingers (θ_1, θ_2 and θ_3, θ_4), the object tilt (θ_{ob}), the left and right tendon forces (F_{TL}, F_{TR}) and the X and Y components of the contact force for the left

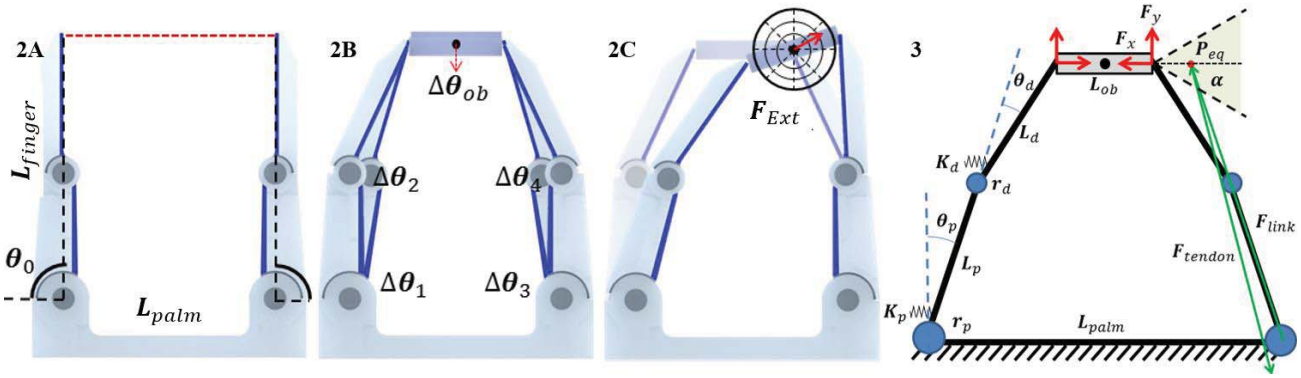

Figure 2. The process for evaluating stability for two-fingered precision grasping including (a) the starting position of the hand and (b) a constrained optimization of the six bar mechanism to determine reconfiguration and (c) evaluating the stability of configurations to external wrenches .
Figure 3. A kinematic model of the two fingered system describing the starting positions, design parameters, kinematics and contact model.

and right finger (F_{XL}, F_{YL} and F_{XR}, F_{YR}). First, the tendon tension must balance the actuator force (F_{act}) so that the fingers remain in equilibrium with the actuator. Coupled tendons also inferred that the tendon length change in the fingers (ΔL_{TL}, ΔL_{TR}) must be equal. The next two constraints, evaluated at an initial configuration (θ_0), required that the six bar linkage closure constraints were unviolated to ensure object contact was maintained throughout the grasp.

$$\boldsymbol{F}_{act} = F_{TL} + F_{TR} \tag{5}$$

$$r_1\theta_1 + r_2\theta_2 = r_3\theta_3 + r_4\theta_4 \tag{6}$$

$$\begin{bmatrix} L_1c_1 + L_2c_{12} \\ L_1s_1 + L_2s_{12} \end{bmatrix} + \begin{bmatrix} L_{ob}c_{ob} \\ L_{ob}s_{ob} \end{bmatrix} = \begin{bmatrix} L_3c_3 + L_4c_{34} + L_{palm} \\ L_3s_3 + L_4s_{34} \end{bmatrix} \tag{7}$$

Where s_{12} and c_{34} are shorthand for $\sin(\theta_1 + \theta_2)$ and $\cos(\theta_3 + \theta_4)$ and angles are evaluated in the direction of closure. The finger torque balance provides four equations and ensures both fingers are in static equilibrium while grasping the object. In this formulation, the actuator torque must equal the elastic element restoring torque plus the contact torque. The product between the actuator jacobian, describing the actuation lever arms $\boldsymbol{J}_{act}^T = [r_1\ r_2\ r_3\ r_4]$, and the tendon force ($\boldsymbol{F}_{act}$), consisting of F_{TL} and F_{TR}, produces the actuator torque. The product of diagonalized spring stiffness ($\boldsymbol{K}_{1-4}$) and the net closure $\Delta\boldsymbol{\theta}_{1-4}$ produces the spring restoring torque. Last, the product of the contact jacobian, mapping the moment arms of the joints to the contact point, $\boldsymbol{J}_c^T(\theta_i, \theta_{ob})$, and the contact forces $\boldsymbol{F}_c = [F_{XL}\ F_{YL}\ F_{XR}\ F_{YR}]$ produces the contact torque. The last three constraint equations are generated from the object static equilibrium conditions that must balance an applied external wrench. In this constraint which $\boldsymbol{F}_c$ is the concatenated contact force vector for each finger, $\boldsymbol{G}$ is the grasp matrix that maps the contact forces to the object frame and $\vec{F}_{ext}$ is the external wrench. The contact jacobian $\boldsymbol{J}_c^T(\theta_i, \theta_{ob})$ and grasp matrix $\boldsymbol{G}$ form are explained in further detail in [13].

$$\boldsymbol{J}_{act}^T\boldsymbol{F}_{act} = \boldsymbol{K}_i\Delta\boldsymbol{\theta}_i + \boldsymbol{J}_c^T(\theta_i, \theta_{ob})\boldsymbol{F}_c \tag{8}$$

$$\boldsymbol{G}\boldsymbol{F}_c + \boldsymbol{F}_{ext} = 0 \tag{9}$$

Constraints and failure criteria were considered in every step of the constrained optimization. Configurations that violated the constraints or failure criteria were eliminated during each step of the parameter search. The initial set of stable solutions were configurations that remained stable at contact and during reconfiguration up to a determined maximum tendon force (F_{Tmax}) for objects from 0% to 50% of the finger length. These percentages were chosen to represent precision grasping of a variety of small to large objects. The configurations that passed this initial stability heuristic were passed through two additional criteria to evaluate their performance for practical robotic grasping focused on reliably grasping a large variety of object sizes and reducing post-contact work.

C. Evaluating Optimal Configurations

Two additional criteria were established to evaluate stable configurations for favorable performance in grasping tasks. Due to instability in two-fingered underactuated precision grasping from slipping or ejection [15], one is usually limited to grasping a small variety of objects. This is partly attributed to reconfiguration that can occur in underactuated hands post-contact requiring compensatory movement to adequately place an object [14]. Thus, favorable designs of underactuated hands include the ability to stably grasp a variety of object sizes with minimal system reconfiguration.

The first objective was to find configurations that produce the maximum reliable object size which we defined as L_{objmax} normalized to the finger length. This was calculated using the previous constrained optimization and varying L_{obj} > 50% finger length until failure. The second objective was to minimize post-contact work of the hand-object system to reduce post-contact joint motion and object reconfiguration. Post-contact work (ΔW_{pc}) was calculated as the integral of product of the post-contact change in tendon force, $F_{Tpc} = F_{Tmax} - F_{Ti}$, and the difference in tendon length $\Delta L_{Tpc} = L_{Tf} - L_{Ti}$. Where F_{Tmax} is the maximum actuator force, F_{Ti} is the tendon force at contact, L_{Tf} is the tendon length after reconfiguration and L_{Ti} is the tendon length at contact. Minimizing this metric reduces the amount of compensation a robotic system may have to do to account for this motion.

$$\Delta W_{pc} = \int F_{Tpc}\,\Delta L_{Tpc} \tag{10}$$

To evaluate configuration performance, an optimization function was incorporated to produce a weighted score of the given configuration combining the stable grasp width and post-contact work. This weighted score (C_{score}) is a maximization of the three elements, the post-contact work for a very small object $S_1 = 1/\Delta W_{pc0\%}$, the post-contact work for a large object $S_2 = 1/\Delta W_{pc50\%}$, and the normalized maximum reliable grasp span $S_3 = L_{objmax}/L_{finger}$. The constant A_i determines the weight of each element in the optimization function. Each individual value is normalized against the maximum and minimum range of values in the stable configuration solution space to eliminate bias in the case elements have different variability.

$$C_{score} = \sum A_i \frac{\boldsymbol{S}_i - \min(\boldsymbol{S}_i)}{\max(\boldsymbol{S}_i) - \min(\boldsymbol{S}_i)} \tag{11}$$

D. External Disturbance Analysis

Once weighted values were determined, an external wrench was applied to the already grasped object for the top 40% of maximally performing configurations to determine configuration stability. The external disturbance was applied in the global frame and acted in the center of the grasped object to determine the maximum resistible wrench, a measure of configuration post-contact stability [16]. This metric also further evaluates the stability of fringe cases where the maximally performing solutions fall close to the stability solution hull. External disturbances can create force asymmetry which removes the mirrored motion of the

TABLE I. SIMULATION RESULTS

Parameter	Stable Reconfiguration (0% to 50% L_f)				
	Min	*Mean*	*Max*	*Range*	*Tested*
Link Length Ratio (L_d/L_p)	0.680	1.085	1.460	[0.68-1.46]	1.403
Transmission Ratio (R_d/R_p)	0.383	0.503	0.583	[0.01-1]	0.583
Stiffness Ratio (K_d/K_p)	0.548	0.719	0.833	[0.01- ∞]	0.833
Palm Width (L_{palm}/L_{finger})	0.500	0.945	1.500	[0.5-1.5	0.770

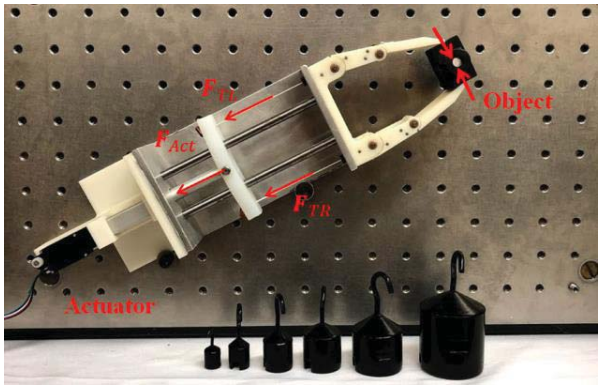

Figure 4. Experimental test setup including a linear actuator, coupled tendons, a hand and object. Weights were applied to the center of the object with gravity applying a force in the global frame.

proximal and distal joints (θ_p, θ_d), allowing nonzero object tilt (θ_{ob}) and differences in tendon force (F_{TL}, F_{TR}). For simplicity the system can be modeled as an asymmetric constrained six bar linkage, subject to elastic elements and joint limits, to solve for displacement of hand-object system.

To experimentally test and validate the simulation a two-fingered precision grasper was developed using parameters from a sample optimal solution seen in Fig. 4. A single linear actuator drove two symmetric fingers in open loop force control. The 30 gram object was acquired and the actuator tendon was tensioned to a designated force allowing the system to reconfigure. To simulate an external disturbance in the global frame, the apparatus was placed in a variety of orientations and weights were slowly added to the center of the object until object slip occurred. The maximum resistible wrench and external disturbance profile was calculated and compared to the simulation results.

III. RESULTS AND DISCUSSION

A. Precision Grasp Stability

A parameter search of three independent variables (r_d, L_d, L_{palm}), bounded by initial sampling constraints on anthropomorphism and kinematic feasibility, was conducted to determine stable configurations using gradient descent of a constrained nonlinear multivariable function in MatLab [17]. The free swing trajectory constant (c_{fs}) was set to 0.7 to resemble an anthropomorphic hand [18] with a large grasp envelope. Given our initial model, 0.1% of tested configurations (n = 3.2 million) remained stable for an object size of 0% to 50% finger length in the bounded parameter search (Table 1). The simulated friction coefficient was conservative at μ = 0.7.

The link length ratio was sampled from 0.68 to 1.46 which represented a 10% L_{finger} variation of the PIP joint location from the middle of the finger. This limitation was imposed as an anthropomorphic design constraint to sample joint positions near the location of the human PIP joint [19]. The entire sampled range provided stable configuration existing at varying transmission ratios, stiffness ratios and palm lengths. The mean link length ratio for a stable configuration was approximately one, inferring stable link length ratios with anthropomorphic joint positions exist. The transmission ratio was sampled from 0.01 to 1 to avoid kinematical infeasible zero distal radius r_d= 0 and diverging force action lines at R_i > 1 for grasp reliability. The stable parameter space was only 20% of the initial sample space with a mean transmission ratio of R_i = 0.503. A proximal tendon level arm being twice that of the distal tendon lever arm when paired with the mean link length ratio produces an equilibrium point centered in the friction cone for small angles. This alignment is intrinsically favorable for stably grasping objects that are large relative to the palm width.

The stiffness ratio was calculated from the anthropomorphic free swing trajectory and transmission ratio. Configurations with a stiffer proximal spring were preferred with a mean K_r= 0.719; this would decrease if a larger motion envelope ($\Delta\theta_p \gg \Delta\theta_d$) is preferred or increase if a smaller motion envelope ($\Delta\theta_p \ll \Delta\theta_d$) is preferred. Palm width normalized to finger length was sampled from 50% to ensure an object 50% of the finger length could fit within the grasp, to 150%, to ensure symmetric contact of a very small object. There was at least one stable configuration for every sampled palm width, although the transmission ratio, link length ratio and stiffness ration parameters varied. The average normalized palm width was slightly below one, however, optimal solutions discussed in the next section exist slightly higher than this average.

B. Maximizing Reliable Object Width

After stable configurations were determined for an object ranging from 0% to 50% finger length, the maximum reliable grasp span was calculated for each configuration. In Fig. 5a, the solution volume was reduced to a planar representation of varying transmission ratios (R_i). These specific ratios were chosen because most of the stable solution hull existed within the anthropomorphic constraints. The graph axis compares the link length ratio to the normalized palm width and solution spaces are graded by their respective optimal criteria or combined optimal criteria.

For the smallest listed transmission ratio R_1 = 0.42 the local maximum was L_{objmax}/L_{finger} = 0.946 and for the largest R_5 = 0.42 the local maximum was L_{objmax}/L_{finger} = 1.081. A trend of increasing max reliable object width with increasing transmission ratio was observed. The local optimum solution by transmission ratio occurred at palm widths slightly larger (1.0 < L_{palm}/L_{finger}< 1.1) than the

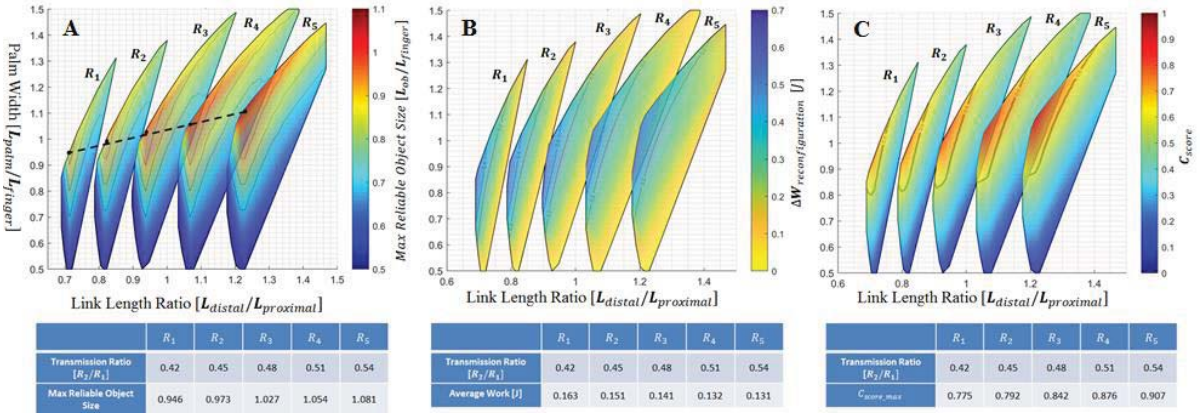

	R_1	R_2	R_3	R_4	R_5
Transmission Ratio $[R_2/R_1]$	0.42	0.45	0.48	0.51	0.54
Max Reliable Object Size	0.946	0.973	1.027	1.054	1.081

	R_1	R_2	R_3	R_4	R_5
Transmission Ratio $[R_2/R_1]$	0.42	0.45	0.48	0.51	0.54
Average Work [J]	0.163	0.151	0.141	0.132	0.131

	R_1	R_2	R_3	R_4	R_5
Transmission Ratio $[R_2/R_1]$	0.42	0.45	0.48	0.51	0.54
C_{score_max}	0.775	0.792	0.842	0.876	0.907

Figure 5. (A) Results of the max reliable object size segmented by transmission ratio with accompanied table displaying the max reliable object size for each transmission ratio labeled and connected by a dotted line. (B) The post-contact work for configurations contacting an object that is 50% finger length with accompanied table showing average work in each transmission ration segment. (C) The weighted score received from an optimization function weighing the post-contact reconfiguration for 0% and 50% finger length and the max reliable object size with accompanied table of max scores.

length of the finger. The global optimum L_{objmax}/L_{finger} = 1.15 was recorded at the largest transmission ratio R_{objmax} = 0.583. Without anthropomorphic sampling limitations, we would expect this value to increase as the allowable palm width and link length ratio increase. It is noted that although there is a favorable correlation for increasing palm width and link length ratio for a given transmission ratio, the local optimum of our model is located at palm lengths near the finger length. Palm designs of similar width to the finger length could be favorable for contact stability in underactuated robotic hands. It is noted that the normalization of maximum reliable object width to finger length skews the optimal solution space towards larger palms, which have a greater potential to grasp larger objects because they have a larger initial grasp span.

The approximately linear relationship between the design parameters when evaluating max stable grasp span provides a practical guideline of relative palm width, link lengths and transmission ratios for effective two-fingered precision graspers. We can conclude that the wider the range of object sizes that can be reliably grasped improves the quality of the device, especially when it comes to underactuated grippers where precision grasp is typically difficult to stabilize under arbitrary loading conditions in open loop [15].

C. Minimizing Post-Contact Work

When calculating post-contact work for the second evaluation criteria, a max actuator force of 60 N was applied, dividing 30 N to each tendon. This force represents a value near the max force production for compact highly geared DC motors commonly found in robotic hands. A reasonably strong proximal spring stiffness K_p = 0.044 $\frac{N}{m}$ was selected. The post-contact work was simulated for the same transmission ratios R_i for objects that were 0%, 25% and 50% of the finger length.

The minimum average post-contact work by transmission ratio and the global optimum post-contact work were observed for grasping the 50% finger length object. In Fig. 5b, the local average minimum of ΔW = 0.131 J was observed at R_5, this was also true for the 0% finger length configurations where minimum average ΔW = 0.407 J at R_5 and at the 25% finger length configurations where minimum average ΔW = 0.263 J at R_5. The transmission ratio being inversely proportional to average post-contact work was consistent across the three object widths. We believe this because a higher r_d increases the tendon force and excursion required to contact a given object, reducing the required work to reconfigure to a max actuator load. Increased performance with increased object width was also observed. Less finger motion $(\Delta\theta_p, \Delta\theta_d)$ to contact an object produces a longer lever arm, reducing reconfiguration because force is less effectively transferred to the object from the actuation tendon. The global minimum for both the 25% and 50% graphs is essentially ΔW = 0 J and is located at the maximum transmission ratio, minimum palm length and largest link length ratio. The contact line, centered in the friction cone, acts as an asymptote in which incrementally larger increases in tendon force are required for an equilibrium point to reconfigure towards this line, reducing the overall magnitude of finger reconfiguration. The low reconfiguration of these solutions indicates that the system is already near a stable position at contact where the equilibrium point is on or approaching the contact line.

The combined weighted score from the optimization function is displayed in Fig. 5c. The weighted values for this evaluation were $A_1 = 0.25$, $A_2 = 0.25$ and $A_3 = 0.50$ to equally balance max reliably object width with post-contact reconfiguration. The average C_{score} increased with increasing transmission ratio and the optimal solution was observed to be C_{score} = 0.907. The maximally performing 40% of stable solutions are located in the bounded lines for each transmission ratio, these values were considered for the additional stability testing.

D. Resistance to System Disturbances

Stability of the top 40% of stable solutions from the optimization function were evaluated by applying external

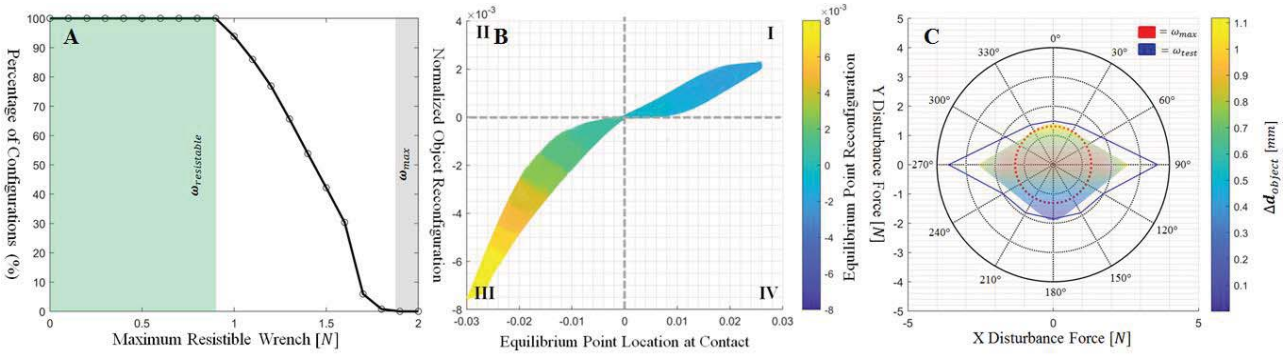

Figure 6. Three criteria were used to evaluate the stability of the top 40% of maximum performing configurations. (A) Displays the percentage of configurations that can resists a certain maximum wrench in any direction, the green section shows the wrench at which all configurations could resist and grey section describes the cutoff for maximum resistible wrench. (B) Displays the equilibrium point reconfiguration relative to object reconfiguration to show that stable solutions reconfigure towards the contact force line of action, which acts as a force asymptote. In (C) simulated and experimental external disturbance plots are compared, the simulated resistible wrench is overlaid with object motion at the force and direction.

disturbances. When evaluating these configurations, the link lengths were determined to be the anthropomorphic basis for the physical values. The finger length was set to 74mm or the size of a small female index finger [19] and the proximal tendon radius was 6mm for practical design considerations. The starting position of the configuration was the acquisition of a 37 mm object that reconfigured to an actuator load of 60 N. Each configuration was radially applied a force in 30° increments until failure criteria were reached. It was seen that all of these configurations were stable to external disturbances being able to resist a minimum of 0.98 N in all directions with the optimal configuration being able to resist 1.85 N in all directions or about 3.1% of the actuator force (Fig. 6A). A maximum resistible wrench greater than zero verifies that final stable configurations are in force closure and can resist arbitrary external wrenches. This is important to note because a significant amount of the final configurations exist on the hull of the stable solutions. Nominally the configurations were weakest in the ±Y direction to force resistance and strongest in the ±X direction. This is becuase the slipping failure mode was the most common and the vertical disturbance forces in the initial configuration were more likely to move the contact force $\boldsymbol{F}_c$ out of the friction cone.

In Fig. 6B, reconfiguration of the object and equilibrium point location were plotted to further understand how the system would adjust to additional actuator force. In quadrants I and III, It was seen that for all solutions the object reconfigured towards the equilibrium point. No solutions existed in quadrants II and IV which would display an object reconfiguring away from the equilibrium point with force, heading towards unstable finger poses. We can assume these configurations will remain stable with additional actuator force because the contact force line of action acts as a kinematic force asymptote and our solution space is reconfiguring towards this asymptote,.

A sample configuration in the top 40% of maximally performing solutions, parameters displayed in Table 1 and test setup in Fig. 4, was simulated and experimentally tested for external wrench resistivity (Fig. 6C). The simulation provided stable resistance of approximately 2.5 N in the ±X directions while resisting 1.3 N in the +Y and 1.9 N in the -Y directions. The minimal resistible wrench of this configuration in simulation was 1.31 N, approximately 2.2% of the actuation force. The physical test displayed an external disturbance profile similar to that of the simulation that was slightly elongated in the X directions. The gripper saw a stable resistance of approximately 3.5 N in the ±X directions, 1.5 N in the +Y direction and 1.8 N in the –Y direction. The minimal resistible wrench of this configuration was 1.53 N which was similar to the 1.31 N of the simulation. Although the profile was similar, the average error between the simulated and experimental results was 22%. This can be primarily attributed to a slightly higher coefficient of friction and difficulties of visually assessing slip in the horizontal configuration where rolling instead of slipping tends to occur. When planning to manipulate an object, it is favorable to know the direction of maximum force resistance so the operator can orient the gripper such that external loading is applied in the direction of maximal disturbance resistance or so that gravity is optimally resisted.

IV. Conclusion

A multi-stage optimization framework was developed to evaluate the stability of symmetric two finger underactuated grippers from a single actuator in open loop force control. Anthropomorphic design parameters were sampled and key relationships between these parameters were established for the design of underactuated robotic precision graspers that can stably grasp a large variety of object sizes with minimized reconfiguration with additional grasp force. An optimal experimental design using these relationships produced a gripper was able to withstand applied object disturbances nearly five times the weight of the initial object in all directions. These relationships provide insight for the development of a variety of prosthetic hands that can successfully grasp an object in precision grasp, be proprioceptively secure and be robust to interactions with its environment. Future work includes the evaluation of higher dimensional asymmetric index-thumb precision grasping configurations using this framework.

REFERENCES

[1] C.M. Gosselin, F. Pelletier and T. Laliberté. “An Anthropomorphic Underactuated Robotic Hand with 15 Dofs and a Single Actuator.” *IEEE Int. Conf. on Robotics and Automation*, California, USA, 2008.

[2] M.G. Catalano, G. Grioli, E. Farnioli, A. Serio, C. Piazza and A. Bicchi. “Adaptive synergies for the design and control of the Pisa/IIT Softhand.” *The Int. Journal of Robotics Research*, Vol.33, No.5, pp.768-782, 2014.

[3] M.C. Carrozza, C. Suppo, F. Sebastiani, B. Massa, F. Vecchi, R. Lazzarini, M.R. Cutkosky and P. Dario. “The SPRING Hand: Development of a Self-Adaptive Prosthesis for Restoring Natural Grasping,” *Autonomous Robots*, Vol. 16, pp. 125-141, 2004.

[4] M.T. Leddy and A.M. Dollar. “Preliminary Design and Evaluation of a Single-Actuator Anthropomorphic Prosthetic Hand with Multiple Distinct Grasp Types”, *IEEE Int. Conf, on Biomedical Robotics and Biomechatronics*, Enschede, Netherlands, 2018.

[5] H. Stuart, S. Wang, O. Khatib and M. Cutkosky. “The Ocean One hands: An adaptive design for robust marine manipulation,” *The Int. Journal of Robotics Research*, Vol.36, No. 2, pp.150-166, 2017.

[6] A. Rodriguez, M.T. Mason and S. Ferry. “From Caging to Grasping.” *Robotics: Science and Systems*, California, USA, 2011.

[7] L. Birglen, T. Laliberté and C.M. Gosselin. *Underactuated Robotic Hands*. Springer-Verlag, 2008.

[8] A. Bicchi and V. Kumar. “Robotic Grasping and Contact: A Review.” *IEEE Int. Conf. on Robotics Research and Automation*, California, USA, 2000.

[9] L. Birglen and C. Gosselin. “On the Force Capability of Underactuated Fingers.” *IEEE Int. Conf. on Robotics Research and Automation*, Taipei, Taiwan, 2003.

[10] S.A. Spanjer, R. Balasubramanian, J.L. Herder and A.M. Dollar. “Improved Grasp Robustness through Variable Transmission Ratios in Underactuated Fingers.” *IEEE Int. Conf. on Intelligent Robots and Systems*, Algarve, Portugal, 2012.

[11] M. Ciocarlie and P. Allen. “A constrained optimization framework for compliant underactuated grasping.” *Mech. Sci.*, Vol.2, pp. 16-26,2011.

[12] M. Haas-Heger, G. Iyengar and M. Ciocarlie. “Passive Reaction Analysis for Grasp Stability.” *Trans on. Automation Science and Engineerin*g, Vol.15, No.3, pp.955-966, 2018.

[13] D. Prattichizzo, M. Malvezzi, M. Gabiccini and A. Bicchi. “On Motion and Force Controllability of Precision Grasps with Hands Actuated by Soft Synergies.” *IEEE Trans. on Robotics*, Vol.29, No.6, pp.1440-1456, 2013.

[14] M.V. Liarokapis and A.M. Dollar. “Post-Contact, In-Hand Object Motion Compensation with Adaptive Hands.” *IEEE Trans. on Automation Science and Engineering*, Vol.15, No.2,pp.456-467, 2017.

[15] L.U. Odhner, R.R. Ma and A.M. Dollar. “Open-Loop Precision Grasping With Underactuated Hands Inspired by a Human Manipulation Strategy.” *IEEE Trans. on Automation and Engineering*, Vol. 10, No.3, pp.625-633, 2013.

[16] C. Ferrari and J. Canny. “Planning Optimal Grasps.” *IEEE Int. Conf. on Robotics and Automation*, Nice, France, 1992.

[17] MATLAB and Parallel Computing Toolbox Release 2018a, The MathWorks, Inc., Natick, Massachusetts, Unite States.

[18] A.M. Kociolek and P.J. Keir. “ Design methodology for a multifunctional hand prosthesis.” *Journal of Rehabilitation Research and Development*, Vol. 32, No. 4, pp.316-324, 1995.

[19] A.R. Tilley. *The Measure of Man and Woman: Human Factors in Design,* John Wiley and Sons, New York, 2002.

State of the Art in Artificial Wrists: A Review of Prosthetic and Robotic Wrist Design

Neil M. Bajaj, *Student Member, IEEE*, Adam J. Spiers, *Member, IEEE*, and Aaron M. Dollar, *Senior Member, IEEE*

***Abstract*—The human wrist contributes greatly to the mobility of the arm/hand system, empowering dexterity and manipulation capabilities. However, both robotic and prosthetic research communities tend to favor the study and development of end-effectors/terminal devices (hands, grippers, etc.) over wrists. Wrists can improve manipulation capabilities, as they can orient the end-effector of a system without imparting significant translational motion. In this paper, we review the current state of the art of wrist devices, ranging from passive wrist prostheses to actuated robotic wrist devices. We focus on the mechanical design and kinematic arrangements of said devices and provide specifications when available.**

***Index Terms*—Amputee, commercial, design, mechanism, parallel, prosthetic, review, robot, serial, wrist.**

I. Introduction

THE spatial orientation of an end-effector such as a hand or a gripper is closely tied to its ability to perform a desired task, and nearly all robotic and prosthetic arms incorporate some type of wrist for this purpose. Yet both the academic and industrial research communities have tended to place more focus on hand/gripper development than that of wrist systems. Recent prosthetics investigations, however, have shown that increased dexterity in wrist prostheses may contribute more to manipulation capacity than a highly dexterous terminal device with limited wrist capability [1]. The role of the wrist becomes particularly significant when using a simple end-effector, or when an object fully constrains the fingers of the hand, such as during a cylindrical grasp.

The objective of this paper is to thoroughly review the design of artificial wrist devices in order to identify design strengths and trends, as well as suggest future directions for wrist development. We consider both prosthetic and robotic wrists in this review, as they share many of the same features. We characterize a prosthetic wrist as a unit that changes the orientation of a terminal device and is used by upper-limb amputees. In contrast, a robotic wrist is a device used in a nonhuman, robotic system to orient an end-effector. In many cases, the end-effector of a robot is a manipulation device, such as a robotic hand. However, orientation sensitive devices, such as tactile sensors or solar panels also feature often as end-effectors.

We focus on the mechanical design of the presented wrist devices, specifically: mobility in terms of degrees of freedom (DOF), kinematic architecture, actuation details, and physical design parameters when available. We examine both commercial devices and research prototypes.

In particular, we only consider devices that replace or create wrist function as opposed to those that augment it. Wrist exoskeletons fall into the latter category, as they support intact wrist capacity. As they are generally placed in parallel with the intact human wrist, these exoskeletons have different motion constraints and design requirements imparted on them that most standalone wrist designs do not. The design principles, requirements, and objectives within exoskeletons make them separate enough from standalone wrists to warrant their exclusion from this review.

Furthermore, we exclude works that only discuss the kinematic representation of a wrist from the review. While these representations are key for determining the workspace characteristics and singularities of (mostly parallel) mechanism, they do not fully address the physical implementation of the kinematic architecture into hardware. These kinematic representations generally do not address all the physical design issues, namely, size scale, weight, actuator selection, physical interference/collision of components, or passive joint limitations. These issues may in turn limit the application of a design due to torque, speed, weight/size, or range of motion requirements.

Very few previous reviews of wrist devices have been published. A preliminary version of this paper was published by the authors, covering only wrist prostheses [2], in which design trends, strengths, and deficiencies were identified. Otherwise, the only other published review is [3], which reviews the major advancements in wrist technology up to 1989, focusing primarily on devices utilized in industrial settings as well as some additional designs by the author. The inclusion criteria for this review are the following.

1) The wrist devices discussed herein must have been physically implemented.
2) Details regarding the actuation and kinematic arrangement must have been published in a refereed journal or

Manuscript received December 1, 2017; revised June 21, 2018; accepted July 10, 2018. Date of publication January 23, 2019; date of current version February 4, 2019. This paper was recommended for publication by Associate Editor M. O'Malley and Editor P. Dupont upon evaluation of the reviewers' comments. This work was supported by the U.S. Army Medical Research and Materiel Command under Contract W81XWH-15-C-0125. *(Corresponding author: Neil M. Bajaj.)*

The authors are with the Department of Mechanical Engineering and Materials Science, Yale University, New Haven, CT 06511 USA (e-mail: neil.bajaj@yale.edu; adam.spiers@yale.edu; aaron.dollar@yale.edu).

Color versions of one or more of the figures in this paper are available online at http://ieeexplore.ieee.org.

Digital Object Identifier 10.1109/TRO.2018.2865890

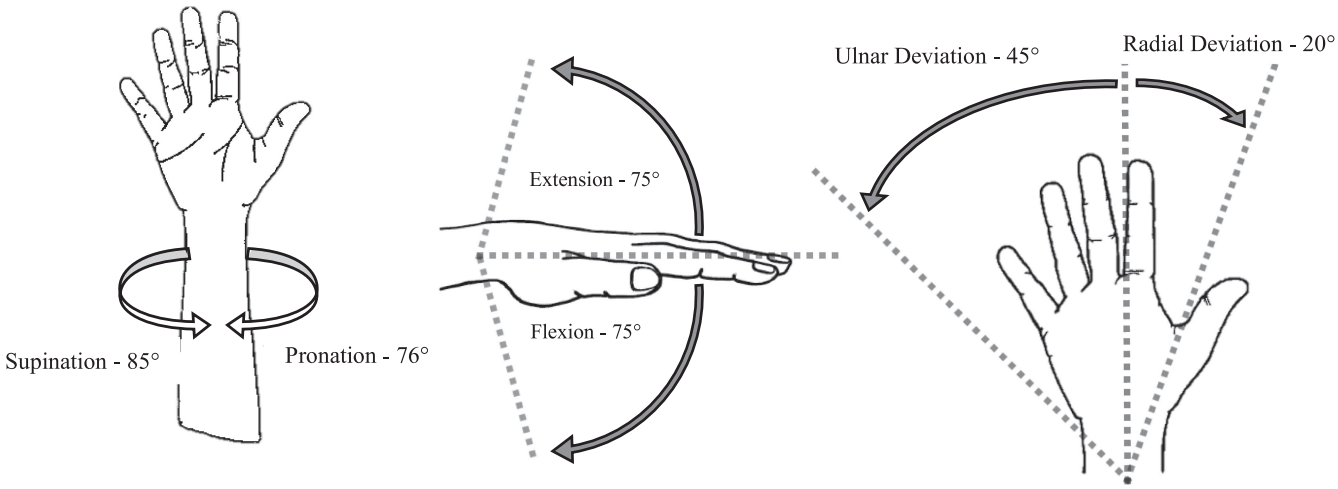

Fig. 1. DOFs of the human wrist and their ranges, shown from a neutral position. From left to right, pronation/supination, flexion/extension, and radial/ulnar deviation.

conference proceedings, patents, or within commercial product catalogs.

3) The devices must primarily impart rotational motion to the respective terminal devices or end-effectors.

We begin with an overview of human wrist biomechanics to provide a baseline of comparison for both prosthetic and robotic wrist devices. We subsequently introduce terminology relevant to the mechanical design of the devices regarding their topology and physical architecture. The following sections review wrist devices and their characteristics, organized by DOFs in the ascending order, then by mechanism type, and actuation method when appropriate. Physical specifications (such as weight, length, and torque) of the devices are provided when made available. Finally, we present the takeaways regarding wrist design as findings of the review.

II. Background

A. Human Wrist Capabilities

The healthy human wrist serves as an effective baseline toward which prosthetic wrists are designed, and a point of reference for which any orientation device may be considered. It is capable of motion in 3-DOFs, namely pronation/supination, flexion/extension, and radial/ulnar deviation. Each DOF is a paired set of motions, referring to positive and negative motion within each DOF. Henceforth, each DOF shall only be referred to by its positive direction of motion.

For an unaffected wrist, the maximal ranges of motion generally fall between 76°/85°, 75°/75°, and 20°/45° for pronation/supination, flexion/extension, and radial/ulnar deviation, respectively [4]–[6]. These DOF are coupled, meaning motion in one DOF may serve to limit the range of motion in the other two.

Healthy individuals only utilize a portion of each joint's full range of motion during activities of daily living (ADL). Investigations into these "functional" ranges of motion suggest that they fall between 65°/77°, 50°/70°, and 18°/40° for pronation/supination, flexion/extension, and radial/ulnar deviation, respectively [7]–[10]. The DOF and their ranges of motion can be seen in Fig. 1.

B. Wrist Terminology and Characteristics

In this section, we define relevant terminology for the review, which we use to both structure the review and discuss the individual devices.

1) Degrees of Freedom (DOFs): We primarily categorize the devices by the number of DOFs. Each DOF is defined (at least instantaneously) by rotation about an axis in space. An *n*-DOF wrist will typically have *n* linearly independent axes of rotation, except at any singular points in the workspace of the mechanism.

2) Mechanism Type: Depending on the kinematic arrangement of its joints and linkages, a mechanism may be classified as a serial, parallel, or hybrid mechanism.

A serial mechanism, or serial chain, consists of a sequential connection of joints and links, resulting in motion of the end-effector relative to the static base. The types of joints that comprise a serial chain are Revolute (R), Prismatic (P), Universal (U), and Spherical (S) joints. Each type of joint and their DOF are shown in Fig. 2. The human wrist may effectively be considered a serial RU chain, indicating it is kinematically equivalent to a universal joint (located at the carpal bones) in series with a revolute joint (within the forearm).

A parallel mechanism consists of two or more serial chains that connect a (generally fixed) common base to a mobile common platform. With respect to wrist deceives, the platform is usually the end-effector or terminal device. An example parallel mechanism, the S, 3SPS is shown in Fig. 3. The "3SPS" portion of the name indicates that there are three serial chains, all of which have a spherical, prismatic, and another spherical joint in series. The preceding "S" indicates there is another serial chain comprising solely of one spherical joint, though it is still in parallel with the other three SPS chains.

A hybrid mechanism is simply a chain of serial and parallel mechanisms. An example hybrid mechanism could be a 2DOF

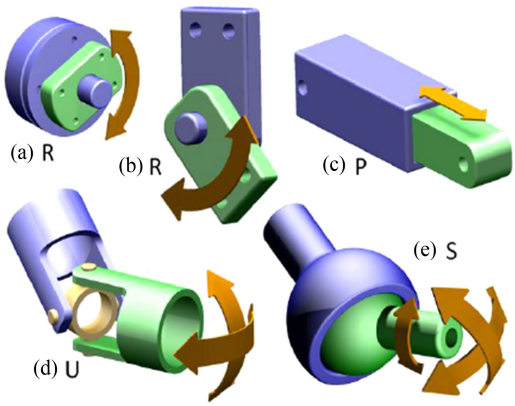

Fig. 2. Mechanical joint types and corresponding DOFs. (a) Revolute rotator (R). (b) Revolute flexor (R). (c) Prismatic (P). (d) Universal (U). (e) Spherical (S).

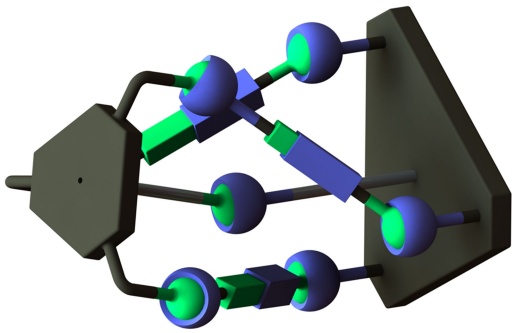

Fig. 3. S, 3-SPS parallel mechanism.

parallel mechanism that has a single revolute joint on the platform, allowing for "roll" motion of the end-effector.

3) Actuation Method: In the context of this review, a wrist may be passively, body powered, or actively actuated. This classification is useful mainly for prosthetic wrists, as neither passive nor body-powered wrists are used outside of prosthetics to our knowledge.

With passively actuated wrists, external forces and torques are used to reorient the end-effector. In prosthetics, such devices are usually manually articulated by the amputee user. They often use the opposite hand to twist or adjust their wrist device, but forces that arise due to manipulation may also reorient the wrist, though purposefully or unintentionally.

Body-powered prosthetic devices affect articulation by using motion and forces generated elsewhere on the body of the user. A typical arrangement involves a Bowden cable that connects a wrist or end-effector to a shoulder harness (or, more recently dermal anchor patches). As the user moves their shoulder relative to their arm, force is transmitted along the cable and results in prosthetic device articulation.

Actively actuated wrists utilize powered actuators to generate motion of the end-effector. These systems often feature electric motors, but may also be pneumatic or hydraulic systems. We consider a device to be actively actuated only if the actuator causes motion of the end-effector or terminal device. Thus, an active hand with a passive wrist would not be considered to be an active wrist.

C. Wrist Design Objectives

Though varied in design and appearance, most wrist devices seek to achieve similar objectives. Namely, devices should be designed to provide spherical rotational motion, meaning that the axes of rotation of a multi-DOF wrist should intersect, or the distance between axes should be minimized. Linear movements of the end-effector are generally accomplished via proximal joints in the arm system. Generally, weight and rotational inertia should be minimized as well, as wrists are often located near the distal end of the arm. Minimizing mass and inertia often involves minimization of the total size of the wrist (especially length along the forearm axis), although this objective is more critical in prosthetic and mobile robots than in industrial robots.

III. Single-DOF Wrists

We first begin the review by discussing single-DOF wrist units, then discuss 2- and 3-DOF devices within their own subsequent sections. Within these sections, we arrange the wrists by the mechanism type, and, when appropriate, by the articulation type as well.

A. Serial 1-DOF

A serial 1-DOF wrist is, by the definition of serial mechanism, a standalone revolute joint placed immediately proximal to the end-effector or terminal device. We may discuss these devices broadly as belonging to one of two categories: rotators and flexors. While kinematically equivalent as a single revolute joint, the wrists in these two categories often have differing packaging requirements, aspect ratios, and additional functionality.

1) Passive Serial 1-DOF: As discussed in Section III-C, both passive and body-powered mechanisms are used exclusively as prosthetic wrists. Thus, discussion of these two types of wrists, regardless of their DOFs, will be limited to prostheses, and not robotic applications. Discussions of active wrists shall cover both prosthetic and robotic wrist devices.

Passive single-DOF wrist prostheses have been the most common wrist devices for the past 75 years, mainly due to their compactness, mechanical simplicity, and low weight. These devices may broadly be separated into two categories, namely, rotators and flexors. Rotators serve to pronate or roll the terminal devices along the longitudinal forearm axis, whereas flexors will, as their name suggests, flex or pitch the terminal device.

Passive rotators, such as [11]–[21], are the first and more common of these two categories. To enhance their functionality, these devices often include additional features. One such device, the *Hosmer-Dorrance (HD) Friction Wrists* utilizes an adjustable clutch in order to hold the terminal device at any rotated position [11]. Other friction clutch rotators are described in [12] and [13]. Some rotators incorporate locking mechanisms [11], [15]–[17], which lock the terminal device at a discrete number of points until a latch or button is pressed, unlocking the device. One such wrist, the *OttoBock (OB) Ratchet Type*

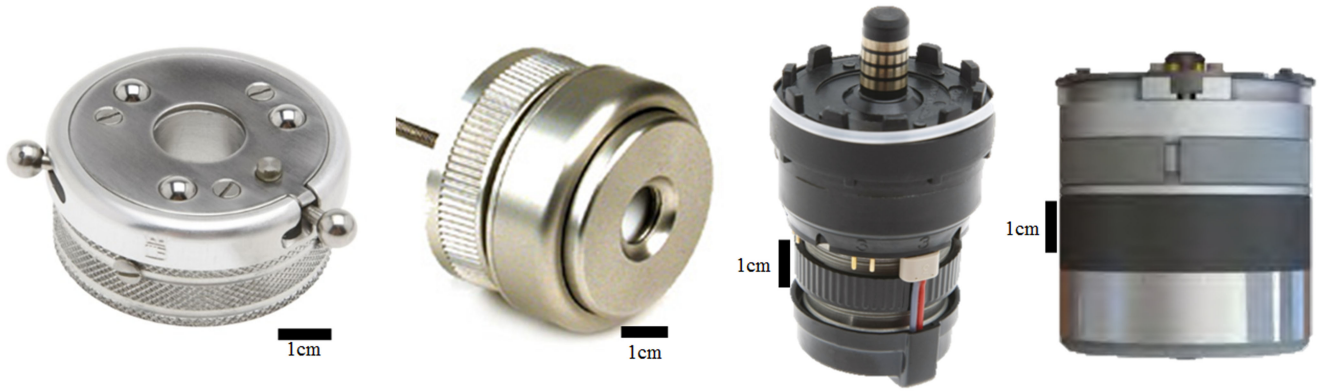

Fig. 4. Single-DOF prosthetic wrists. (a) OB Ratchet Type Rotation (R) [15]. (b) HD Rotation Wrist (R) [11]. (c) OB Electric Wrist Rotator [15]. (d) TB Supro Wrist. Size scales indicated by black bars are shown.

Rotation, can be seen in Fig. 4(a). Locking of passive wrist devices may also be achieved through the use of nonbackdriveable mechanisms, as in [19] and [20], in which the user must manually twist a collar on the wrist in order to rotate the terminal device. Further additional functionality may include the use of a "quick disconnect," allowing the users to easily switch their terminal devices [19]–[21].

Passive flexors, which are the second category of passive single-DOF wrists, are generally the devices which lock at discrete flexion intervals [11], [15], [22]–[24]. Commercially available locking flexion wrists include the *HD Sierra*, *HD Flexion Friction Wrist* [11], *OB MyoWrist Transcarpal* [22], [23], and the *OB MyoWrist 2Act* [15]. These devices usually may lock in 3–5 positions within their ranges of motion. Locking wrists of this nature are often used in concert with body-powered terminal devices, as the cable actuating the terminal device will not cause the wrist to change its position. For more continuous motion, the *OB Adapter with Flexion* [15] incorporates a frictional disk to hold the wrist in a flexed position, under limited loads. Though specifically integrated into the *i-Limb* series of prosthetic hands, the *Touch Bionics (TB) Flexion Wrist* [25] offers both locking in some flexed positions and offers spring loaded flexion while unlocked. Notably, the hydraulically actuated hand in [26] utilizes a check valve system to provide wrist flexion locking at an arbitrary position. Many flexor units are used in series with either active or passive rotators, allowing for 2-DOF motion.

All of the aforementioned passive rotators require external forces (from the user's other limb or environmental features) not only to rotate the terminal device, but also to access any additional functionality, such as locking or adjusting the friction within the clutches. This may be problematic for bilateral amputees, who will tend to experience greater difficulty in adjusting the passive wrists with a nonintact opposite arm.

2) Body-Powered Serial 1-DOF: To alleviate some of the issues of passive prostheses, body-powered prosthetic wrists employ a Bowden cable system to exert control over the wrist. As described in Section III, body-powered systems involve a body-harness-connected cable, which may either serve to actuate a prosthetic wrist or toggle a motion-locking mechanism. An example of a device actuated by body-powered cable is discussed in [27], which alternates between pronation and supination of the terminal device with subsequent cable pulls, locking when there is no tension on the cable. Alternatively, the *HD Rotation Wrist* [11] [see Fig. 4(b)] uses a cable to unlock and pronate the wrist. Pronation is resisted by a torsional spring, which tends to supinate the wrist. Releasing tension on the cable reengages the lock.

Some wrists which are considered passive in the context of this review use a Bowden cable system not to directly actuate the wrist, but to toggle or release locking mechanisms on passive joints. Devices such as the *OB Ratchet Type Rotation Series* [15] and the device detailed in [20] all utilize an elastic element for the wrist to return to a neutral pronation position when unlocked. As such, the user does not need to use their other hand to unlock the wrist.

3) Active Serial 1-DOF: Active 1-DOF wrists are often found in both prosthetic and robotic applications. Within the field of prosthetics, these are generally used with myoelectric (EMG) systems that enable a user to control rotation through muscle signals. Active wrists may be standalone units [15], [28] integrated into a prosthetic hand [29]–[32], or integrated into the forearm within larger prosthetic arms [33]. In robotics applications, single DOF units are commonly used but rarely discussed due to their simplistic nature. Similar to the passive wrists, active 1-DOF units may also be categorized into rotators and flexors.

Active rotators [15], [28]–[30], [32], [34]–[36] are the most common powered units in wrist prostheses. Standalone devices include the *Motion Control (MC) Electric Rotator* [28] and the *OB Wrist Rotator* [15] [see Fig. 4(c)], both of which have been designed for compatibility with many terminal devices, leading to relatively widespread use. The noncommercial standalone design described in [34] employs pronation about an axis skewed from the forearm longitudinal axis, with the authors claiming rotation about this axis leads to better manipulation performance when compared to other 1-DOF devices.

As powered rotators are much less compact than their passive counterparts (due to motor and drive train packaging), some rotators are incorporated directly into a terminal device in an

attempt to shorten the overall length of the prosthetic system. Both the *OB Michelangelo Hand* [30] and *TB i-Limb Quantum* [36] utilize compact rotators, namely *AxonRotation* and *SuproWrist* [see Fig. 4(d)], respectively, which fit within the prosthetic socket and lower palm of the respective hands. In [32], a small motor and a spur gear pair incorporated into the base of the hand are used to impart wrist rotation with few components. The MANUS Hand [29] utilizes an ultrasonic motor and a low reduction gear train to achieve compact packaging as well as a hollow channel to pass wiring from socket to hand through the wrist.

Active flexors also tend to be incorporated into existing robotic hand or terminal device systems. In both [33] and [31], the wrist flexion mechanism and rotary actuators are located within the body of the hands. In contrast, in [37], prismatic actuators responsible for flexion are located within the forearm of the robotic arm assembly.

B. Parallel 1-DOF

As single-DOF wrists are kinematically equivalent to a single rotational joint, parallel mechanisms generally are not used as single-DOF wrist devices. The mechanical simplicity of serial devices compared to parallel devices appears to outweigh potential benefits of using a single-DOF parallel mechanism, such as a four-bar linkage. However, single-DOF parallel mechanisms often find use in other devices, such as ankle prostheses. For example, in [38], a four-bar linkage with compression springs as links serves as a passive single-DOF ankle prosthesis. This device stores and releases energy in the compression springs to provide powered push-off during gait. A four-bar mechanism is also used in an active ankle prosthesis in [39], with an electric motor injecting power during gait. In both of these cases, the customizable kinematics and increased load bearing capacity of four-bar mechanisms were reasons for incorporating them over simple revolute joints. Single-DOF wrist prostheses with similar requirements may be suitable candidates for using 1-DOF parallel mechanisms in their design.

C. Single-DOF Wrist Discussion

The clearest theme within single-DOF wrists is that most of the devices are passive prostheses with serial mechanism architecture. As these have been the standard wrist prosthesis for the most of the last century, it is not surprising they are the most prevalent in this category.

Compared to their passive counterparts, active single-DOF wrists tend to incur significantly greater length in their designs, especially with rotators. By the content of this review, it may seem that active 1-DOF wrists are either standalone wrist prostheses or additional features in hand designs, but the commonality of 1-DOF units in all fields minimizes discussion on devices outside of these applications. Improvements to the torque production, strength, and compactness of active 1-DOF rotators will allow for increased manipulation capabilities for both amputees and mobile robots. These units currently do not match the capabilities of the human wrist in terms of torque production, strength, and compactness. This limits the manipulation capabilities of amputees as well as for robotic systems (e.g., mobile humanoid robots).

IV. 2-DOF Wrists

Unlike single-DOF wrists, 2-DOF devices not only include prosthetic wrists, (including those proposed in academic environments), but wrists used in robotic applications, such as solar panel and camera orientation, as well.

A. Serial 2-DOF

There are only two combinations of serial wrist mechanisms resulting in 2-DOF rotational motion, namely, revolute-revolute (RR) chains or universal (U) joints (see Fig. 2). Both are employed regularly to achieve 2-DOF rotational motion.

1) Passive Serial 2-DOF: While not as common as single-DOF passive wrist prostheses, there exists a variety of passively articulated, commercially available 2-DOF wrists. Many of these devices [40], [41] consist of a flexor unit in series with a rotator, forming a U joint. One such device, the *OB RoboWrist* [40], provides simultaneously lockable pronation and flexion, and while unlocked, provides frictional resistance against motion that can be adjusted by turning a collar on the wrist. The *MC Flexion Wrist* [41] similarly consists of a lockable pronation and flexion mechanism, but utilizes elastic elements to bias the wrist to a neutral position when unlocked. The *HD Four-Function* [11] wrist is a serial combination of the *HD Rotation Wrist* and *HD Sierra Wrist*, incorporating both body powered and locking functionality.

Other commercial wrist prostheses opt for a simpler and more compact design by using a constrained spherical joint to achieve passive 2-DOF motion. In both the *OB Myolino* [15] [see Fig. 5(a)] and *Liberating Technologies OmniWrist* [42], a circumferential groove around ball is constrained with a pin, thus only allowing flexion and radial deviation. Set screws around the circumference of the socket are used to adjust the amount of friction on the joint, allowing for greater torque resistance.

Noncommercial 2-DOF devices are detailed in [43] and [44]. In [43], two lockable single-DOF units are stacked with axes of rotation orthogonal (but nonintersecting) to one another, resulting in a relatively long resultant wrist. To achieve more length reduction, the wrist design in [44] [see Fig. 5(b)] uses a bevel gear differential with elastic elements connected to the input gears. This arrangement achieves flexion and radial deviation with spring return. Additionally, this wrist actively switches between two stiffness levels, allowing for different types of manipulation to occur.

Passive 2-DOF wrists also may be found integrated into some prosthetic hand designs [45], [46]. In [45], the mechanism that attaches the hand to the prosthetic socket comprises two revolute joints with intersecting axes, but the geometry of the hand and near-parallel orientation of the axes appear to limit the wrist to virtually 1-DOF motion. In [46], a universal joint serves as a 2-DOF wrist, but also as a means to transmit power from a motor in the forearm to a grasping mechanism in the hand.

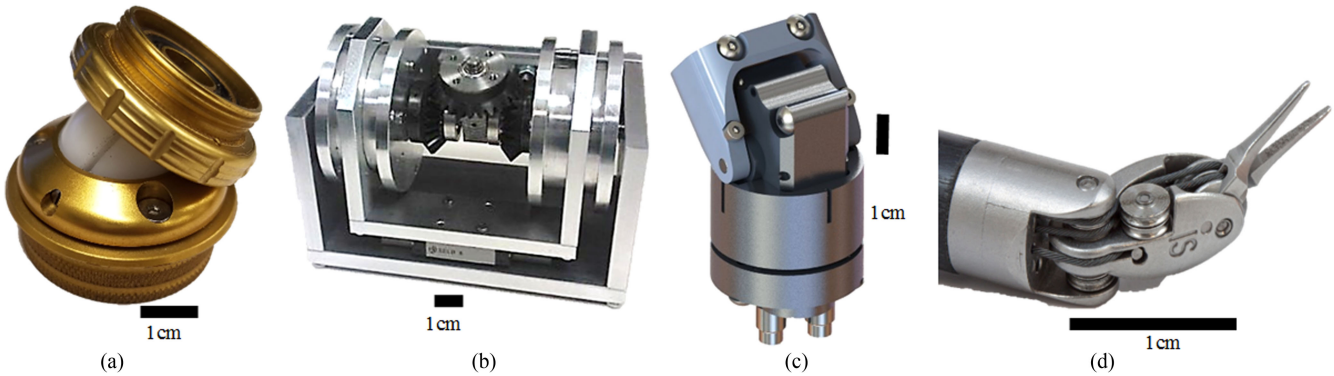

Fig. 5. Serial 2-DOF prosthetic and robotic wrists. (a) OB Myolino (U) [15]. (b) Montagnani switchable stiffness wrist (RR) [44]. (c) Verleg Hydraulic Wrist Prosthesis (RR) [61]. (d) Intuitive Surgical EndoWrist with forceps (RR) [70]. Size scales indicated by black bars are shown.

2) Body-Powered Serial 2-DOF: Due to the nature of tendon-driven systems, body-powered devices become less practical as the number of DOFs in the prosthetic system increases. Namely, each actuated DOF requires at least one tendon. Thus, in [47], two cables are routed into the wrist prosthesis to separately lock/unlock and control pronation and flexion of the wrist. Additional cables require more harnessing as well as a corresponding unique motion to "select" and apply tension to a particular cable. This leads to unwieldly systems that may sacrifice actuation of other DOF (such as the opening and closing of a terminal device).

3) Active Serial 2-DOF: Active serial 2-DOF wrists are the point at which prosthetic and robotic systems begin to overlap. Similar designs may be employed between transradial/transhumeral prostheses and the arms of humanoid robots.

Like passive 2-DOF wrists, some active designs simply place two active 1-DOF units in series with one another. Prosthetic wrists, such as [48]–[51], are composed of a pronation and a flexion unit placed together in this way. In [48], two motors are placed directly next to each other within the forearm volume, and use slightly different gearing systems to actuate their DOFs (internal ring gear versus bevel gear). In [49], however, the flexion motor is placed directly on the top of the pronation motor, resulting in an uncomplicated yet large design, occupying the forearm volume. Notably, this wrist could generate torques comparable to that of a healthy adult, though achievable speeds were not discussed.

As 2-DOF motion cannot fully replicate the capabilities of the human wrist, some wrist designs [52], [53] have implemented coupling between the flexion and radial deviation DOFs. In [52], motion statistics during ADLs were used to determine which axis (perpendicular to the pronation axis) was used most often. The subsequently proposed wrist design proposed implements a pronation unit with the coupled flexion/deviation axis in series, with the coupled axis 35° from the nominal flexion axis. Similarly, the forearm portion of the notable *DEKA Arm* [53] prosthesis uses coupled flexion/deviation in series with a powered pronation unit, presumably for similar reasons as in [52]. The designs of both of these wrists are indicative of the tradeoff between the mechanical complexity and anthropomorphic motion.

The *RIC Arm* [54], a research transhumeral prosthesis designed to be within the form factor of a 25th percentile female arm, makes use of orthogonal cycloidal drives housed within the forearm to impart pronation and flexion to the terminal device. The *ToMPAW* [55], a research device designed to be a modular prosthetics testing platform (especially for myoelectric control systems), utilizes a similar pronation and flexion configuration.

The arms of humanoid robots are often similar to transhumeral prostheses, though their applications may determine size and additional functionality required in their design. One such example, the "table-top" sized *NAO humanoid* [56], [57], produced by SoftBank Robotics, is designed to mimic human motion and gesturing, but must accomplish these goals in a much smaller package. It achieves pronation and wrist flexion using micromotors and high reduction gear stages. Alternatively, the DLR TORO humanoid features an arm design [58] similar in size to the human arm, as its primary applications are related to manipulation tasks. The wrist of this robot consists of the pronation and flexion units in series with one another. As compliant manipulation is a particular application of this robot, both DOFs were designed to be variable stiffness actuators, and thus employ two motors each (to control both position and stiffness at each joint).

In order to eliminate the necessity of a constant holding torque, the wrists in [59] and [60] use worm gearing in their pronation and flexion mechanisms, rendering both DOFs in each wrists nonbackdriveable. Moreover, as these are both transhumeral prostheses, the wrist actuation motors occupy the forearm volume.

To reduce weight or mechanical complexity of wrist designs, some systems employ hydraulic [61] [see Fig. 5(c)] or pneumatic [62] actuation. Though these may achieve the aforementioned goals, additional reservoir systems, pumps, or compressors are needed in tandem with these devices, leading to additional equipment that must be transported by the user.

Constrained S joints may be used for powered 2-DOF motion. One such example is the *RSL Steeper BeBionic Wrist* [63], which constrains motion of 2-DOFs of the spherical joint at any instant via another pin-and-groove system (similar to the *OB Myolino* [15]). The unconstrained DOF is actuated by a single motor,

and via a button press, may be changed from flexion to radial deviation by the user.

In [64], a bevel gear differential is used to create a wrist with pronation and flexion motors placed obliquely to the forearm longitudinal axis. While this design places more mass distally, the compact design occupies less forearm volume, making it more suitable for amputees with distal amputations. A similar differential design is employed in the transradial prosthesis design of [65], though motors are placed within the forearm volume and a tendon drive is used to actuate the input bevel gears. In both of these cases, both motors may contribute to actuate the same DOF, potentially allowing for greater mechanical power input to each DOF, though only actuated one at a time.

Other tendon-driven serial 2-DOF wrists have been designed for a variety of applications, such as transradial prostheses [66], [67], anthropomorphic robotic arms [68], surgical robots [69]–[71], and solar tracking systems [72].

The wrist of the transradial prosthesis in [66] utilizes Bowden cables to actuated a constrained S joint (resulting in a U joint). Though three motors were required for 2-DOF actuation, the motor could be placed in a way to reduce loads on the elbow or outside the forearm (due to the use of Bowden cables).

Similar to transradial prostheses, anthropomorphic robotic hands attempt to replicate the capabilities and appearance of the human hand. The anthropomorphic University of Bologna IV hand (UB-Hand IV) [68] contains a wrist composed of two R joints offset by a small distance with perpendicular axes, with each R joint driven by an antagonistic tendon pair. Tendons that actuate the hand pass through channels in line with the wrist axis, causing no net torque on the wrist due to hand actuation.

The tendon-driven surgical robotic wrists in [69]–[71] are examples of the *EndoWrist* instruments [see Fig. 5(d)] for use with the *da Vinci* surgical system produced by *Intuitive Surgical*. In [69], a coupled tendon drive actuates both the pitch and the yaw of the surgical wrist device, with the tendons routed through extruded channels on the surface of the wrist. Friction is potentially reduced in [70], in which pulleys are used for tendon routing, though the same tendon coupling scheme is used. In [71], slight modifications are implemented to the wrist design of [70] to allow for the tool distal to the wrist to be exchanged. As these wrists are intended to be used in a laparoscopic surgery, these wrists must be rather compact. Utilizing a tendon drive system allows for the actuators to be placed in a separate housing away from the wrist, and the tendons routed to the wrist through a long shaft, thus the wrist need only be large enough to route tendons. However, the size and drive system make these wrist devices exceedingly prone to friction and wear, thus requiring replacement after one to ten operations [73].

The solar tracking system in [72] utilizes two tendon drive systems to actuate the DOFs of a U joint, allowing a solar panel to track the sun optimally. Motors with pulleys route and actuate the tendons, and each tendon attaches to the panel underside on each end via a tension spring, maintaining tensegrity even when the panel is buffeted by the wind.

B. Parallel 2-DOF

Excluding planar linkages, much of parallel mechanism research and design focuses on creating mechanisms with two or more DOFs. When these mechanisms are nonplanar, either by implementing 3-DOF translational motion or 2-DOF rotational motion, these mechanisms may be called spatial linkages.

The subsequently presented parallel mechanisms are all active devices. While it is likely passive parallel mechanisms find their uses in other cases, within wrist devices, only active wrists appear to have incorporated such mechanisms.

1) Active Parallel 2-DOF: To achieve 2-DOF rotational motion in a parallel mechanism, a passive U joint may be placed in parallel with multiple actuated legs with different joint topologies. The passive U joint constrains the motion of the actuated legs, which are often higher DOF serial linkages with one actuator each. This approach is implemented in wrists used in a variety of applications [74]–[77].

The wrists of the *NASA Robonaut 2* humanoid robot [74] utilize a U, 2PSU parallel mechanism. The U joint connects the hand to the forearm of the robot, and the PSU linkages, via P joint actuation, differentially actuate flexion and radial deviation. In [75], the same mechanism architecture is used in a solar tracking system. The workspaces, packaging constraints, and optimization goals are different between the two applications of this mechanism; thus, the geometry of these mechanisms varies quite largely. A similar mechanism is described for the use for endoscopic surgery in [76], though this instance employs 3 PSU linkages in parallel with the central U joint. Though [76] is a 2 DOF system, all three P joints are actuated, thus resulting in redundant actuation. While this may improve load bearing properties, the actuators must be carefully coordinated to result in permittable motion. All of these mechanisms impart flexion and radial deviation to their respective end-effectors.

The mechanism detailed in [77] is a U, 2RRR configuration [see Fig. 6(a)]. The platform and the base are coupled with a passive U joint, and the two RRR legs actuate the two DOF via rotary motors that drive the most proximal R joints. The axes of the R joints in the legs intersect the center of rotation of the U joint, theoretically making this a spherical mechanism. In such configurations, every component rotates about the same fixed center of rotation.

Other 2-DOF spherical mechanisms include [78]–[80]. As these are only 2-DOF mechanisms, they do not truly recreate full spherical motion. In [78], a five-bar linkage consisting of only R joints is used to preposition a camera for endoscopic surgery. As before, the revolute joints all point toward a common center of rotation, which results in all links of the mechanism being constrained to move on virtual spherical surfaces. As none of the links pass through the center of rotation, the camera may be placed such that it only undergoes rotational motion with no translation. In [79], an overconstrained, singularity free, six-bar mechanism (also utilizing only R joints with center-pointing axes) is designed to have a hemisphere of reachable workspace. However, to avoid link interference, some links use circular tracks and sliders instead of simple pin joints to create R joints, resulting in considerably more friction in the mechanism.

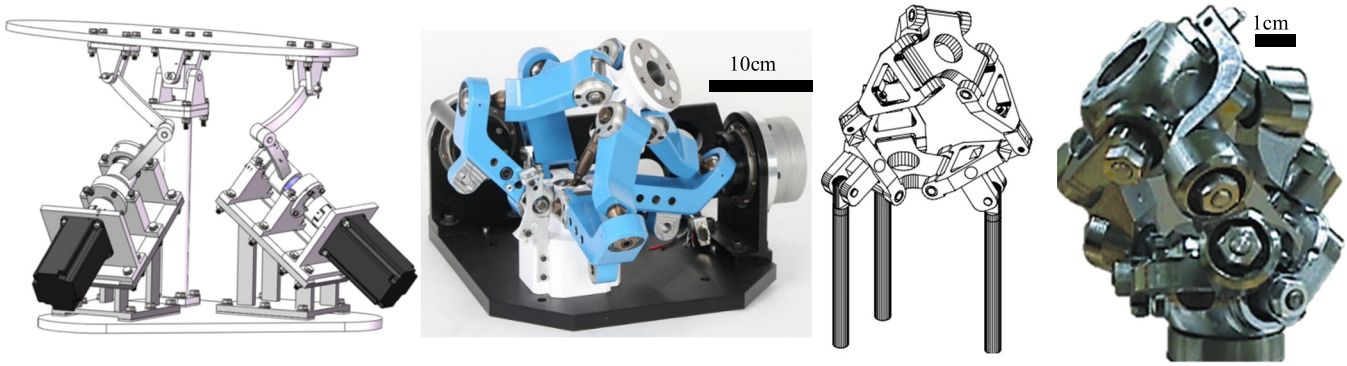

Fig. 6. Parallel 2-DOF robotic wrists. (a) Duan parallel mechanism (U, 2RRR) [77]. (b) Rosheim Omni-Wrist VI (SS, 4RSR) [82]. (c) Canfield Carpal Robot Wrist (3RSR) [83]. (d) Sone High Angle Active Link (3RRRR) [81]. Size scales indicated by black bars are shown when known.

The wrist described in [80] uses two spherical cam-roller systems in parallel to control pitch and roll of the end-effector. The geometric complexity of the cams, rollers, and other elements to support these components in this mechanism makes its fabrication quite difficult, with the spherical cams milled on a five-axis computer numerical control machine.

A design that includes only R joints, but is neither a spherical mechanism nor a single closed-loop linkage, is described in [81] [see Fig. 6(d)] capable of hemispheric pitch and yaw motion. This design uses a 3RRRR mechanism, where two of the three base R joints are actuated and the third is passive. The lower six R joints have a common center of rotation, as do the upper six (as the mechanism is symmetric from base to platform), resulting in two spherical mechanisms in series with one another. The mechanism is designed to be used as a constant-velocity joint for optical applications, though it also appears to be a 2-DOF orientation unit in its own right.

The *Omni Wrist (OW)* series [82] by Rosheim is a series of singularity free, hemispherical workspace wrist devices using similar parallel kinematic structures. The *OW V* and *OW VI* [see Fig. 6(b)] employ an SS, 3RSR and an SS, 4RSR structure, respectively. In both cases, the central SS chain constrains the platform to the surface of a virtual sphere, and two of the base R joints are actuated for active pitch and yaw motion. Careful kinematic design allows the S joints in the RSR chains to only utilize a small portion of their ranges of motion. Between, the two mechanisms, the OW VI, utilizing four RSR legs, may loosely have better load bearing properties.

Similar to both of the aforementioned designs is the Carpal Robot Wrist [83] [see Fig. 6(c)], which employs a 3RSR structure. Though this mechanism nominally has a third translational DOF, it may be constrained through the use of an SS chain in the center as well. Notably, this mechanism uses three intersecting pinned R joints to implement the S joints in the RSR chains, leading to a much greater workspace of the S joint, as the ball and socket constraints are removed. This is particularly useful if the translational motion is desired.

A variety of other 2-DOF parallel wrist units are designed for a variety of applications for specific functionality. In [84], a solar tracking mechanism using a PU, PUR architecture capable of pitch and yaw motion is described. The actuated P joints lie against the ground and offer nonbackdrivability and high force transmission with a low profile, all of which are desirable characteristics in solar power applications.

The 2-DOF wrist described in [85] uses two slider crank mechanisms in parallel, connected with a universal joint, to impart flexion and radial deviation to a humanoid robot wrist. In both the slider cranks, the sliders are linear series elastic actuators, which allows the wrist to be position or torque controlled. The *RoboRay* wrist [86] implements a flexion and radial deviation wrist using a U, 2PUR mechanism. The central U joint's flexion axis is designed with pulleys, routing tendons from the forearm to the hands for finger actuation This approach compensates for tendon length changes passively due to wrist motion, though the mechanism does twist individual tendons, which may result in wear or failure.

C. Hybrid 2-DOF

By the definition of hybrid mechanisms, hybrid 2-DOF wrists consist solely of a single DOF rotator in series with a 1-DOF parallel mechanism. Only active hybrid mechanisms were found, thus passive and body-powered sections shall be omitted.

1) Active Hybrid 2-DOF: The two hybrid 2-DOF mechanisms described subsequently [87], [88] are both incorporated into transradial prostheses. The SVEN Hand [87] was one of the earliest actuated transradial prostheses and actuated hands. It utilizes a rotator placed in series with a four-bar linkage that actuates flexion. Alternatively, the wrist described in [88] consists of a four-bar linkage, actuating a plate to impart flexion. Within the plate, a linearly actuated rack drives a pinion to impart pronation to the end-effector.

D. 2-DOF Wrist Discussion

Serial 2-DOF wrists are applied across a variety of applications. No single actuation system appears to be most successful within these wrists, though many have individual features particularly useful for their applications.

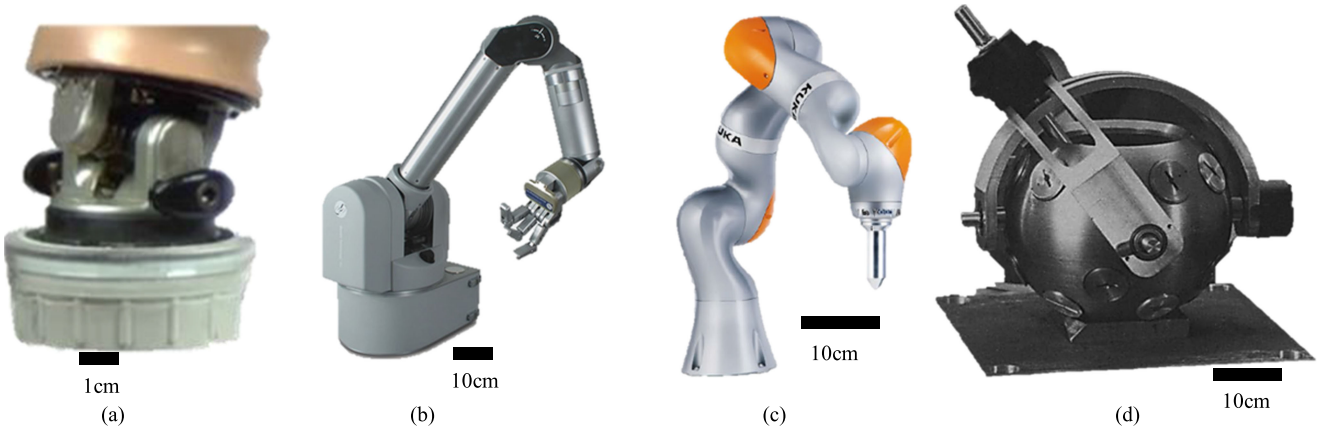

Fig. 7. Serial 3-DOF wrists. (a) MC MultiFlex (RU) [89]. (b) Barrett WAM Arm (RRR) [98]. (c) Kuka LBR iiwa (RRR) [106]. (d) Chirikjian Spherical Stepper Motor (S) [112]. Size scales are indicated by black bars.

The majority of 2-DOF passive prostheses have only been available for the relatively recent past. Elastic bias [41], [44], frictional [15], [42], or continuous locking mechanisms are included in these devices more often than their 1-DOF counterparts, potentially better enabling manipulation with the prosthetic hand.

As active wrist prostheses are not often able to match the torque production capacity of the human wrist, differential mechanisms [64], [65] allowing synergistic actuation of a single DOF can result in higher torque production in a small package. The tradeoff between size and torque-production/robustness is the biggest challenge to address in these devices. Though a wrist may be able to achieve human torque levels [49], it cannot do so without occupying a larger volume than the human wrist and significant portion of the forearm. On the other hand, when compactness is required, such as in the NAO humanoid [56] or minimally invasive surgical robots, both fabrication difficulty and fragility of the devices increase significantly. Some compromise between weight/size savings and strength can be achieved by using hydraulic [61] or pneumatic [62] actuation, although these systems come with the separate considerations and issues of additional hardware requirements, such as reservoirs and pumps.

Parallel 2-DOF wrists employ a variety of different types of designs. Constraining the end-effector with a passive U joint circumvents the necessity of having a purely spherical mechanism and allows more freedom in addressing the other issues common with parallel mechanisms, such as joint limits and singularity. Moreover, many of these devices can achieve large singularity free workspaces [74], [75], [81], [82], [84].

V. 3-DOF Wrists

Wrist designs capable of 3-DOF rotational motion can arbitrarily orient their end-effectors (up to a workspace limit). While the human wrist is naturally capable of 3-DOF motion, some of the subsequently described wrists outperform the human wrist in some aspects, such as range of motion or torque output, but generally not size or compactness.

A. Serial 3-DOF

Serial 3-DOF wrist devices are prevalent in robotic applications, though some prosthetics incorporate 3-DOF wrists into their designs. As no 3-DOF body-powered wrists were found, we shall not dedicate a subsection to them.

1) Passive Serial 3-DOF: Few 3-DOF passive wrists exist outside of those that are simply combinations of off-the-shelf 1-DOF prosthetic wrist units, which were described in Section IV-A-1. However, the *MC Multiflex* [89] [see Fig. 7(a)] uses a 1-DOF rotator in series with an elastically biased U joint, forming an RU chain. The design is similar to the MC *Flexion Wrist* [41], described in Section V-A-1, though incorporating the third DOF (radial deviation) into the *Multiflex* only results in a 6 mm length increase compared to the *Flexion Wrist*.

The prosthetic hand described in [90] employs a passive S joint as a wrist in its design. The S joint is a simple ball and socket design, though the ball has a channel running through it, allowing tendons to pass from the forearm to the hand. The encapsulation required for the ball and socket joint restricts the range of motion, and as the wrist cannot be locked, manipulation may be difficult due to instability without high friction in the joint. Passing the tendons through the center of the ball does decrease their respective torques on the wrist, however.

2) Active Serial 3-DOF: The most common approach for achieving 3-DOF active motion is by arranging active rotators in series, with axes at different orientations. This approach is used within both prosthetics and robotics. The Modular Prosthetic Limb [91], designed by the Johns Hopkins University's Applied Physics Laboratory, uses a rotator located proximally to pronate, and two identical motorized units placed in series with a 90° offset between the two for flexion and deviation. The same approach is used in the Osaka City University Hand [92].

The serial RRR approach is exceedingly common within industrial robot arm applications. Many commercially available industrial arms, such as the *Kuka KR-16* [93], *Kawasaki K-Series* [94], *Fanuc M Series* [95], *Durr EcoPaint* [96], *Hon Hai / Foxconn* robot arms [97], and *Barrett WAM* [98] [see Fig. 7(b)], utilize the roll-pitch-roll arrangement for their wrist design. The axes of the three joints intersect at a common point, allowing for

spherical end-effector motion, and for the more proximal joints of the robot arms to provide translational movements decoupled from the spherical wrist motion. This design often results in a singularity at the zero position, when the two "roll" axes are collinear. However, the range of motion and flexibility in packaging constraints (roll motors and gear train can be placed away from the center of rotation) make this configuration appealing and suitable for industrial arms. It is worth noting that the pitch and one of the roll DOFs within these arms are often actuated via a bevel gear differential, which allows motors to be placed along the longitudinal direction of the wrist, saving space and potentially reducing rotational inertia.

The roll-pitch-roll design is also used in humanoid robots [99], [100], robotic arms for satellite servicing [101], and in surgical robotic wrists [102].

Instead of using a second inline roll joint, some wrist designs achieve 3-DOF motion via a roll-pitch-yaw configuration. In this case, the yaw axis is perpendicular to both the roll and pitch axes and would correspond to radial deviation in the human wrist. When the yaw axis intersects the pitch and roll axes, the mechanism is generally considered a spherical wrist, and could be considered an RU chain. This architecture is used in surgical robots, such as the *DLR Mirosurge* [103] and in some of the *EndoWrist Instruments* by *Intuitive Surgical* [104], [105], all of which use tendon-driven systems for actuation due to packaging constraints (merits and disadvantages common of tendon-driven surgical wrists systems were discussed in Section V-A-3). Compared to roll-pitch-roll wrists, the relative workspaces of roll-pitch-yaw wrists tend to be smaller due to geometric constraints, as the pitch and yaw joints cannot usually achieve 360° rotation without physically colliding with other parts of the wrist. The same issue can be seen with two-yoke universal joints [see Fig. 2(d)], which can be described as pitch-yaw devices. Some robotic arms, such as the *Kuka LBR iiwa* [106] [see Fig. 7(c)] alleviate this issue by not using the dual-yoke type of geometry, and only constrain the R joints on a single side. The resulting geometry looks much like a roll-pitch-roll wrist with the pitch joint at 90°, which is considered the neutral position of the wrist. This allows for a larger range of motion while potentially sacrificing strength or payload.

Besides surgical and industrial arms, roll-pitch-yaw wrists are often used in humanoid or anthropomorphic robotic arms due to their resemblance to the human wrist. The *ARMAR III* humanoid [107] as well as the anthropomorphic arm described in [108] utilizes direct drive to actuate the pronation (roll) DOF, and two tendon drives actuated via ball screws to actuate the universal joint at the wrist for flexion and radial deviation (pitch and yaw, respectively). The *Humanoid Robot Prototype HRP-4* [109] utilizes a servo motor and harmonic drive in each of its three wrist DOF, and use a belt system to ensure the axes all intersect despite the motors being placed serially. In [110], McKibben actuators are used to actuate each DOF of an RU wrist mechanism of an anthropomorphic arm, reducing the mass and rotational inertia of the arm, though requiring an air compressor.

An interesting RU mechanism that uses slotted disks is implemented in the hand/wrist system described in [111]. A motor and an internal ring gear pronate the distal end of the forearm, which houses the flexion, radial deviation, and hand actuators. An S joint with a pin protruding radially is actuated by two disks: one with a spiral track cut into it, and the other with a simple diametric track. The pin is constrained to lie in the track of both disks, which are stacked upon one another. By rotating the disks either in opposition or together, the wrist is flexed or radially deviated, respectively.

Some serial wrist designs opt to use a single spherical joint instead of a serial chain [112]–[114]. Spherical stepper motors are described in both [112], [113] [see Fig. 7(d)]. While the overall geometry is that of a ball and socket joint, the ball is actually the rotor and the socket is the stator. The ball is impregnated with permanent magnets, and the socket houses a plurality of electromagnet windings, thus no wires cross the joint. Activating the electromagnets in different configurations and sequences results in rotation of the ball about different axes. Using a more traditional approach, the prosthetic wrist detailed in [114] actuates a spherical joint with five equally spaced tendons connecting to its platform. As tendons are only capable of exerting tension, the authors determined that at least five were necessary to actuate the 3-DOF joint.

B. Parallel 3-DOF

Parallel 3-DOF motions are capable of exhibiting fully spherical motion, though some mechanisms are cable of coupled translation with 3-DOF rotation. Moreover, these mechanisms are all active devices, so passive and body-powered subsections shall be omitted.

1) Active Parallel 3-DOF: Of all purely rotational parallel mechanisms, the most well known is the *Agile Eye* [115] [see Fig. 8(a)]. This mechanism, designed for camera orientation, is a symmetric 3RRR mechanism, with base R joints actuated with rotary motors. As all of the R joint axes must intersect at a central point, high precision is necessary in both fabrication and assembly of the Agile Eye. However, the Agile Eye remains a point of inspiration for 3-DOF spherical mechanisms.

A mechanism that uses similar architecture to the Agile Eye is the *Spherical Haptic Device* [116], hereon known as *SHaDe*, is a 2RRR, RRRU spherical mechanism designed to be used as a haptic feedback tool for spherical MC. The RRRU leg is used in place of an RRR chain to allow for a larger unobstructed volume between the base and platform of the mechanism. This allows the user to operate *SHaDe* over a large range of motion without their hand contacting any of the legs of the mechanism.

Though the *Agile Eye* has a large pitch and yaw workspace, roll capability is small in comparison. To achieve continuous rotation, a 3RRR, RUR mechanism was designed and described in [117]. This mechanism essentially consists of the standard Agile Eye design with an additional RUR mechanism running centrally from the base to the platform with actuation at the base R joint. The platform contained a bearing in which the distal R joint was housed, thus the 3RRR portion of the mechanism resulted in redundant actuation. Torsional movement was achieved by rotating the U joint, allowing for continuous rotation up to certain angular limits dictated by the U joint.

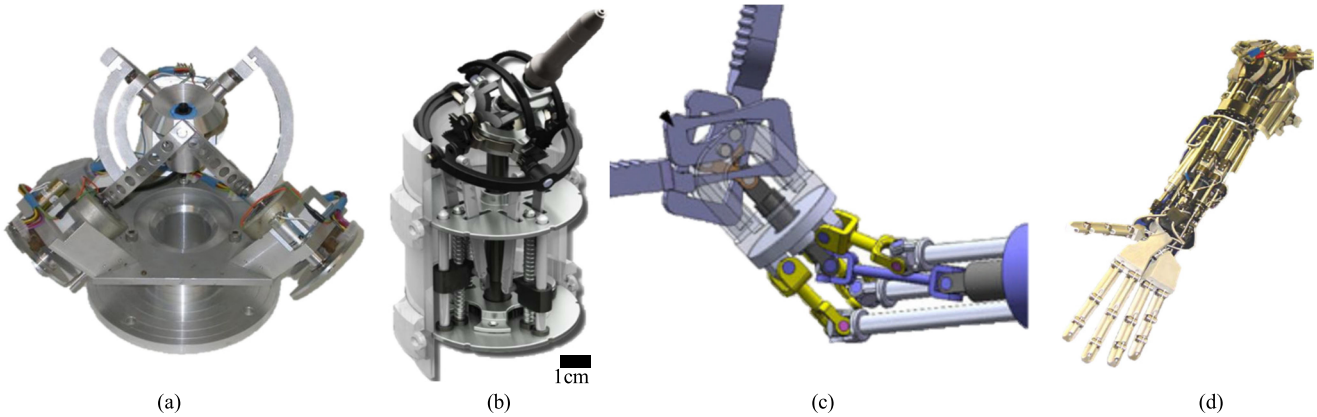

Fig. 8. Parallel and hybrid 3-DOF mechanisms. (a) Agile Eye (3RRR) [115]. (b) Hammond Micromanipulation Wrist (2PRRU, RUUR) [122]. (c) Hong Surgical Wrist and instrument (3PSR, RUUR) [121]. (d) Vanderbilt Gas Actuated Arm Prosthesis (Hybrid: [R][RPR, SPS]) [123]. Size scales indicated by black bars are shown when known.

To address the difficulty in precision fabrication of the Agile Eye, the *Agile Wrist* [118] was designed, employing a 3RRRP architecture. In this mechanism, the revolute joint axes are not required to intersect exactly at the center of rotation, and the addition of a passive prismatic joint prevents the mechanism from becoming overconstrained if intersection does not occur. Though the motion of the end-effector is not perfectly spherical, the spatial displacements apply small contributions to the overall platform pose.

Another mechanism that attempted to simplify the manufacturing issues of the Agile Eye while still only allowing spherical motion is *Argos* [119]. Argos is nominally a 3RRRS mechanism, with the base R joints actuated via rotary motors. However, the second and third R joints in each of the legs are implemented via a steel cable pantograph mechanism. As a result, each of the legs is a planar mechanism, simplifying the fabrication process, and the combination of the three legs then fully constrains the platform. Argos is suggested to be the rotational equivalent of the translational Delta parallel robot [120].

A spatial mechanism intended for use in minimally invasive surgery is described in [121] [see Fig. 8(c)]. The wrist described therein uses a 3PSR, RUUR parallel architecture, in which the P joints and the base R joint are actuated. While the 3PSR portion of the mechanism can accomplish 3-DOF motion, the central RUUR constrains the motion and enables roll of the end-effector, as the distal R joint sits in a bearing.

A wrist meant for micromanipulation is detailed in [122] [see Fig. 8(b)]. The architecture is a 2PRRU, RUUR. Similar to the previously described wrist, the RUUR provides unlimited roll motion to the end-effector. The 2PRRU mechanism actuates an intermediate platform, coupled to the distal platform with a rolling gear pair for each leg. This results in the distal platform having twice the pitch and yaw of the intermediate platform.

C. Hybrid 3-DOF

Hybrid 3-DOF mechanisms generally use a 2-DOF parallel mechanism in series with a rotator, either proximal or distal to the 2-DOF orientation mechanism. Once again, we limit the discussion to solely active mechanisms for the same reasons stated previously.

1) Active Hybrid 3-DOF: Hybrid mechanisms wrists incorporated in transradial prostheses [123]–[125] all consist of a pronation mechanism in series with a 2-DOF flexion and radial deviation mechanism. In [123] [see Fig. 8(d)], the pronation mechanism is driven via pneumatic actuation of a lead-screw against a slotted cylinder. The flexion and radial deviation mechanism employs a U, RPR, SPS configuration. The prismatic joints are pneumatically actuated, and all actuators are placed near the elbow. Alternatively, in [124], the pronation mechanism, a simple rotator, is placed distal to the 2-DOF flexion/radial deviation device, which uses an SS, 2RPU mechanism.

The surgical wrist robot detailed in [126] uses a spherical five-bar mechanism to actuate pitch and yaw motion, and a rotary motor with a center pointing axis rolls the end-effector.

D. 3-DOF Wrist Discussion

Perhaps most striking observation regarding 3-DOF wrists is the similarities in architecture and even physical design between devices. Robots across all applications utilize a roll-pitch-roll configuration due to the simple design and high range of motion. As evidenced by the industrial arms, roll-pitch-roll and roll-pitch-yaw systems can be used in high load applications, despite their serial construction.

As serial 3-DOF wrists are often part of larger arm systems, it is a priority for actuators to be far from the wrist, and as proximal to the elbow as possible. This can be accomplished simply through tendon systems, as in [102], [105], [107], and [108]. However, these systems are far weaker than the standard transmission counterparts, such as gear and belt drives. A trade-off clearly exists between the actuator placement flexibility and torque production capabilities.

The 3-DOF parallel mechanisms previously presented appear to belong to two groups: namely, those that utilize a central passive constraining joint (universal or spherical) which has lower mobility than the actuated legs [117], [121], [122], and

those that have legs of equal mobility to the platform [115], [116], [118], [119], [126]. Though the former category often requires more components than the latter as the legs have higher mobility, the legs need not to be fabricated as precisely. The passive central constraint enforces the lower DOF mobility of the platform, as opposed to the legs themselves limiting its mobility. This relaxes some of the constraints on the leg design and geometry, such as intersecting joint axes in the *Agile Eye* [115], potentially making their fabrication simpler.

VI. Discussion

Physical specifications of a number of wrist devices are presented in Table I. Because the joint axes do not always follow the same order that they appear in the human wrist for some of the presented wrist devices, the torque and range of motion values in the table appear in the same order of the joints when listed from proximal to distal. As industrial robotic arms may come in a large variety of form factors with different physical specifications, the smallest arm (by mass) from each catalog was selected to be featured in Table I for better comparability with other mechanisms.

Apart from the major trends identified at the conclusion of each section, other comparisons may be made between various groups of wrists. Namely, we discuss differences between serial and parallel wrists, commercial and research devices, and prosthetic and robotic wrists.

A. Serial Versus Parallel

A great number of differences exist between serial and parallel wrist mechanisms. Notably, serial mechanisms tend to be longer than their parallel counterparts when comparing across devices with the same number of DOFs, though the use of tendon drives and bevel gear differentials may alleviate this issue, due to some freedom conferred in actuator placement. If differential couplings are not used, only a single actuator is responsible for an output DOF. Though this only allows power input from a single motor, it is much simpler to introduce compliance [41], [44], [89] or measure loads than it would be in a parallel counterpart.

With serial mechanisms, range of motion and torque specifications is often simply determined by actuator selection (in the case of active devices) and basic shape geometry, and is not configuration dependent. Moreover, the use of fewer components can potentially lead to greater robustness, though loads must be transferred through the entire wrist mechanism.

Parallel mechanisms often have many more architectures and geometric design parameters that can affect the ROM and producible torque. However, this additional complexity allows greater freedom in the design process. For example, collocating axes of rotation may be feasible (e.g., [78], [81], [115], and [116]), and actuators may be placed proximally to reduce inertia of the device (e.g., [74], [84], and [86]. Passive constraints, such as a central universal joint [74]–[77], [117], [123], can be used to bear loads away from actuators and increase stiffness of the mechanisms. However, issues that are not present in serial wrists, such as link/end-effector interference [74], [116] and individual joint ROM, must be addressed in successful implementations of parallel wrist designs. These issues become more difficult to deal with as the desired workspace of a mechanism grows larger, indicating a tradeoff between range of motion and stiffness. This tradeoff not only serves as a major difference between serial and parallel mechanisms, but also within parallel mechanisms themselves.

In most of the parallel wrist mechanisms, motion along an arbitrary DOF requires tandem actuation of multiple motors [74], [75], [119]. This coupling allows multiple actuators to contribute to a single motion. However, in some configurations, actuators may actually work in opposition to one another, or the wrist may be in a singular configuration, unable to actuate in a particular direction. Singular configurations also exist in serial wrists, such as in the roll-pitch-roll configuration when the pitch is neutral, but other configurations such as roll-pitch-yaw only experience a singularity when either pitch or yaw reaches 90°. The singularities are much more predictable, and mechanisms are easily designed for singularities to lie outside of the desired workspace.

The variety of architectures within parallel mechanisms leaves much room for wrist development within the subfield, especially when compared to serial mechanisms. Within serial wrist mechanisms, only a few types of architectures are possible, though improvements to the actuation systems (motors, transmission, etc.) in terms of size, reliability, and power density still may be made. Though the architectures of many parallel mechanisms, and specifically spherical mechanisms, have been described exhaustively and indexed in atlases, physical implementations remain scarce. Part of this may be attributed to the difficulty in creating the successful physical implementation of a parallel mechanism. Small manufacturing errors can lead to overconstraint and large increases of internal forces. Difficulty can also arise in the software and method used to control the mechanism as the forward kinematics are difficult to solve. For some redundantly actuated parallel mechanisms, mitigation of internal forces requires additional sensors and sophisticated control methods.

B. Commercial Versus Research Wrists

Stark differences exist between commercial and research-based wrists as well. Commercially available wrists come as standalone devices in prostheses or are an integrated part of industrial and surgical arms. Commercial prosthetic wrists tend to be passive devices with discrete locking positions, adjustable friction clutches, or elastic joints, all of which are potentially useful for manipulation. Active wrist prostheses are also commercially available [15], [28], [36], though they are restricted to 1-DOF devices.

Almost all multi-DOF commercial active wrists covered in this review utilize a serial roll-pitch-roll (e.g., [93] and [102]) or roll-pitch-yaw architecture (e.g., [98] and [105]), driven by belts (or tendons) and/or bevel gear differentials. Tendon drives are popular among commercially available surgical robots, whereas belt drives are more common amongst heavy duty industrial robots. Both of these drivetrain systems allow for actuator placement away from the wrist and end-effector, this reducing size

TABLE I
WRIST SPECIFICATIONS

TABLE. I. WRIST SPECTFICATIONS

Name / Reference	Commercial (Yes/No)	#-DOF	Actuation (Passive/ Active)	Configuration	Diam. (mm)	Length (mm)	Weight* (g)	Range of Motion** (°)	Torque*** (Nm)
HD Rotation Wrist [11]	Y	1	P	R	--	--	--	360	–
HD Sierra Wrist [11]	Y	1	P	R	50	36	113	50	–
Plettenburg [13]	N	1	P	R	50	38	20	360	–
OB Ratchet Type Rotation [15]	Y	1	P	R	50	25	120	360	–
OB Ratchet Type Rotation- Short [15]	Y	1	P	R	50	19	100	360	–
OB Myowrist 2Act [15]	Y	1	P	R	36	26	55	80	–
OB Myolino [15]	Y	2	P	U	40	39	49	60	–
TB Flexion Wrist [25]	Y	1	P	R		32	161	80	–
MC Wrist Rotator [28]	Y	1	A	R	47	70	143	360	1.13
Pons et. al. (MANUS Hand) [29]	N	1	A	R	--	--	--	170	2
Zinck et al. [34]	N	1	A	R	40	65	87	360	0.06
TB SuproWrist [36]	Y	1	A	R	--	57	154	--	–
OB RoboWrist [40]	Y	2	P	RR	50	41	164	360, 86	–
MC Flexion Wrist [41]	Y	2	P	RR		48	54	--	–
Montagnani et. al. [44]	N	2	P	RR	95	65	450	90, 90	–
Abd Razak et al. [49]	N	2	A	RR	--	--	690	--	3.9, 3.9
Ito et al. [51]	N	2	A	RR	--	115	700*	162, 133	0.17, 1.02
Fan et al. [52]	N	2	A	RR	--	--	200	360, 90	–
Sensinger et al. (RIC Arm) [54]	N	2	A	RR	--	--	325	360, 180	0.9, 1.0
Kyberd et al. [55]	N	2	A	RR	96	50	200	--	0.07, --
Gouaillier et al. (NAO) [56]	N	2	A	RR	--	--	143	240, 210	8.0, --
Friedl et al. (DLR Toro) [58]	N	2	A	RR	--	--	1200	180, --	–
Verleg [61]	N	2	A	RR	30	52.5	73	90, 90	0.75, --
Polhemus et al. (u-GRIP II) [62]	N	2	A	RR	--	--		90, 90	–
Controzzi et al. [65]	N	2	A	RR	76	--	240	--	–
Ahmad et al. [66]	N	2	A	U	47	--	870	175, 60	–
Sone et al. [81]	N	2	A	3RRRR	49	48	75*	360, 90	–
Kim et al. [86]	N	2	A	U, 2PUR	--	--	--	180, 90	2.5, 0.5
Roose [88]	N	2	A	RRRR, R	53	--	95	84, 103	0.32, --
Mahmoud et al. [92]	N	3	A	RRR	--	--	--	--	0.93, 0.21, 0.21
Kawasaki KF121 [94]	Y	3	A	RRR	--	--	--	270, 145, 360	7.8, 7.8, 2.9
Fanuc CR-4iA [95]	Y	3	A	RRR	--	--	48000*	380, 200, 720	8.86, 8.86, 4.9
Wyrobeck et al. [99]	N	3	A	RRR	--	--	--	360,--,360	2.5, 3.6, 4.7
Schuler et al. (DEXARM) [100]	N	3	A	RRR	114	108	--	360, 180, 360	72, --, --
Kuka LBR iiwa [106]	Y	3	A	RRR	--	--	23900*	170, 120, 175	110, 40, 40
Gosselin et al. (Agile Eye) [115]	N	3	A	3RRR	--	--	--	140, 140, 30	–
Birglen et al. (SHaDe) [116]	N	3	A	2RRR, RRRU	350	290	6500	90, 45, 45	1.0, 0, 0
Hess-Coelho [117]	N	3	A	3RRR, RUR	--	--	--	140, 140, 360	–
Hammond et al. [122]	N	3	A	2PRRU, RUUR	--	--	--	180, 180, 360	–
Fite et al. [123]	N	3	A	R, RPR, SPS	--	--	--	170, 60, 150	–
Degirmenci et al. [126]	N	3	A	RRRRR, R	--	--	--	72, 144, 360	4.5, 4.5, 4.2

*Indicates weight of the entire arm system, including wrist device.
**For multi-DOF devices, ROM is listed for each DOF, separated by commas. If ROM of a particular DOF is unknown, a null sign (--) appears in the list.
***For multi-DOF devices, torque is listed for each DOF, separated by commas. If torque of a particular DOF is unknown, a null sign (--) appears in the list.

in surgical robots and inertia in industrial arms. Industrial arms utilize bevel gear differentials [93], [95], [96], [98] to collocate axes of revolution in a compact volume, and potentially allow multiple motors to contribute to a single DOF. Though many commercial products exist that use these designs already, there is likely a room to develop devices that depart from this architecture and actuation scheme.

As most of these wrists belong to industrial robots, their designs show high robustness and torque capacity when compared to research wrists, which have varied designs and design goals.

Research wrists are seen in broad applications, including from prostheses, humanoids, solar trackers, and surgical robots. The designs employ serial, parallel, and hybrid mechanisms. As expected, research devices incorporate a greater variety of coupling schemes [34], [52], [86] and actuation technology [29], [51], [112].

C. Prosthetic Versus Robotic

Though robotic wrists encompass a wide variety of applications, many comparisons may still be made between prosthetic and robotic wrists. Many of the differences are enforced simply by the fact that prostheses require direct human interaction to function. For example, prosthetic wrists may be passive or body powered, whereas robotic wrists are solely active devices. Prosthetic wrists also include externally adjustable functionality, such as adjustable friction or locking. Any adjustment of robotic wrists is generally accomplished within the control system.

Still, a number of nonobvious differences exist between these two categories. Whereas robotic wrists may be serial, parallel, or hybrid devices, all standalone prosthetic wrists are serial chains, though in a few cases transradial and transhumeral prostheses may incorporate parallel or hybrid wrists [123]–[125]. This may be indicative of a minimum amount of space needed to implement a parallel mechanism based wrist with comparable performance to a serial chain.

Coupling of output DOFs is more common amongst prosthetic wrist devices [34], [52], [53] as well. These devices are results of efforts to reduce the complexity, size, etc., of wrist prostheses by sacrificing actuation and motion capabilities. Robotic applications instead tend to utilize the normal design approach of multiple orthogonal axes of rotation, such as those seen in roll-pitch-roll wrists and similar architectures.

Though intended for use as prostheses, there are no major differences between transhumeral/transradial prostheses and anthropomorphic humanoid arms besides the control scheme (inputs generated from user instead of autonomous system). However, design and design goals are more varied in anthropomorphic robots (such as tendon decoupling mechanisms in [68], [86] or housing power components in [74]), which often utilize portions of the forearm to house actuation drivetrains or power components for the end-effector. On the other hand, the thrust for prostheses design is to generally reduce weight. Moreover, limitations on available control inputs to prostheses, especially multiarticulated hands and limbs, reduce the need or feasibility of dexterous wrists in prosthetics compared to anthropomorphic humanoid robots.

While it may appear that active prosthetic wrists are simply a subset of robotic wrist technologies, backdrivability is often different between the two. As a prosthetic wrist user must also carry the power source, a device with low power consumption is generally beneficial. Use of nonbackdrivable transmission elements such as lead screws is an effective way to minimize power consumption by resisting external loads passively when the motors are deactivated. The design goals of minimized size and weight make it sensible for prostheses to utilize small, though highly geared rotary motors to achieve somewhat human levels torque output, rather than heavy motors with minimal gearing. These high gear ratios make even the nonlocking transmission relatively nonbackdrivable. Heavily geared systems also introduce significant backlash when multiple gear stages are placed in series. Combined with the nonbackdrivabililty, this may make prosthetic wrists rather vulnerable to impulsive loading and collisions.

While some robotic wrists also use screw elements or highly geared motors, the looser size restrictions allow use of larger motors with smaller gear ratios, or even direct drive. Backdrivability can then be implemented on some robotic hardware, which may then allow the "teaching" of a robotic arm by physically manipulating the robot externally. These low gear ratios also may enable force sensing at the actuator, or even force control.

VII. Conclusion and Takeaways

Considering the entire group of designs, it is apparent that the intended use of the design greatly affects the performance and physical implementation of a particular wrist. Where miniaturization or low distal inertia is key, tendon drives are a clear strategy for successful implementation. Alternatively, implementation of wrists in industrial settings tends to use a variety of gear drives. Investigating ways to take smaller wrist designs and scaling them to the larger size (and taking larger wrist designs and scaling them to the smaller size) would likely yield interesting solutions and different implementations of specific transmission elements that would enable them for the different size scale.

Though wrist designs have not been a particularly active field of study over the last few decades (compared to hand development), a number of gaps in the literature would benefit from additional focus. Namely, identifying factors that make parallel mechanisms more tractable or appropriate for commercial cases would allow their benefits to be conferred more easily. Automating parallel mechanism design to allow for entry into commercial devices such that expert knowledge is not required, or developing more utilitarian architectures is one such development direction. Mechanically, developing ways to more easily be fabricate the passive subcomponents of parallel mechanisms (especially at small size scales) and making these subcomponents more robust may also lead to more confidence and adoption of these architectures.

While it appears that serial wrists may have little room left for development, the design of a 3-DOF serial wrist which does not occupy the entire forearm volume of a prosthesis, humanoid

robot arm, industrial arm, etc., is still a challenge. While this is likely due to the fact that actuators have greater constraints on their positioning, some transmission elements (tendons, belts, etc.) can be leveraged to achieve more freedom in actuator position.

The use of hybrid mechanisms (combinations of serial and parallel mechanisms) could be especially beneficial in achieving this remote positioning without the complexity of coupled DOFs. For example, using separate four-bar linkages in parallel with one another could allow for proximal actuator positioning, with only simple, passive elements at the wrist joint itself.

The majority of the active wrists described herein use electric motors as the primary source of actuation. Use of pneumatics, whether in rigid pistons, McKibben Actuators [127], or other soft actuators, may be a good method to distribute weight and actuation away from the wrist, though practicality may be limited outside of fixed base robotic systems. Similarly, shape memory alloy (SMAs) actuation systems such as that in [90], or ultrasonic motors as in [29] and [51] may be beneficial in future wrist designs, though the technology still appears relatively immature compared to electric motor, or even pneumatic, actuation.

As of yet, it appears quite difficult to achieve torque and speed capacity of the human wrist while maintaining similar size, weight, and inertia. Many robotic systems easily outperform the human wrist in terms of torque and speed, but their use of large motors with high gear ratios prevent miniaturization and can also preclude backdrivability. While the latter point may not be as important in systems specifically requiring accurate positioning, systems which are meant to interact with an external environment in a manner similar to humans generally require some amount of compliance or modulable impedance, especially when trying to control forces. Developing lightweight, compact actuators, and transmissions with high torque capacity would be of great benefit in the fields of prosthetics and humanoid robots.

Finally, establishing methods to evaluate wrists, and developing insightful metrics and sets of hardware specifications required to complete tasks, may further help designers and end users alike assess suitability of a particular wrist device for their purposes, and drive development toward useful goals.

REFERENCES

[1] F. Montagnani, M. Controzzi, and C. Cipriani, "Is it finger or wrist dexterity that is missing in current hand prostheses?" *IEEE Trans. Neural Syst. Rehabil. Eng.*, vol. 23, no. 4, pp. 600–609, Jul. 2015.

[2] N. M. Bajaj, A. J. Spiers, and A. M. Dollar, "State of the art in prosthetic wrists: Commercial and research devices," in *Proc. IEEE Int. Conf. Rehabil. Robot.*, 2015, pp. 331–338.

[3] M. E. Rosheim, *Robot Wrist Actuators*. New York, NY, USA: Wiley, 1989.

[4] M. M. Marshall, J. R. Mozrall, and J. E. Shealy, "The effects of complex wrist and forearm posture on wrist range of motion," *Human Factors*, vol. 41, no. 2, pp. 205–213, 1999.

[5] D. C. Boone and S. P. Azen, "Normal range of motion of joints in male subjects," *J. Bone Joint Surg. Amer.*, vol. 61, pp. 756–759, 1979.

[6] J. M. Soucie *et al.*, "Range of motion measurements: Reference values and a database for comparison studies," *Haemophilia*, vol. 17, pp. 500–507, 2011.

[7] J. Ryu, W. P. C. Iii, L. J. Askew, K. An, and E. Y. S. Chao, "Functional ranges of motion of the wrist joint," *J. Hand Surg.*, vol. 16, pp. 409–419, 1991.

[8] D. L. Nelson, M. A. Mitchell, P. G. Groszewskv, S. L. Pennick, and P. R. Manske, "Wrist range of motion in activities of daily living," in *Advances in the Biomechanics of the Hand and Wrist*. Boston, MA, USA: Springer, 1994, pp. 329–334.

[9] M. Sardelli, R. Z. Tashjian, and B. A. MacWilliams, "Functional elbow range of motion for contemporary tasks," *J. Bone Joint Surg. Amer.*, vol. 93, pp. 471–477, 2011.

[10] R. H. Brumfield and J. A. Champoux, "A biomechanical study of normal functional wrist motion," *Clin. Orthopaedics Related Res.*, vol. 187, pp. 23—25, 1984.

[11] Hosmer, Chattanooga, TN, USA, Homer Dorrance, 2017. [Online]. Available: www.hosmer.com

[12] W. C. Prout, "Prosthetic wrist unit," U.S. Patent 3 159 847, 1965.

[13] D. H. Plettenburg, "The WILMER passive hand prosthesis for toddlers," *JPO J. Prosthetics Orthotics*, vol. 21, pp. 97–99, 2009.

[14] S. C. Jacobsen, D. F. Knutti, and R. T. Johnson, "Electrically driven artificial arm," U.S. Patent 4 521 924, 1985.

[15] Otto bock, Duderstadt, Germany, 2017. [Online]. Available: http://www.ottobock.com/

[16] D. R. W. May, "Prosthetic wrist fitting," U.S. Patent 4 156 945, 1979.

[17] Northrop Aircraft, "Prosthetic wrist," U.S. Patent 2457316A, 1946.

[18] G. M. Motis, "Artificial arm with stepped up wrist drive and automatic wrist lock," U.S. Patent 2638604A, 1953.

[19] K. Vesper, "Wrist mechanism for artificial arms," U.S. Patent 2605476A, 1952.

[20] W. C. Prout, "Universal wrist system," U.S. Patent 3798680, 1974.

[21] E. Horvarth, "Artificial wrist and arm prosthesis," U.S. Patent 4010495, 1977.

[22] T. Bertels, "Biomechanic aspects and patient needs lead the path to a unique wrist joint for myoelectric prosthesis," in *Proc. MEC Conf.*, 2005, pp. 17–20.

[23] T. Bertels and T. Grob, "Verriegelbares prothesengelenk," Eur. Patent 1 852 092 A1, 2007.

[24] G. M. Motis, "Wrist flexion unit," U.S. Patent 2692390, 1954.

[25] H. Gill, "Wrist device for a prosthetic limb," WO Patent 2016051138 A1, 2016.

[26] I. N. Gaiser, C. Pylatiuk, S. Schulz, A. Kargov, R. Oberle, and T. Werner, "The FLUIDHAND III: A multifunctional prosthetic hand," *JPO J. Prosthetics Orthotics*, vol. 21, no. 2, pp. 91–96, 2009.

[27] G. M. Motis, "Linear to rotational movement converter," U.S. Patent 3466937, 1969.

[28] Motion Control, Salt Lake City, UT, USA, "Motion control wrist rotator and ProWrist electric wrist rotator," 2000.

[29] J. L. Pons *et al.,* "The MANUS-HAND dextrous robotics upper limb prosthesis: Mechanical and manipulation aspects," *Auton. Robots*, vol. 16, pp. 143–163, 2004.

[30] G. Puchhammer, "Michelangelo hand (articulated hand prosthesis)," U.S. Patent 8 690 963, 2014.

[31] G. Rennerfelt, "Artificial hand," E.P. Patent 0219478A1, 1988.

[32] J. Zajdlik, "The preliminary design and motion control of a five-fingered prosthetic hand," in *Proc. Int. Conf. Intell. Eng. Syst.*, 2006, vol. 2, pp. 202–206.

[33] M. Johnsson and C. Balkenius, "LUCS haptic hand III an anthropomorphic robot hand with proprioception," Tech Rep., Lund Univ. Cognitive Sci., 2006, pp. 1–5.

[34] A. Zinck, Ø. Stavdahl, E. Biden, and P. J. Kyberd, "Design of a compact, reconfigurable, prosthetic wrist," *Appl. Bionics Biomech.*, vol. 9, no. 1, pp. 117–124, 2012.

[35] M. Troncossi, E. Gruppioni, M. Chiossi, A. G. Cutti, A. Davalli, and V. Parenti-Castelli, "A novel electromechanical shoulder articulation for upper-limb prostheses: From the design to the first clinical application," *JPO J. Prosthetics Orthotics*, vol. 21, pp. 79–90, 2009.

[36] Touch Bionics, Livingston, U.K., SuproWrist, 2017.

[37] I. Kato, S. Yamakawa, K. Ichikawa, and M. Sano, "Multifunction myoelectric hand prosthesis with pressure sensory feedback system. Waseda hand 4P," in *Proc. 3rd Int. Symp. External Control Human Extremities*, 1963, pp. 155–170.

[38] J. J. Rice, J. M. Schimmels, and S. Huang, "Design and evaluation of a passive ankle prosthesis with powered push-off," *J. Mech. Robot.*, vol. 8, no. 2, 2015, Art. no. 21012.

[39] B. J. Bergelin and P. A. Voglewede, "Design of an active ankle-foot prosthesis utilizing a four-bar mechanism," *J. Mech. Des.*, vol. 134, no. 6, 2012, Art. no. 61004.

[40] OttoBock, Duderstadt, Germany, 10V41 Robo-Wrist, 2017.
[41] S. L. Archer *et al.*, "Wrist device for use with a prosthetic limb," U.S. Patent 7144430B2, 2006.
[42] Liberating Technologies, Inc., Holliston, MA, USA, 2017. [Online]. Available: http://www.liberatingtech.com/.
[43] M. W. Razink, "Prosthetic wrist," U.S. Patent 8795387, 2014.
[44] F. Montagnani, M. Controzzi, C. Cipriani, and S. Member, "Preliminary design and development of a two degrees of freedom passive compliant prosthetic wrist with switchable stiffness," in *Proc. IEEE Int. Conf. Robot. Biomimetics*, Dec. 2013, pp. 310–315.
[45] B. D. Veatch and J. D. Scott, "Pre-positionable prosthetic hand," U.S. Patent 20080188952A1, 2008.
[46] N. Dechev, W. L. Cleghorn, and S. Naumann, "Multiple finger, passive adaptive grasp prosthetic hand," *Mech. Mach. Theory*, vol. 36, pp. 1157–1173, 2001.
[47] J. H. Rouse, R. H. Farquharson, and C. G. Betts, "Multifunction body powered prosthetic wrist unit and method," U.S. Patent 7048768B1, 2003.
[48] S. L. Phillips, K. J. De Laurentis, and C. E. I. Pfeiffer, "Joint prosthetic device," U.S. Patent 20090326677, 2009.
[49] N. A. Abd Razak, N. A. Abu Osman, H. Gholizadeh, and S. Ali, "Development and performance of a new prosthesis system using ultrasonic sensor for wrist movements: A preliminary study," *Biomed. Eng. Online*, vol. 13, 2014, Art. no. 49.
[50] K. Ohnishi, T. Morio, T. Takagi, and I. Kajitani, "Multimodal sensor controlled three degree of freedom transradial prosthesis," in *Proc. IEEE 13th Int. Conf. Rehabil. Robot.*, 2013, pp. 1–6.
[51] K. Ito, T. Tsuji, A. Kato, and M. Ito, "An EMG controlled prosthetic forearm in three degrees of freedom using ultrasonic motors," in *Proc. 14th Annu. Int. Conf. IEEE Eng. Med. Biol. Soc.*, 1992, vol. 4, pp. 1487–1488.
[52] S. Fan, S. Fan, L. Jiang, and H. Liu, "A design of a miniaturized prosthetic wrist based on repetition rate of human wrist daily tasks," in *Proc. Int. Conf. Robot. Biomimetics*, 2016, pp. 1643–1648.
[53] L. Resnik, S. L. Klinger, and K. Etter, "The DEKA arm: Its features, functionality, and evolution during the veterans affairs study to optimize the DEKA arm," *Prosthetics Orthotics Int.*, vol. 38, pp. 492–504, 2013.
[54] J. Sensinger *et al.*, "Initial experiences with the RIC arm," in *Proc. Myoelect. Controls Symp.*, 2014, pp. 227–229.
[55] P. J. Kyberd, A. S. Poulton, L. Sandsjo, S. Jonsson, B. Jones, and D. Gow, "The ToMPAW modular prosthesis - a platform for research in upper limb prosthetics," *J. Prosthetics Orthotics*, vol. 19, pp. 15–21, 2007.
[56] D. Gouaillier *et al.*, "Mechatronic design of NAO humanoid," in *Proc. IEEE Int. Conf. Robot. Automat.*, Jun. 2009, pp. 769–774.
[57] Aldebaran Robotics, Tokyo, Japan, "All purpose humanoid robot," 2012.
[58] W. Friedl, H. Hppner, F. Petit, and G. Hirzinger, "Mechanical design, shape analysis and experimental validation wrist and forearm rotation of the DLR hand arm system," in *Proc. IEEE/RSJ Int. Conf. Intell. Robots Syst.*, 2011, pp. 1836–1842.
[59] R. A. Frosch, G. A. Wiker, and W. A. Mann, "Compact artificial hand," U.S. Patent 4149278, 1979.
[60] D. Gow, "Upper limb prosthesis," U.S. Patent 6 361 570, 2002.
[61] M. N. Verleg, "Wrist prosthesis: New two degrees-of-freedom hydraulic wrist mechanism for hand prostheses," M.S. thesis, Dept. Biomech. Eng., TU Delft, Delft, The Netherlands, 2015.
[62] A. Polhemus, B. Doherty, K. Mackiw, R. Patel, and M. Paliwal, "uGrip II: A novel functional hybrid prosthetic hand design," in *Proc. Annu. Northeast Bioeng. Conf.*, 2013, no. 39, pp. 303–304.
[63] RSL Steeper, Leeds, U.K., Bebionic wrist, 2015.
[64] P. J. Kyberd *et al.*, "Two-degree-of-freedom powered prosthetic wrist," *J. Rehabil. Res. Develop.*, vol. 48, no. 6, pp. 609–617, 2011.
[65] M. Controzzi, C. Cipriani, B. Jehenne, M. Donati, and M. C. Carrozza, "Bio-inspired mechanical design of a tendon-driven dexterous prosthetic hand," in *Proc. Annu. Int. Conf. IEEE Eng. Med. Biol. Soc.*, 2010, pp. 499–502.
[66] S. Ahmad, A. Masood, and U. S. Khan, "Bowden cable based powered ball and socket wrist actuator," *Int. J. Mech. Aerosp., Ind. Mechatronic Manuf. Eng.*, vol. 6, no. 9, pp. 932–935, 2012.
[67] H. Takeda, N. Tsujiuchi, T. Koizumi, H. Kan, M. Hirano, and Y. Nakamura, "Development of prosthetic arm with pneumatic prosthetic hand and tendon-driven wrist," in *Proc. 31st Annu. Int. Conf. IEEE Eng. Med. Biol. Soc.*, 2009, pp. 5048–5051.
[68] U. Scarcia, C. Melchiorri, and G. Palli, "Towards simplicity: On the design of a 2-DOFs wrist mechanism for tendon-driven robotic hands," in *Proc. IEEE Int. Conf. Robot. Biomimetics*, 2015, pp. 1317–1322.
[69] W. A. Burbank, "Four-cable wrist with solid surface channels," U.S. Patent 8 821 480, 2014.
[70] T. E. Murphy and M. M. Nixon, "Surgical instrument wrist," U.S. Patent 8 540 748, 2013.
[71] S. Manzo and L. Heaton, "Wristed robotic surgical tool for pluggable end-effectors," U.S. Patent 8 398 634, 2013.
[72] S. Lo *et al.*, "Design, operation, and performance evaluation of a cable-drawn dual-axis solar tracker compared to a fixed-tilted system," *Energy Sci. Eng.*, vol. 3, no. 6, pp. 549–557, 2015.
[73] Intuitive Surgical, Sunnyvale, CA, USA, "EndoWrist instrument & accessory catalog," 2015.
[74] L. B. Bridgwater *et al.*, "The robonaut 2 hand-designed to do work with tools," in *Proc. IEEE Int. Conf. Robot. Automat.*, 2012, pp. 3425–3230.
[75] A. Cammarata, "Optimized design of a large-workspace 2-DOF parallel robot for solar tracking systems," *Mech. Mach. Theory*, vol. 83, pp. 175–186, 2015.
[76] D. Sanchez and S. Barbara, "Surgical instrument with a universal wrist," U.S. Patent 7 121 781, 2006.
[77] X. Duan, Y. Yang, and B. Cheng, "Modeling and analysis of a 2-DOF spherical parallel manipulator," *Sensors (Switzerland)*, vol. 16, no. 9, pp. 1–15, 2016.
[78] B. M. Schena, "Center robotic arm with five-bar spherical linkage for endoscopic camera," U.S. Patent 8 469 945, 2013.
[79] J. M. Wiitala and M. M. Stanisic, "Design of an overconstrained and dextrous spherical wrist," *J. Mech. Des.*, vol. 122, no. 9, pp. 347–353, 2000.
[80] S. Hernandez, S. Bai, and J. Angeles, "The design of a chain of spherical stephenson mechanisms for a gearless robotic pitch-roll wrist," *J. Mech. Des.*, vol. 128, no. 2, pp. 422–429, 2006.
[81] K. Sone, H. Isobe, and K. Yamada, "High angle active link," NTN, Osaka, Japan, Tech. Rev., 2004, pp. 70–73.
[82] M. E. Rosheim, "Multiple rotatable links robotic manipulator," U.S. Patent 5 893 296, 1999.
[83] S. L. Canfield and C. F. Reinholtz, "Development of the carpal robotic wrist," in *Experimental Robotics V*. Berlin, Germany: Springer, 1998, pp. 423–434.
[84] L. Barker, M. Neber, and H. Lee, "Design of a low-profile two-axis solar tracker," *Sol. Energy*, vol. 97, pp. 569–576, 2013.
[85] Y. Lee, C. Chu, J. Xu, C. Lan, and S. Member, "Two-dimensional series elastic actuation for accurate force/torque interaction," *IEEE/ASME Trans. Mechatronics*, vol. 21, no. 3, pp. 1315–1325, Jun. 2016.
[86] Y. J. Kim *et al.*, "RoboRay hand: A highly backdrivable robotic hand with sensorless contact force measurements," in *Proc. IEEE Int. Conf. Robot. Automat.*, 2014, pp. 6712–6718.
[87] H. Lymark and F. Mohl, "An electromechanical forearm and hand," in *Advances in the Control of Human Extremities*. *3rd Int. Symp. Control of Human Extremities*, Dubrovnik, Croatia, 1966, pp. 142–150.
[88] C. Roose, "Pneumatically powered wrist prosthesis," Master's thesis, TU Delft, 2014.
[89] S. L. Archer *et al.*, "Wrist device for use with a prosthetic limb," U.S. Patent 7 914 587, 2011.
[90] K. J. De Laurentis and C. Mavroidis, "Mechanical design of a shape memory alloy actuated prosthetic hand," *Technol. Health Care*, vol. 10, pp. 91–106, 2002.
[91] M. S. Johannes, J. D. Bigelow, J. M. Burck, S. D. Harshbarger, M. V. Kozlowski, and T. Van Doren, "An overview of the developmental process for the modular prosthetic limb," *Johns Hopkins APL Tech. Dig. (Appl. Phys. Lab.)*, vol. 30, no. 3, pp. 207–216, 2011.
[92] R. Mahmoud, A. Ueno, and S. Tatsumi, "Dexterous mechanism design for an anthropomorphic artificial hand: Osaka City University Hand I," in *Proc. 10th IEEE-RAS Int. Conf. Humanoid Robot. Humanoids*, 2010, pp. 180–185.
[93] S. Roth, "Robot arm," U.S. Patent 2014/0165771 A1, 2014.
[94] T. Inada, T. Tsujimori, S. Kitamura, and R. Taniuchi, "Robot," U.S. Patent 7 622 001, 2009.
[95] N. Torii, K. Mizuno, and H. Iwasaki, "Wrist assembly for an industrial robot," U.S. Patent 4 972 735, 1990.
[96] T. Hezel, I. Leiensetter, F. Herre, B. Maxharraj, and N. Maxaharaj, "Multi axis robot wrist and method," U.S. Patent 7 870 807, 2011.
[97] Z.-X. Liu, "Robot arm assembly," U.S. Patent 2012/0103127 A1, 2012.
[98] N. Ulrich and W. T. Townsend, "Robotic wrist," U.S. Patent D 352, 050, 1989.

[99] K. A. Wyrobek, E. H. Berger, H. F. M. Van Der Loos, and J. K. Salisbury, "Towards a personal robotics development platform: Rationale and design of an intrinsically safe personal robot," in *Proc. IEEE Int. Conf. Robot. Automat.*, 2008, pp. 2165–2170.
[100] S. Schuler, V. Kaufmann, P. Houghton, and G. S. Székely, "Design and development of a joint for the dextrous robot arm," in *Proc. 9th ESA Workshop Adv. Space Technol. Robot. Automat.*, 2006, no. 1, pp. 1–8.
[101] R. D. Howard, "Design of a robotic wrist and tool-exchange mechanism for satellite servicing," Univ. Maryland, College Park, MD, USA, Presentation, 2002.
[102] T. A. Morley and D. T. Wallace, "Roll-pitch-roll surgical tool," U.S. Patent 7 398 707, 2008.
[103] U. Hagn *et al.*, "DLR MiroSurge: A versatile system for research in endoscopic telesurgery," *Int. J. Comput. Assisted Radiol. Surg.*, vol. 5, no. 2, pp. 183–193, 2010.
[104] A. J. Madhani and J. K. Salisbury, "Articulated surgical instrument for performing minimally invasive surgery with enhanced dexterity and sensitivity," U.S. Patent 5 792 135, 1998.
[105] T. A. Morley and D. T. Wallace, "Roll-pitch-roll-yaw surgical tool," U.S. Patent 6 676 684, 2004.
[106] Kuka AG, Augsburg, Germany, 2017. [Online]. Available: www.kuka.com
[107] A. Albers, S. Brudniok, J. Ottnad, C. Sauter, and K. Sedchaicharn, "Upper body of a new humanoid robot - the design of ARMAR III," in *Proc. 6th IEEE-RAS Int. Conf. Humanoid Robots*, 2006, pp. 308–313.
[108] K. Berns, H. Vogt, T. Asfour, and R. Dillmann, "Design and control architecture of an anthropomorphic robot arm," in *Proc. 3rd Int. Conf. Adv. Mechatronics*, 1998, vol. 35, pp. 945–962.
[109] K. Kaneko *et al.*, "Humanoid robot HRP-4 - humanoid robotics platform with lightweight and slim body," in *Proc. IEEE Int. Conf. Intell. Robots Syst.*, 2011, pp. 4400–4407.
[110] B. Tondu, S. Ippolito, J. Guiochet, and A. Daidie, "A seven-degrees-of-freedom robot-arm driven by pneumatic artificial muscles for humanoid robots to cite this version," *Int. J. Robot. Res.*, vol. 24, no. 4, pp. 257–274, 2005.
[111] G. T. Pinson, "Digitally controlled artificial hand," US patent 4,246,661, 1981.
[112] G. S. Chirikjian and D. Stein, "Kinematic design and commutation of a spherical stepper motor," *IEEE/ASME Trans. Mechatronics*, vol. 4, no. 4, pp. 342–353, Dec. 1999.
[113] R. B. Roth and K.-M. Lee, "Design optimization of a three degrees-of-freedom variable-reluctance spherical wrist motor," *J. Eng. Ind.*, vol. 117, pp. 378–388, 1995.
[114] S. K. Mustafa, G. Yang, S. H. Yeo, W. Lin, and C. B. Pham, "Development of a bio-inspired wrist prosthesis," in *Proc. IEEE Conf. Robot. Automat. Mechatronics*, 2006, vol. 1, pp. 3–8.
[115] C. M. Gosselin, E. St. Pierre, and M. Gagné, "On the development of the agile eye," *IEEE Robot. Automat. Mag.*, vol. 3, no. 4, pp. 29–37, Dec. 1996.
[116] L. Birglen, C. Gosselin, N. Pouliot, B. Monsarrat, and T. Laliberté, "SHaDe, a new 3-DOF haptic device," *IEEE Trans. Robot. Automat.*, vol. 18, no. 2, pp. 166–175, Apr. 2002.
[117] T. A. Hess-Coelho, "A redundant parallel spherical mechanism for robotic wrist applications," *J. Mech. Des.*, vol. 129, pp. 891–895, Aug. 2007.
[118] K. Al-Widyan, X. Q. Ma, and J. Angeles, "The robust design of parallel spherical robots," *Mech. Mach. Theory*, vol. 46, no. 3, pp. 335–343, 2011.
[119] P. Vischer and R. Clavel, "Argos: A novel 3-DoF parallel wrist mechanism," *Int. J. Robot. Res.*, vol. 19, pp. 5–11, 2000.
[120] R. Clavel, "Device for the movement and positioning of an element in space," U.S. Patent 4 976 582, 1989.
[121] M. B. Hong and Y. H. Jo, "Design of a novel 4-DOF wrist-type surgical instrument with enhanced rigidity and dexterity," *IEEE/ASME Trans. Mechatronics*, vol. 19, no. 2, pp. 500–511, Apr. 2014.
[122] F. L. H. Iii, R. D. Howe, and R. J. Wood, "Dexterous high-precision robotic wrist for micromanipulation," in *Proc. 16th Int. Conf. Adv. Robot.*, 2013, pp. 1–8.
[123] K. B. Fite, T. J. Withrow, X. Shen, K. W. Wait, J. E. Mitchell, and M. Goldfarb, "A gas-actuated anthropomorphic prosthesis for transhumeral amputees," *IEEE Trans. Robot.*, vol. 24, no. 1, pp. 159–169, Feb. 2008.
[124] D. S. V. Bandara, R. A. R. C. Gopura, K. T. M. U. Hemapala, and K. Kiguchi, "A multi-DoF anthropomorphic transradial prosthetic arm," in *Proc. BIOROB*, 2014, vol. 1, pp. 1039–1044.
[125] S. K. Kundu and K. Kiguchi, "Development of a 5 DOF prosthetic arm for above elbow amputees," in *Proc. IEEE Int. Conf. Mechatronics Automat.*, 2008, pp. 207–212.
[126] A. Degirmenci, F. L. Hammond, J. B. Gafford, C. J. Walsh, R. J. Wood, and R. D. Howe, "Design and control of a parallel linkage wrist for robotic microsurgery," in *Proc. IEEE Int. Conf. Intell. Robots Syst.*, Dec. 2015, pp. 222–228.
[127] C. Chou and B. Hannaford, "Measurement and modeling of McKibben pneumatic artificial muscles," *IEEE Trans. Robot. Automat.*, vol. 12, no. 1, pp. 90–102, Feb. 1996.

Neil M. Bajaj (S'18) received the B.S. degrees in mechanical engineering and in kinesiology, both in 2014, from University of Massachusetts, Amherst, MA, USA, and the M.S. and M.Phil. degrees in mechanical engineering in 2016 and 2017, respectively, from Yale University, New Haven, CT, USA, where he is currently working toward the Ph.D. degree in mechanical engineering.

His research focuses on the design, construction, and evaluation of powered prosthetic wrists for upper limb amputees.

Adam J. Spiers (M'17) received the B.Sc. degree in cybernetics and control engineering and the M.Sc. degree in engineering and information sciences from University of Reading, Reading, U.K., in 2004 and 2006, respectively, and the Ph.D. degree in mechanical engineering from University of Bristol, Bristol, U.K., in 2011.

He is currently a Research Scientist with the Haptic Intelligence Department, Max Planck Institute for Intelligent System, Stuttgart, Germany. His research interests include haptic interfaces, human and robot manipulation, and upper limb prosthetics.

Aaron M. Dollar (SM'13) received the B.S. degree in mechanical engineering from University of Massachusetts, Amherst, MA, USA, in 2000, and the S.M. and Ph.D. degrees in engineering sciences from Harvard University, Cambridge, MA, USA, in 2002 and 2007, respectively.

He is currently the John J. Lee Associate Professor of mechanical engineering and materials science with Yale University, New Haven, CT, USA. He was involved in two years of postdoctoral research with the Massachusetts Institute of Technology Media Lab. His research interests include human and robotic grasping and dexterous manipulation, mechanisms and machine design, and assistive and rehabilitation devices, including upper limb prosthetics and lower limb orthoses.

Prof. Dollar is the recipient of the 2014 NASA Early Career Faculty Award, the 2013 DARPA Young Faculty Award, the 2011 AFOSR Young Investigator Award, the 2010 Technology Review TR35 Young Innovator Award, and the 2010 NSF CAREER Award.

Kinematic Optimization of a 2-DoF U, 2PSS Parallel Wrist Device

Conference Paper · August 2019

CITATIONS
0

READS
56

2 authors, including:

Neil Bajaj
Yale University
5 PUBLICATIONS **22** CITATIONS

SEE PROFILE

Proceedings of the ASME 2019
International Design Engineering Technical Conferences
and Computers and Information in Engineering Conference
IDETC/CIE2019
August 18-21, 2019, Anaheim, CA, USA

IDETC2019-98108

KINEMATIC OPTIMIZATION OF A 2-DOF U, 2PSS PARALLEL WRIST DEVICE

Neil M. Bajaj[1], Aaron M. Dollar
Yale University
New Haven, CT, USA

ABSTRACT

The wrist plays the crucial role of orienting a hand or end effector without significant translational motion, a critical requirement of successful manipulation. In this paper, we present the kinematic design optimization a two degree of freedom universal, two-prismatic-spherical-spherical (U, 2-PSS) parallel wrist mechanism. By varying the geometric parameters of the mechanism, we examine configurations that maximize the Global Conditioning Index, a metric describing the quality of the motion and torque, over the desired workspace, which mimics a healthy human wrist range of motion in circumduction (flexion/extension and abduction/adduction). We further investigate the effects of sizing constraints on the resulting optimized design which satisfies the imposed sizing constraints.

Keywords: Parallel Robots, Robot Kinematics, Design Optimization

1. INTRODUCTION

Wrist joints allow for manipulator devices to decouple translational motion from rotational motion due to their close proximity to the end effector. In an anthropomorphic arm system, this may allow the shoulder and elbow to determine the spatial location of the hand while the wrist determines its orientation, up to certain limits. Many robotic or artificial wrists employ a serial type architecture, with joints placed one after another in series. This series configuration may limit the compactness of a wrist, rendering it unsuitable for some applications [1] [2]. Though generally more complex, parallel mechanisms can mitigate potential disadvantages of serial mechanisms, such as excessive length, large distal inertia, and size constraints. This additional complexity arises from both kinematic and implementation issues, such as singularities and link interference, and passive joint ranges. These complexities can be further exacerbated as the number of degrees of freedom (DOFs) of a mechanism increases.

Parallel mechanisms are used to orient end effectors in a variety of applications, and employ many different types of architectures Notably, the Agile Eye [4] is a 3RRR parallel manipulator used to quickly orient a camera. Variants on the Agile Eye include an RUR, 3RRR mechanism [5] meant to impart infinite platform roll, the Agile Wrist [6], designed to mitigate manufacturing errors, and ShaDe [7], a tool meant for haptic feedback with a less obstructed center. In [8], a five-bar linkage is used to orient a surgical device. In [9], a PUR, PU 2-DOF mechanism is used a solar panel orientating device. A rotational complement to the linear positioning Delta Robot, Argos [10] three symmetric spatial pantograph arms to orient its platform in 3 DOF.

Other wrist devices employ the same U, 2PSS (or kinematically equivalent) architecture within their designs. Notably, the NASA Robonaut Humanoid [11] utilizes this design to actuate its 2DOF wrists. In both [12], [13], a U, 2PSU mechanism is used in a solar tracking device to maximize power generation. With these two implementations, the parameter space was limited by at least two parameters by enforcing the P joints were both vertical and parallel. In [14] and [15], similar architectures were used to achieve 3-DOF wrist motion.

In this paper, we present the kinematic optimization of a 2-DOF parallel wrist mechanism with a universal, 2-prismatic-spherical-spherical (U, 2PSS) architecture (Fig. 1). In each of the PSS legs, the prismatic joints are actuated, leading to 2-DOF rotation about end effector points in, though without the ability to rotate about the instantaneous pointing axis. As opposed to previous work regarding the optimization of this particular mechanism architecture, we vary all of the geometric parameters of the symmetric version of this mechanism, thus potentially resulting in more optimal configurations.

The optimization described herein entails varying the geometric parameters which uniquely define the mechanism in

[1] Contact author: neilmbajaj@gmail.com

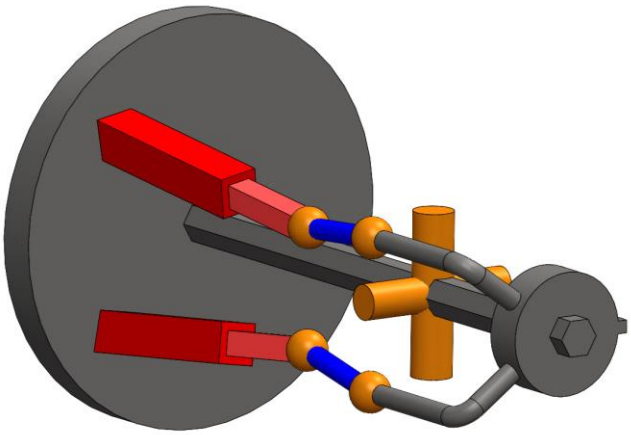

FIGURE 1: An example configuration of the U, 2PSS mechanism. The actuated prismatic joints are shown in red, the passive universal and four spherical joints in gold, the intermediate links in blue, and the base and platform in grey.

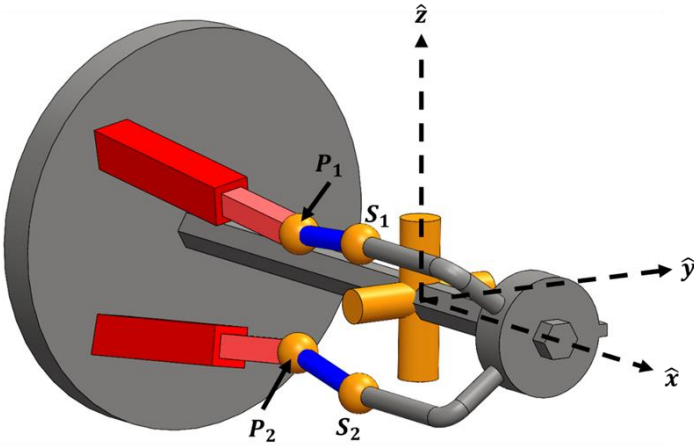

FIGURE 2: Coordinate system and named points of the mechanism. The three unit vectors corresponding to the coordinate axes intersect at the center of the U joint.

order to maximize an index called the Global Conditioning Index (GCI) [3], an index which describes the quality or evenness of the motion. We present the resulting optimal design configurations, and then explore the ability to trade GCI for better satisfying sizing metrics, namely clearance and overall size.

We begin with a discussion of the parallel mechanism in consideration, defining the geometric parameters and detailing the inverse kinematics. We subsequently define the optimization metric and other important quantities and present the simulation methodology. The resulting configurations and effects of tightening sizing constraints on the overall performance of the mechanism are detailed, and a discussion of the simulation results and design tradeoff concludes the paper.

2. MATERIALS AND METHODS

2.1 Mechanism Description

The mechanism designed and optimized herein is a parallel U, 2PSS mechanism. The mechanism is symmetric about the horizontal plane (denoted as the x-y plane), thus each of the two PSS legs are mirrored versions of one another, reducing the overall number of design parameters and ensuring a symmetric workspace about this plane. The central, passive U-joint constrains the motion of the platform to 2-DOF circumduction. Note that in either PSS chain, one of the S joints may be replaced by a U joint without altering the characteristics of the mechanism, though individual ranges of motions of the joints may affect the kinematics in a physical implementation.

A base coordinate system (Fig. 2) is placed at the center of the U joint, with the positive x axis pointing towards the platform when in the zero position (0º flexion and abduction, called ZP hereafter). The y axis points along the proximal axis of the universal joint, running horizontally, and the z axis points vertically along the axis of the secondary U joint axis when in the ZP.

Changing the stroke of the prismatic joints rotates the distal platform with respect to the base of the mechanism. Roughly speaking, actuating both prismatic joints in the same direction results in yaw motion, whereas actuating the in opposite directions changes the pitch. Both actuators may generally contribute to torque production in an arbitrary direction as a result.

In total, eight design parameters consisting of four lengths and four angles are required to uniquely define a mechanism configuration. These parameters may be seen in Figs 2-4. Four of the parameters are used to describe the line of action (LoA) of one of the P joints. As we stipulate that the P joints may not actuate completely vertically, each line of action must have a single intercept point with the y-z plane, with an x value of 0. For the upper PSS linkage, this intercept point $\boldsymbol{P_{O1}}$ is defined as

$$\boldsymbol{P_{O1}} = \left[0, -\boldsymbol{r_p}\cos(\boldsymbol{\alpha_p}), \boldsymbol{r_p}\sin(\boldsymbol{\alpha_p})\right]^T \quad [1]$$

where $\boldsymbol{r_p}$ is the radial distance parameter of the intercept, and $\boldsymbol{\alpha_p}$ is the angle in the y-z plane measured from the negative y axis. The corresponding intercept of the lower PSS linkage is the mirror of $\boldsymbol{P_{O1}}$ about the x-y plane, changing the z value to $-\boldsymbol{r_p}\sin(\boldsymbol{\alpha_p})$.

Two more angles, $\boldsymbol{\beta}$ and $\boldsymbol{\gamma}$ (shown in Fig. 3), are used to determine the P joint LoA unit direction, denoted by the unit vector $\hat{\boldsymbol{v}}_1$. These angles define the unit direction:

$$\hat{\boldsymbol{v}}_1 = \boldsymbol{R_x}(-\boldsymbol{\alpha_p})\boldsymbol{R_y}(\boldsymbol{\beta})\boldsymbol{R_z}(\boldsymbol{\gamma})\hat{\boldsymbol{x}} \quad [2]$$

where $\boldsymbol{R_x}$, $\boldsymbol{R_y}$, and $\boldsymbol{R_z}$, are rotation matrices about the x, y, and z axes, respectively, and $\hat{\boldsymbol{x}}$ is a unit column vector in the positive x direction. Mirroring $\hat{\boldsymbol{v}}_1$ about the x-y plane yields $\hat{\boldsymbol{v}}_2$, the unit direction of the lower P joint. With $\boldsymbol{P_{O1}}$ and $\hat{\boldsymbol{v}}_1$, the LoA may be parametrically expressed with respect to the stroke $\boldsymbol{t_1}$ as

$$\boldsymbol{P_1}(\boldsymbol{t}) = \boldsymbol{P_{O1}} + \hat{\boldsymbol{v}}_1 * \boldsymbol{t_1}. \quad [3]$$

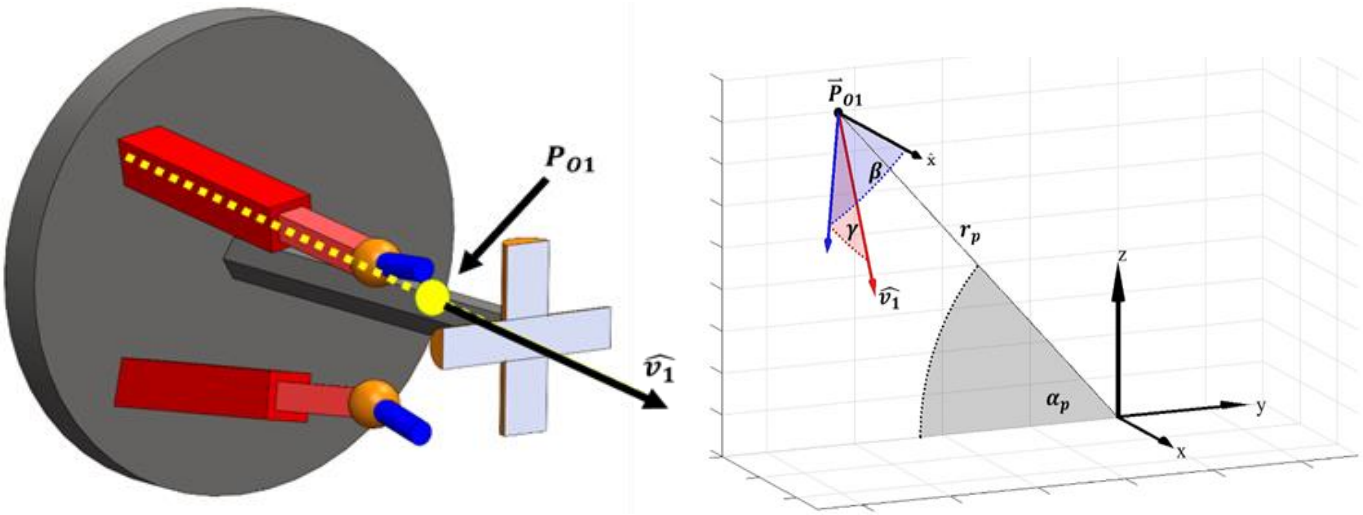

FIGURE 3: (Left) Cutaway view at the x=0 plane showing prismatic joint line of action and intercept point PO1. (Right) Geometric definition of parameters of prismatic joint LoA.

The proximal spherical joint in the upper PSS linkage is located at the point $\boldsymbol{P_1}$, and thus changes as a function of the stroke.

Three parameters are required to define the geometry of the platform (Fig. 4). As the distal S joints of each PSS linkage are fixed with respect to the platform, these three parameters are used to determine the location of these joints within a platform fixed coordinate system, or relative to the ZP. The locations are defined cylindrically, with an axial translation, a radius, and an angle about the center axis, which is the x axis. Namely, these three parameters are $\boldsymbol{d_x}$, (the x coordinate of the spherical joints in the ZP), $\boldsymbol{\alpha_s}$ (the angle about the x-axis measured w.r.t. the y axis), and $\boldsymbol{r_s}$ (the radial distance from the x axis. We then define the position of the second spherical joint in the ZP as

$$\boldsymbol{S_{1o}} = [\boldsymbol{d_x}, -\boldsymbol{r_s}\cos(\boldsymbol{\alpha_s}), \boldsymbol{r_s}\sin(\boldsymbol{\alpha_s})]^T \quad [4]$$

The final parameter is simply the length of the intermediate link in the PSS linkage, which corresponds to the distance between the two spherical joints. This parameter is denoted by the variable $\boldsymbol{l_i}$. When the geometric parameters are set, we call the resulting mechanism a configuration. Note that all length parameters are unitless for the purpose of this simulation, and can be scaled up or down to any particular size scale.

2.2 Kinematic Analysis

With the eight design parameters fixed, the configuration is a 2-DOF mechanism which can achieve a set of flexion and abduction values by changing the stroke of the P joints. While the forward kinematics of the mechanism must be solved by an iterative numerical method, the inverse kinematics, shown subsequently, may be solved simply without an iterative scheme.

In inverse kinematics for parallel mechanisms, the pose of the platform is specified and the resulting actuator excursion values are calculated. The platform pose is defined by two angles, $\boldsymbol{\varphi}$ and $\boldsymbol{\theta}$, corresponding to flexion and abduction, respectively. The platform is first rotated about the fixed z axis by $\boldsymbol{\theta}$, and then about the negative y axis by $\boldsymbol{\varphi}$. In particular, the positions of the distal S joints are required to solve the inverse kinematics, and can be calculated by

$$\overrightarrow{\boldsymbol{S_1}}(\boldsymbol{\varphi}, \boldsymbol{\theta}) = \boldsymbol{R_y}(-\boldsymbol{\varphi})\boldsymbol{R_z}(\boldsymbol{\theta})\overrightarrow{\boldsymbol{S_{1o}^T}}. \quad [5]$$

and the position $\boldsymbol{S_2}$ may be calculated similarly.

After calculating the location of the distal S joint in the PSS linkage, the stroke value of the P joint must be determined. This nominally corresponds to finding the intersection(s) of a sphere centered at $\boldsymbol{S_1}$ with radius $\boldsymbol{l_i}$ with the P joint LoA and then determining the resulting stroke. The intersection point is the location of the proximal S joint when the mechanism is in the specified pose. The intersection(s) of a sphere and line in $\mathbb{R}^3$ may be simply computed using basic geometry.

Generally speaking, there may be zero, one, or two intersection points. In the case of no intersections, the LoA and sphere are too far apart to intersect, meaning the current pose is physically unreachable within the current configuration. With one intersection, the LoA is tangent to the sphere, and the pose on a workspace boundary, as further separation of the LoA and sphere result in unreachable configurations, and is singular, as the P joint is perpendicular to the intermediate link and thus transfers zero force.

In the case of two intersection points, this corresponds to the particular pose being reachable. The two intersection points are both feasible, though one of the points would require the intermediate link to go past perpendicular to the LoA, which is not possible as it would run through a singular point. Thus, we may eliminate one of the intersection points and keep the one that results in the intermediate link falling in front of the P joint LoA. Computing the stroke simply involves finding the distance between the resulting intersection point and the location of the proximal S joint when the mechanism is in the ZP.

Once the pose of the mechanism has been determined, the Jacobian matrix $\boldsymbol{J}$ may be calculated via static equilibrium. The Jacobian, which relates velocities of the P joints to velocities of the platform, also relates the forces of the input P joints (labeled

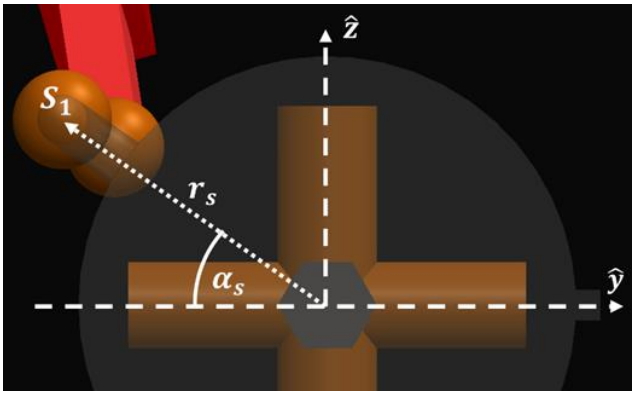

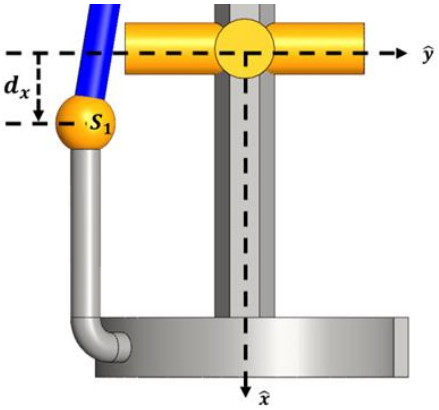

FIGURE 4: (Left) Front view of spherical joint location S_1 in the ZP, projected onto the plane x = d_x, corresponding to the offset the spherical joint has from the *x=0* plane. The positive x-axis runs out of the page. (Right) Top view of S_1 in the ZP , highlighting the offset d_x.

as the vector $\vec{u}$) to output torques on the platform $\vec{\tau}$ via the relationship

$$\vec{u} = J^T \tau. \quad [6]$$

As there are two actuators and two output DoFs in this mechanism, the Jacobian is square, and generally invertible away from singular poses. To more intuitively define the Jacobian, we multiply Eqn. 6 by its inverse to yield

$$[J^T]^{-1}\,\vec{u} = [J^{-1}]^T\,\vec{u} = K\,\vec{u} = \tau. \quad [7]$$

The matrix K, which is the transpose of the inverse Jacobian, is thus a mapping from input forces to output torques. Generally speaking, we may consider K to be a matrix of lever arms. To determine the elements of K, we consider the platform to be locked at a particular pose, and then apply a unit force at one of the actuators. The unit force corresponds to an element of $\vec{u}$ being equal to 1. These unit forces propagate through each PSS linkage, from the P joint to the intermediate link, and then generate a torque on the platform. Element by element, the components of the K are:

$$\begin{aligned} K_{11} &= \sec(\rho_1)\left[\hat{l}_1 \times \overrightarrow{S_1}(\varphi,\theta)\right]^T R_y(-\varphi)\hat{z} \\ K_{21} &= -\sec(\rho_1)\left[\hat{l}_1 \times \overrightarrow{S_1}(\varphi,\theta)\right]^T \hat{y} \\ K_{12} &= \sec(\rho_2)\left[\hat{l}_2 \times \overrightarrow{S_2}(\varphi,\theta)\right]^T R_y(-\varphi)\hat{z} \\ K_{22} &= -\sec(\rho_{12})\left[\hat{l}_2 \times \overrightarrow{S_2}(\varphi,\theta)\right]^T \hat{y} \end{aligned} \quad [8]$$

where ρ_1 and ρ_2 are respective the angles between the upper and lower P joint LoA and the intermediate links at the current pose, and $\hat{l}_1$ and $\hat{l}_2$ are the unit vectors in the direction of the upper and lower intermediate links, respectively. Note that K (and thus J) become singular when either of the intermediate links become perpendicular to their associated P joint LoA (ρ_1 or ρ_2 go to 90º). It may also become singular when one of the intermediate links becomes colinear with the line from the origin to $\overrightarrow{S_1}$, corresponding to no mechanical advantage. Further singularity analysis of this particular mechanism may be found in [16]. We may transpose and invert K to yield the original Jacobian, which shall be used to calculate the local optimization metric at a given pose.

2.3 Optimization Framework

By varying the geometric parameters of the mechanism, an index that represents the quality of the motion may be optimized over the desired workspace. As we would like the mechanism to perform well at all parts in the workspace, we opt to average an index which describes the quality of motion at a particular pose, and then average this with other sampled points in the workspace. Specifically, we opt to use the Local Conditioning Index (LCI) χ_{Lp} [17], defined as the inverse condition number of the Jacobian at a particular pose. It is defined as

$$\chi_{Lp} = |\lambda_{min}|/|\lambda_{max}| \quad [9]$$

where λ_{min} is the smaller eigenvalue of the Jacobian matrix at the given pose and λ_{max} is the larger eigenvalue. This ratio is bounded between 0 and 1. It takes a value of 0 when the Jacobian is singular, and takes a value of 1 where the eigenvalues are equal. This latter case represents an isotropic point, where the mechanism can may produce equal torque in arbitrary directions.

A different commonly used local index include the dexterity index, which is simply the absolute value of the determinant of the Jacobian at any given point. Because the Jacobian in this case is dimensionally homogeneous, it is not affected by the scaling issue described in [18]. However, as this index is unbounded, a single point in the workspace with high dexterity can overshadow areas with particularly low, or near singular performance. Moreover, this metric is not scale invariant, meaning that if all linear parameters were halved in total size, the local dexterity of each pose would quadruple. Though we can and do enforce effective size constraints on the parameters, the scaling variance makes it difficult to determine which configurations are actually have better singularity/torque characteristics versus those which enforce a smaller size scale and artificially increase dexterity.

To compute the Global Conditioning Index (GCI) χ_G of a configuration from the LCI of the poses χ_{Lp}, we must first sample points of the desired workspace of a given mechanism parameter configuration, test if they are reachable given the geometric parameters, and then compute the Jacobian and χ_{Lp}.

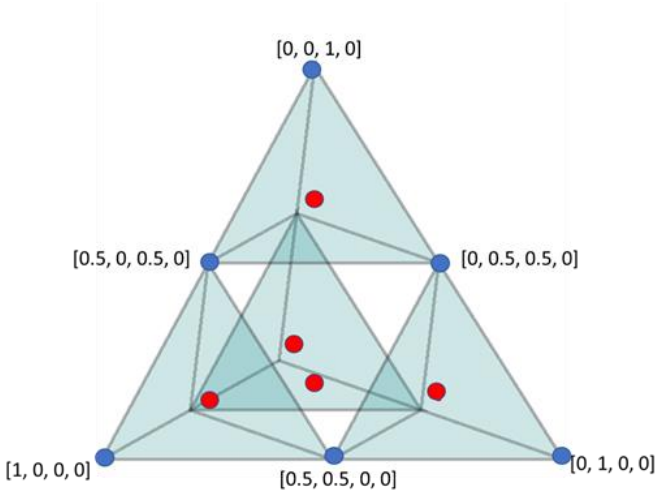

FIGURE 5: Three-dimensional embedding of four-dimensional simplex over length parameters. Each point where lines intersect was a directly sampled point, though only the directly sampled points which fall on nearest face are shown as blue dots, with their respective coordinate values. The center (red dots) of each sub tetrahedron correspond to the indirectly sampled points, generated by finding the center of each sub-tetrahedron. Additional points were added to achieve uniform spacing (equal distance to 3 nearest neighbors). Note each vertex of the overall tetrahedra corresponds to a single length parameter taking a value of unity, while the other three are zero.

Following this, we take a weighted average of all the $\boldsymbol{\chi_{Lp}}$ within the desired workspace, weighting them by the relative area of the workspace they represent to calculate $\boldsymbol{\chi_G}$. If the weight at a particular pose may be denoted as $\boldsymbol{w_p}$, then we may define $\boldsymbol{\chi_G}$ as

$$\boldsymbol{\chi_G} = \sum_{p=1}^{n} \boldsymbol{w_p \chi_{Lp}}$$

where n is the total number of sampled points in the desired workspace (1221 in this work, though points outside of the desired workspace were sampled for visual continuity and singularity analysis). This index also ranges between 0 and 1, with the latter representing best possible performance. The desired workspace is an ellipse in $(\boldsymbol{\varphi}, \boldsymbol{\theta})$ space, with a semi major axis of 80º in the $\boldsymbol{\varphi}$ direction and 40º in the $\boldsymbol{\theta}$ direction. This workspace approximately corresponds to the range of motion in flexion and abduction of the human wrist [19], [20].

In addition to this optimality index, we also examine two size metrics of the configurations. The first of these two is $\boldsymbol{d_{min}}$, the minimum distance an intermediate link comes towards the origin of the mechanism over the desired workspace. This metric relates to clearance of an intermediate link from the central U joint, or the distance from the other intermediate link (whichever is smaller), which informs how large the components may be before interference occurs. A large $\boldsymbol{d_{min}}$ makes a configuration easier to physically construct. The second size metric is $\boldsymbol{d_{max}}$, the maximum distance any point on the intermediate link gets from the origin of the mechanism. This metric relates to the overall size of the mechanism. A smaller $\boldsymbol{d_{max}}$ makes it easier for a configuration to be scaled to fit within certain absolute size constraints (e.g. no longer than 10cm) without forcing any other components to become prohibitively small. Note that both of these metrics may only be calculated after the entire workspace of a configuration has been simulated, and that they are global metrics as well.

To optimize the geometric parameters of the mechanism, we use an exhaustive sampling of the parameter space with a number of adjustments, and follow with a gradient ascent search. Firstly, to avoid sampling configurations which are simply dilations of one another, we constrain all the length parameters to sum to 1. Combining this with the constraint they all be positive valued, the length parameters form a simplex. As there are only four length parameters, the embedded simplex can be represented in only three dimensions (simplified version in Fig. 5). This simplex may be sampled directly forming a basis of vectors orthogonal to the linear summation constraint, and uniformly sampling a space with said basis.

Once the directly sampled points have been obtained, sets of four points with the same pairwise distance in this simplex can form sub-tetrahedra (transparent blue in Fig. 5) within the overall tetrahedron. These points (represented as blue dots in Fig. 5) may lie on the boundary of the overall tetrahedron, where at least one of the length parameters must be 0. These points generally correspond to impossible or impractical mechanism parameter configurations. As a result, the points within the simplex we opt to use, called the indirectly sampled points, are those which correspond to the centers of the sub-tetrahedra, shown as red dots in Fig. 5. They may be obtained by taking the mean of the 4 points which define the sub-tetrahedra. Additional centers are added in to achieve uniform spacing between nearest indirectly sampled points. A total of 385 uniformly spaced indirectly sampled points corresponding to combinations of the length parameters are thus extracted from this simplex.

The angles $\boldsymbol{\alpha_p}$ and $\boldsymbol{\alpha_s}$ are varied between 10º and 80º in 10º increments for a total of 7 values each. Once the four linear parameters and these two angles are chosen, the points $\boldsymbol{S_{1o}}$ a and $\boldsymbol{P_{01}}$ are fully defined, leaving only $\hat{\boldsymbol{v}}_{\boldsymbol{1}}$ to be determined by $\boldsymbol{\beta}$ and $\boldsymbol{\gamma}$. We initially choose $\boldsymbol{\beta}$ and $\boldsymbol{\gamma}$, such that $\boldsymbol{S_{1o}}$ lies on the P joint LoA, and call this fully determined configuration a cardinal configuration. By definition, cardinal configurations are guaranteed to be able to reach the ZP, and the intermediate link will lie directly on the P joint LoA at the ZP. We then construct other fully determined configurations by varying $\boldsymbol{\beta}$ and $\boldsymbol{\gamma}$ each from -15º to 15º in 5º increments from the cardinal configuration while leaving the other parameters the same. We choose $\boldsymbol{\beta}$ and $\boldsymbol{\gamma}$ in this was as opposed to an arbitrary range to ensure the at least the cardinal configurations sampled will have a kinematically feasible ZP, and that deviations about the cardinal configurations likely will as well.

A total of 924,325 configurations are sampled in this exhaustive search of the parameter space. After doing this, we perform a gradient ascent search on configurations within the 5% of the optimum configuration (highest GCI). For each configuration subjected to this procedure, 1000 iterations of ascent steps were permitted. This ascent procedure was still subject to the simplex constraints on the linear parameters and was performed using the fmincon function in MATLAB 2017.

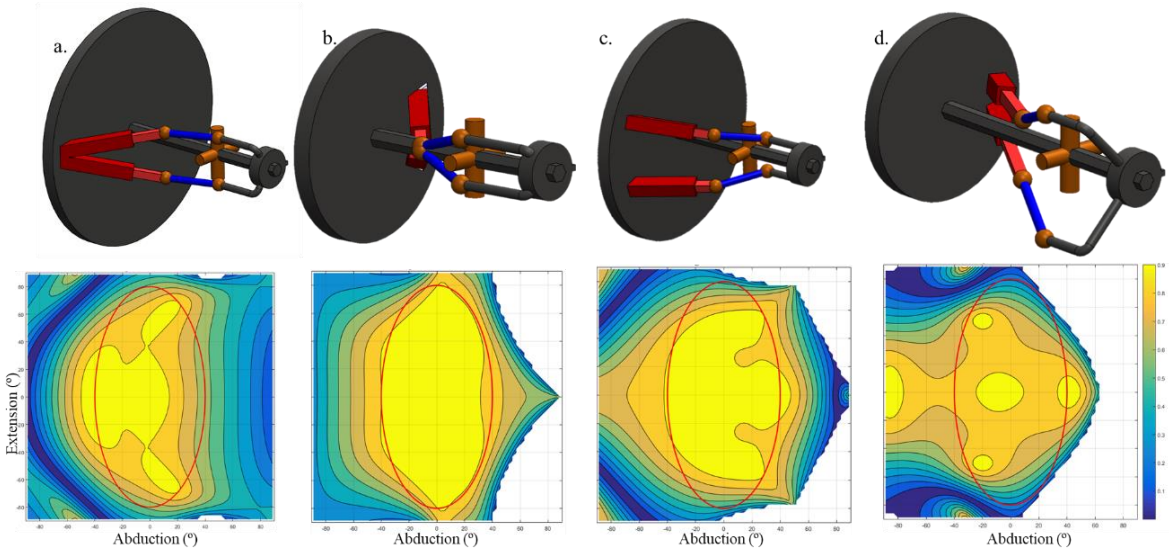

FIGURE 6: Exemplar configurations kinematic layout (top row) and their associated LCI contour plots (bottom row), with the desired workspace denoted by the portion within the red ellipse. a) Configuration C_0, highest χ_G found in exhaustive search. b) Configuration OC, highest χ_G found via gradient search. c) Configuration C_1, a conservative tradeoff which sacrifices less GCI for smaller tightening of sizing constraints d) Configuration C_2, a more aggressive tradeoff with tighter size constraints and lower GCI. Note that all of the contour plots share the same color indexing and axes ranges.

Finally, we also examine the tradeoff between imposing sizing constraints d_{min} and d_{max} and the decrease in maximal GCI as a result. Namely, we take the d_{min} and d_{max} values of the highest χ_G configuration, henceforth called the optimal configuration (OC), as baselines, and tighten the allowable ranges of these metrics to identify the tradeoffs in sizing metrics versus GCI.

.

3. RESULTS AND DISCUSSION

Of the 924,325 configurations sampled via the exhaustive search, 535,287 were feasible configuration which could at least reach the ZP, and 252,943 configurations could reach all points of the discretely sampled desired workspace. The configuration with largest χ_G discovered through this search, called C_0, had a χ_G of 0.8578. This kinematic configuration and the associated LCI contours over the workspace may be seen in Fig. 6a. Subsequently, performing the gradient ascent procedure on configurations within 5% of this optimal value lead to 164 new configurations. This procedure yielded an OC (Fig. 6b) with a χ_G value of 0.945 (LCI contours may be seen in Fig. 6b, lower row). However, this OC would be subject to interference between the intermediate links or the P joints, resulting in a d_{min} of 0. This would prohibit a physical implementation of the mechanism from reaching the entirety of the desired workspace. As a result, we must explore configurations with larger d_{min} values that with similar GCI performance.

Fig. 7 presents the effects of enforcing size constraints on the GCI. Specifically, for a given combination of minimum d_{min} and maximum d_{max}, Fig. 7 shows the highest χ_G of a configuration which met the constraint combination. Moving downward and to the right corresponds to tightening the sizing constraints, while upwards and to the right corresponds to relaxing constraints. By definition, d_{min} must be less than d_{max},

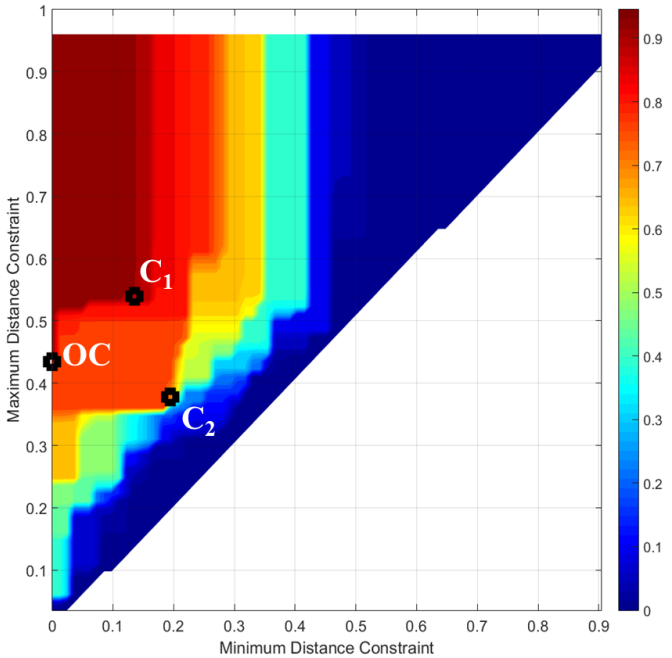

FIGURE 7: Effect of constraints on the GCI. Moving to the right corresponds to requiring a configuration have a higher d_{min}, while moving downward corresponds to requiring a smaller d_{max}. Configurations OC, C_1 and C_2 are denoted as points.

TABLE I. SELECTED CONFIGURATION PARAMETER TABLE

Conf.	d_x	r_s	r_p	l_i	α_p	α_s	β	γ	χ_G	d_{min}	d_{max}
C_0	0.125	0.225	0.225	0.425	165.0	145.0	-40.6	-0.7	0.858	0.101	0.652
OC	0.019	0.179	0.433	0.369	114.2	134.7	0.0	-51.4	0.945	0.000	0.430
C1	0.160	0.125	0.328	0.386	132.1	177.2	-9.1	21.2	0.900	0.160	0.534
C2	0.125	0.325	0.225	0.325	125.0	135.0	15.3	-31.7	0.778	0.189	0.360

therefore no configuration may exist in the empty lower triangular region.

Rather than gradually decreasing as constraints tighten, the GCI appears to fall abruptly between discrete levels. Overall, it is clear that constraints may only be tightened slightly before entering regions of low GCI (blue regions). The regions of high GCI (80% of maximum GCI) only extend up to $d_{min} < 0.2$ and $d_{max} > 0.35$.

As the OC has a d_{min} of 0, it is located on the boundary of feasible configurations, and is shown as such in Fig. 7. To demonstrate the effects of size tradeoffs, two other configurations, C_1 and C_2, are also labeled in Fig. 7. Their kinematic models and associated workspace contours may be seen in Fig. 6c and 6d. These additional configurations were manually chosen by improving the sizing constraint performance (moving down or right in Fig. 7) until there was a sharp decrease in GCI. If the pareto surface in Fig. 7 were smooth, one could define a minimum acceptable GCI as a constraint and optimize over a function of the sizing parameters.

These configurations illustrate the tradeoff between theoretical kinematic performance and physical implementation feasibility. Both configurations lie on boundaries in constraint space which result in sharp drops down to less optimal, better constraint satisfying configurations. As a result, they correspond to how much the constraints may be tightened without significant loss of performance. Configuration C_1 accepts a 5% decrease in GCI and a 20% increase in d_{max} to achieve a d_{min} of 0.16. The prismatic joints are skewed inward but do not result in interference of the intermediate links. Configuration C_2 more aggressively trades performance for size constraint satisfaction,

A list of kinematic parameter values for the configurations presented in Fig. 6 and their associated metrics may be found in Table I.

3.1 Discussion

As maximizing GCI generally entails that local poses be singularity free, it is not surprising that the presented configurations result in singularity curves (dark blue in Fig. 6 lower) located outside of the desired workspace. In fact, LCI appears to be relatively consistent throughout the workspace in the presented configurations, especially within the OC.

Perhaps most notable within these designs is the closeness of the prismatic joints to the horizontal xy plane, and in turn close to the flexion axis. This may be due in particular to the asymmetry in the desired workspace, which includes a significantly higher range of flexion than abduction. Placing actuators close to the flexion axis may decrease the overall required stroke, and thus d_{min}. In turn, this closeness may decrease torque production of the mechanism, though unitless simulations make two configurations difficult to compare outside of predefined scale invariant metrics.

While C_0, C_1, and C_2 will not have collisions due to link interference (under the assumption that the links are thin), an issue that may still affect a physical prototype is the range of motion of the spherical joints. Generally, it is impossible to create a spherical joint with larger than a single hemisphere range of motion due to capture constraints (e.g., a ball must be captured in its socket). In [21], the authors use U joints with asymmetric yokes in series with R joints to achieve the same range of motion, and utilize an elastic biasing element to avoid limiting the range of motion. The complexity of this design may make it intractable for components to be shrunk significantly, precluding their use in small manipulator systems, such as prosthetic wrists.

4. CONCLUSION

In this paper, we present a kinematic architecture for a 2-DOF wrist prosthesis. We perform optimization of the mechanism over its geometric parameters, and also consider some practical implementation issues regarding the size and interference of components of the mechanism. We perform an exhaustive search by discretizing the parameter space, then perform a gradient search to find optimal configurations. We then look at the tradeoffs between sizing issues and performance, and show the extent of changes that can be made without significant loss of performance.

ACKNOWLEDGEMENTS

This work was supported by the US Army Medical Research and Materiel Command, under contract W81XWH-15-C-0125.

5. REFERENCES

[1] N. M. Bajaj, A. J. Spiers, and A. M. Dollar, “State of the art in prosthetic wrists: Commercial and research devices,” in IEEE International Conference on Rehabilitation Robotics, 2015, pp. 331–338.

[2] N. M. Bajaj, A. J. Spiers, and A. M. Dollar, “State of the Art in Artificial Wrists: A Review of Prosthetic and Robotic Wrist Design,” in IEEE Transactions in Robotics, vol. 35, no. 1, pp. 261-277, 2019.

[3] X. J. Liu, Z. L. Jin, and F. Gao, “Optimum design of 3-DOF spherical parallel manipulators with respect to the conditioning and stiffness indices,” Mech. Mach. Theory, vol. 35, no. 9, pp. 1257–1267, 2000.

[4] C. M. Gosselin, E. St. Pierre, and M. Gagné, “On the Development of the Agile Eye,” IEEE Robotics and Automation Magazine, vol. 3, no. 4, pp. 29–37, Dec-1996.

[5] T. A. Hess-Coelho, “A Redundant Parallel Spherical Mechanism for Robotic Wrist Applications,” J. Mech. Des., vol. 129, no. 8, p. 891, 2007.

[6] K. Al-Widyan, X. Q. Ma, and J. Angeles, “The robust design of parallel spherical robots,” Mech. Mach. Theory, vol. 46, pp. 335–343, 2011.

[7] L. Birglen, C. Gosselin, N. Pouliot, B. Monsarrat, and T. Laliberté, “SHaDe, A new 3-DOF haptic device,” IEEE Trans. Robot. Autom., vol. 18, no. 2, pp. 166–175, 2002.

[8] A. Degirmenci, F. L. Hammond, J. B. Gafford, C. J. Walsh, R. J. Wood, and R. D. Howe, “Design and control of a parallel linkage wrist for robotic microsurgery,” in IEEE International Conference on Intelligent Robots and Systems, 2015, vol. 2015–Decem, pp. 222–228.

[9] L. Barker, M. Neber, and H. Lee, “Design of a low-profile two-axis solar tracker,” Sol. Energy, vol. 97, pp. 569–576, 2013.

[10] P. Vischer and R. Clavel, “Argos: A Novel 3-DoF Parallel Wrist Mechanism,” Int. J. Rob. Res., vol. 19, no. 1, pp. 5–11, 2000.

[11] L. B. Bridgwater et al., “The Robonaut 2 hand-designed to do work with tools,” in Proceedings of the 2012 IEEE International Conference on Robotics and Automation (ICRA2012), 2012, pp. 3425–3230.

[12] H. D. Wang, B. H. Yang, K. Zhang, and Y. Q. Bi, “Design and Kinematics Analysis of a New Two DOF Tilter,” Adv. Mater. Res., vol. 591–593, pp. 674–678, 2012.

[13] A. Cammarata, “Optimized design of a large-workspace 2-DOF parallel robot for solar tracking systems,” Mech. Mach. Theory, vol. 83, pp. 175–186, 2015.

[14] S. K. Agrawal, G. Desmier, and S. Li, “Fabrication and Analysis of a Novel 3 DOF Parallel Wrist Mechanism,” J. Mech. Des., vol. 117, no. 6, pp. 343–345, 1995.

[15] N. M, Bajaj and A. M. Dollar, “Kinematic Optimization of a Novel Partially Decoupled Three Degree of Freedom Hybrid Wrist Mechanism,” IEEE International Conference on Robotics and Automation 2018 (ICRA 2018), pp. 6953-6960, 2018.

[16] R. D. I. Gregorio and R. Sinatra, “Singularity Curves of a Parallel Pointing System,” pp. 255–268, 2002.

[17] C. Gosselin, “Kinematic Analysis Optimization and Programming of Parallel Robotic Manipulators.pdf.” p. 252, 1988.

[18] C. M. Gosselin, “Dexterity Indices for Planar and Spatial Robotic Manipulators,” Proc. - IEEE Int. Conf. Robot. Autom., vol. 1, no. May, pp. 650–655, 1990.

[19] D. C. Boone and S. P. Azen, “Normal range of motion of joints in male subjects.,” J. Bone Joint Surg. Am., vol. 61, pp. 756–759, 1979.

[20] J. M. Soucie et al., “Range of motion measurements: Reference values and a database for comparison studies,” Haemophilia, vol. 17, pp. 500–507, 2011.

[21] L.-T. Schreiber and C. Gosselin, “Passively Driven Redundant Spherical Joint With Very Large Range of Motion,” J. Mech. Robot., vol. 9, no. 3, p. 31014, 2017.